TU/e EINDHOVEN UNIVERSITY OF TECHNOLOGY

Investigation of the constricted positive column in neon

Citation for published version (APA):
Mouwen, C. A. M. (1971). *Investigation of the constricted positive column in neon*. [Phd Thesis 1 (Research TU/e / Graduation TU/e), Applied Physics and Science Education]. Technische Hogeschool Eindhoven. https://doi.org/10.6100/IR79299

DOI:
10.6100/IR79299

Document status and date:
Published: 01/01/1971

Document Version:
Publisher's PDF, also known as Version of Record (includes final page, issue and volume numbers)

Please check the document version of this publication:

• A submitted manuscript is the version of the article upon submission and before peer-review. There can be important differences between the submitted version and the official published version of record. People interested in the research are advised to contact the author for the final version of the publication, or visit the DOI to the publisher's website.
• The final author version and the galley proof are versions of the publication after peer review.
• The final published version features the final layout of the paper including the volume, issue and page numbers.

Link to publication

General rights
Copyright and moral rights for the publications made accessible in the public portal are retained by the authors and/or other copyright owners and it is a condition of accessing publications that users recognise and abide by the legal requirements associated with these rights.

• Users may download and print one copy of any publication from the public portal for the purpose of private study or research.
• You may not further distribute the material or use it for any profit-making activity or commercial gain
• You may freely distribute the URL identifying the publication in the public portal.

If the publication is distributed under the terms of Article 25fa of the Dutch Copyright Act, indicated by the "Taverne" license above, please follow below link for the End User Agreement:

www.tue.nl/taverne

Take down policy
If you believe that this document breaches copyright please contact us at:

openaccess@tue.nl

providing details and we will investigate your claim.

Download date: 17. Nov. 2023

INVESTIGATION OF THE CONSTRICTED POSITIVE COLUMN IN NEON

C. A. M. MOUWEN

INVESTIGATION OF THE CONSTRICTED POSITIVE COLUMN IN NEON

C. A. M. MOUWEN

INVESTIGATION OF THE CONSTRICTED POSITIVE COLUMN IN NEON

Proefschrift

TER VERKRIJGING VAN DE GRAAD VAN DOCTOR IN DE TECHNISCHE WETENSCHAPPEN AAN DE TECHNISCHE HOGESCHOOL TE EINDHOVEN OP GEZAG VAN DE RECTOR MAGNIFICUS PROF. Dr. Ir. A. A. TH. M. VAN TRIER, VOOR EEN COMMISSIE UIT DE SENAAT IN HET OPENBAAR TE VERDEDIGEN OP DINSDAG 8 JUNI 1971 DES NAMIDDAGS TE 4 UUR

door

CORNELIS ADRIANUS MARIA MOUWEN

geboren te Breda

Dit proefschrift is goedgekeurd door de promotor
Prof. Dr. A.A.Kruithof .

ter nagedachtenis aan mijn vader

CONTENTS.

Chapter I General introduction 10

1.1 Constriction theories 11
1.2 Experimental methods 13
1.2.1. Spectrum line broadening experiments 14
1.2.2. Thermocouple measurements 15
1.2.3. Miscellaneous experimental methods 16
1.3 New model of the contricted positive colomn 16
References

Chapter II Experimental Methods

2.1 The discharge tube 18
2.2 Thermocouple measurements 20
2.3 Gas pressure measurements 22
2.4 The order scanning Fabry-Perot interferometer 24
2.4.1. Determination of the dispersion function 25
2.4.2. New method 26
2.4.3. Distortion of the measured line profile 28
2.5 Analysis of the experimental spectrum line profiles 29
2.5.1. Unfolding of the observed line profiles 29
2.5.2 Determination of the resonance halfwidth 31
2.6 Miscellaneous experimental methods 31
2.6.1. Microwave measurements 31
2.6.2. Spectrum line intensity measurements 32
2.6.3. Optical absorption measurements 32
2.6.4. Radiant flux measurements 33
References

Chapter III Spectrum line broadening

3.1.1. General theory of resonance broadening 35
3.1.2. Shape of $n_a(r)$ and $P_{nm}(r)$ for some special cases 38
3.1.3. General representation of $n_a(r)$ and $P_{nm}(r)$ 41
3.1.4. Normalised spectrum line profile 42
3.1.5. Influence of other line broadening mechanisms 47

3.1.5.1. Natural line broadening 48
3.1.5.2. Doppler broadening 48
3.1.5.3. Isotope effects 49
3.1.5.4. Self-absorption 51
3.1.5.5. Stark broadening 52
3.2 Experimental results 53
3.2.1. Spectrum line broadening in the low pressure positive column 56
3.2.2. Spectrum line broadening in the moderate pressure positive column 58
3.2.3. Spectrum line broadening in the constricted high pressure positive column 59
3.2.3.1. Calculation of $n_a(0)$. 59
3.2.3.2. The effective broadening constant $C_{nm_{eff}}$ 60
3.2.3.3. Comparison of experimental and theoretical halfwidths 61
3.3 New method for the determination of gas temperatures 63
3.3.1. Experimental verification of the new method 65
3.4 Conclusion 67
References

Chapter IV Thermocouple measurements

4.1 Introduction 69
4.2 Experimental results 69
4.3 The systematic error in thermocouple measurements 74
4.3.1. Experimental 74
4.3.2. Calculation of the systematic difference 75
4.3.2.1. Heat transfer from the plasma to the thermocouple 77
4.3.2.2. Heat conduction through the capillary and the thermocouple to the wall 77
4.3.2.3. Thermal radiation of the capillary 78
4.3.2.4. Recombination and deexcitation processes at the wall of the capillary 78
4.3.2.5. The energy balance of the thermocouple 79
4.3.3. Approximate solution 79

4.4 Shape of the gas temperature distribution 83
References

Chapter V Plasma model for the constricted positive column

5.1.1. Introduction 85
5.1.2. Basic model 86
5.2 Calculation of the heat dissipation function 86
5.2.1. Electron energy distribution function 87
5.2.2. The energy balance 89
5.2.3. Relation between electron temperature and gas temperature 91
5.2.4. The dissipation function 93
5.3 Relevant atomic processes 94
5.3.1. Resonant and metastable atom densities 95
5.3.2. The ionization mechanism 100
5.3.3. Charged particle balance 102
5.3.4. The heat dissipation function 105
5.4 The solution of the Heller-Elenbaas equation 108
5.5 Approximate solutions 111
5.5.1. The gas temperature distribution 111
5.5.2. The electron temperature distribution 114
5.5.3. The spatial distribution of spectrum line radiation 115
5.5.4. The constriction mechanism 117
5.5.5. Conclusion 117

References

Summary 121

Samenvatting 123

Curriculum vitae 125

CHAPTER I GENERAL INTRODUCTION

INTRODUCTION

When in the familiar low pressure glow discharge of cylindrical symmetry both the gas pressure and the discharge current are increased above a certain critical value, a constriction of the positive column of that discharge will be observed. As a direct consequence of this constriction the emission of light contracts into a narrow channel around the discharge axis. This phenomenon in fact is the most prominent general characteristic of the constricted positive column.

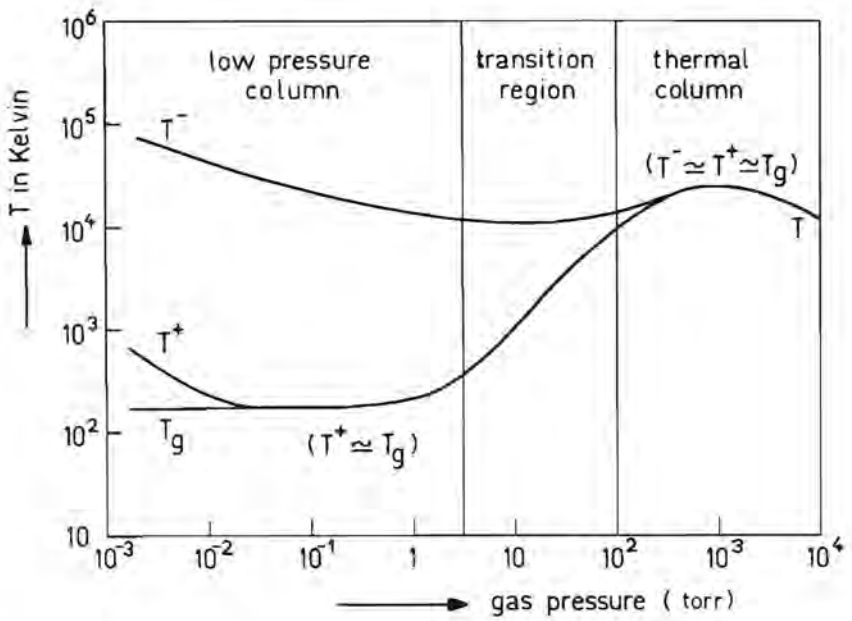

Fig.1.1 Schematic representation of the electron temperature (T^-), the ion temperature (T^+) and the gas temperature (T_g) as a function of the gas pressure.

From measurements presented in this thesis it follows that the constricted positive column can neither be classified as a thermal arc nor as a classical glow discharge; it falls into an intermediate category. This is illustrated schematically in Fig.1.1, where representative curves for electron temperature, ion temperature and gas temperature are shown as functions of the gas pressure. The transition region indicated in the figure is the region in which commonly a constriction of the positive column is observed.

1.1. Constriction theories.

Constricted discharges were studied by several workers. Starting from the basic theory of the positive column described by Schottky[1], more or less complex models were proposed to explain the phenomenon of constriction. A review of the constriction theories up to 1955 was given by Fowler[2], who advanced himself a collision-damping theory for this effect. The most important discharge mechanisms reviewed in his article to explain the phenomenon of constriction may be divided into three categories.

[1] Theories based on the intrinsic non-linearity of the basic differential equations from which the Schottky theory was derived.

[2] In a second category of explanations complexities were introduced into the electron and ion production processes. Ionisation in two steps and volume recombination of electrons and ions both fall into this class.

[3] A third possible basis of explanation was found in the magnetic self-constriction of the positive column. This effect is indeed observed at very large discharge currents, but it is well-known that constricted columns can be maintained with very small currents.

From 1955 up to now (1971) various constriction models were published. The greater part of these were refinements of constriction models described in (2). Apart from these there were some new approaches which are briefly reviewed below.

[4] Kenty[3] studied the constricted discharge in Xenon. He proposed that the main cause for constriction might be an increase of the ion recombination coefficient from the tube axis to the wall.

[5] By Edwin and Turner[4] a constriction model was proposed in which outward diffusion of electrons and ions from the central glowing core is balanced by recombination in the peripheral regions of lower charge density.

[6] Kagan, Lyagustschenko et al.[5] presented a constriction model which was based essentially on the mechanism of stepwise ionisation.

[7] The so called "ionisation controlled" constriction model, proposed and worked out by Wojaczek[6][7][8], is based on the non linear relationship between ionisation rate and electron density. Since this non-linearity , according to Wojaczek, finds its principal origin in the mechanism of stepwise ionisation his new model is only in second order details different from the model proposed by Kagan et al.

[8] In recent publications[9][10][11][12], it has been indicated that thermal effects may influence the constriction mechanism considerably.

Despite of the sometimes very complex models used, the succes of the foregoing theories in describing the constriction of the positive column was very poor. This is not as strange as one would expect at

first glance. Although some of the theories presented are essentially correct, a rough estimate immediately shows that the various models lead to constrictions which are orders of magnitude smaller than those observed in the experiments. The remaining theories fail for the reason that they indicate as the basic constriction mechanism a phenomenon which is a direct consequence of the constriction itself. Concluding it may be stated that although there have been proposed various constriction models, each of which is a specific valuable contribution to a better understanding of the constriction mechanism, there still is a need for a more general concept. Against this background the significance of the present work should be seen. The purpose of the investigation presented in this thesis is to describe the appearance of the constricted positive column at operating pressures up to 1 atm under several conditions of geometry and discharge current and to give the results of thermo-electric and spectroscopic measurements of their characteristics. Based on the experimental results a new thermal model for the constricted positive column is presented which enables us to give an explanation for the most prominent macroscopic features of these discharges.

1.2 Experimental methods.

In order to cope with the strong inhomogeneity of the plasma of the constricted positive column any appropriate diagnostic method should have a good spatial resolution. By this condition various well-known diagnostic methods, which are widely used for the investigation of the homogeneous low pressure discharge, are eliminated in advance, e.g. electric and magnetic probe techniques, microwave measurements etc. Although the last mentioned measurements do not yield an adequate spatial resolution of the quantities to be measured, incidentally a 4 mm microwave interferometer has been used to obtain a rough estimation for the average electron density in the constricted column.

Since in general the plasma of the constricted positive column is not in "Local Thermal Equilibrium" (L.T.E.) neither absolute nor relative spectrum line intensity measurements can yield relevant

information about the electron temperature; they only give data about population densities of the various atomic levels which are not directly interpretable. Strictly speaking, the only definite information which may be obtained from spectrum line intensity measurements is the certainty that the plasma is not in L.T.E.. As in a number of the constriction models, discussed in the foregoing, the assumption is made that the plasma is in L.T.E., the negative experimental information has been used to exclude these models from further consideration.

The emission of light is concentrated in the direct neighbourhood of the discharge axis, but even here the electron density is too small to bring about any noticeable continuum emission, Stark broadening or scattering of radiation. Therefore none of these effects could be used for the determination of the electron temperature or the electron density. After this, from an experimental point of view rather disappointing elimination of the usual experimental techniques, there were only a few experimental methods left which may be applied in principle for the experimental investigation of the constricted positive column. From our thermal model of this column it follows that the constriction is largely determined by the radial gas temperature distribution. For that reason we have chosen two independent methods from the remaining group of diagnostic procedures namely the determination of the resonance broadening of an appropriate spectrum line (λ = 5852 Å) and the determination of the gas temperatures with the aid of thermocouples. Although the methods mentioned are nearly classical ones, both had to be adapted rigorously to the actual experimental conditions as a direct consequence of the strong inhomogeneity of the plasma.

1.2.1 Spectrum line broadening experiments.

In general the broadening of a spectrum line is a rather complicated phenomenon since various broadening effects may take place simultaneously. Fortunately in the region of plasma parameters considered in the actual experiments the influence of resonance broadening on the spectrum line profile largely exceeds that of the other broadening mechanisms like Doppler, Stark and natural broadening. The halfwidth of a resonance

broadened spectrum line is directly proportional to the gas density. Based on this simple relationship, valid for homogeneous plasmas, a new method has been developed to determine spatially resolved gas densities from resonance broadening experiments performed on inhomogeneous plasmas. By this extension of the spectrum line broadening theory to strongly inhomogeneous plasmas, it has been possible to interpret the experimental halfwidths directly in terms of neutral atom densities c.q. gas temperatures. The basic principles of this concept and the experimental results of the line broadening measurements are discussed in chapter 3 of this thesis.

The profiles of the λ = 5852 Å neon spectrum line have been determined with the aid of a Fabry-Perot interferometer. The fixed interference pattern of this interferometer was scanned with a movable fotomultiplier. The principles and the experimental set up of this very simple but accurate method, which was introduced in a previous paper[13] as an "Order scanning Fabry-Perot spectrometer", are discussed in detail in chapter 2 section 4.

1.2.2 Thermocouple measurements.

Although thermocouple measurements are commonly referred to as "classical" untill now no satisfactory answer was given to the following fundamental question: "How large are the systematic errors in such measurements, which are due to various elementary physical processes like: thermal radiation of the thermocouple, recombination and deexcitation at the thermocouple wall, heat conduction etc..?" Moreover it was never investigated in detail in which way the plasma as such is distorted by the presence of the thermocouple. From a quantitative discussion of the energy balance of the thermocouple and a comparison of the experimental results with those obtained from independent line broadening experiments, it could be concluded that taking into account the thermal radiation of the thermocouple, the remaining systematic error due to the other mechanisms does not exceed 5 per cent. This whole matter is discussed, together with the results of the measurements, in chapter 4 whereas the details of the thermocouple measurements are discussed in chapter 2, section 2.

1.2.3 Miscellaneous experimental methods.

In order to get on the one hand some more general information about the constriction mechanism as such, and on the other hand to obtain some more detailed information about certain specific aspects of the high pressure positive column, incidentally, various diagnostic methods have been used. Since in contrast with the line broadening experiments and the thermocouple measurements mentioned, these methods are very common and needed no adaption to the specific requirements of the actual experiments, they are only briefly reviewed in chapter 2 , section 6.

1.3 New model of the constricted positive column.

From the numerous experimental data obtained from the experiments mentioned, it has been possible to conclude that the plasma of the high pressure positive column is essentially determined by its thermal properties. In other words, all characteristic features of this plasma like constriction mode, stabilisation of the column, spectrum line emission etc., strongly depend on the gas temperature distribution. Starting from this concept, in chapter 5 a thermal model for the high pressure positive column is developed which is in good agreement with the various experimental results.

References.

(1) Schottky, W., Phys. Z. 25, 342, 635 (1924).
(2) Fowler, R.G., Proc. Phys. Soc. (London) 68. 130 (1955).
(3) Kenty, C., Phys. Rev. 126, 1235 (1962).
(4) Edwin, R.P., Turner, R., J.Opt.Soc.Am. 60, 448 (1970).
(5) Golubowsky, Ju.B., Kagan, Ju.M., Ljagustschenko, R.J., Michel, P., Beitr.Plasmaphys. 8, 423 (1968).
(6) Wojaczek, K., Beitr.Plasmaphys. 6, 211 (1966).
(7) Wojaczek, K., Beitr. Plasmaphys. 7, 149 (1967).
(8) Wojaczek, K., Beitr. Plasmaphys. 9, 243 (1969).

(9) Massey, J.T., J.Appl.Phys. 36, 373 (1965).
(10) Rakhimov, A.T., Ulinich, F.R., Sovj.Phys.Dokl. 14, 655 (1970).
(11) Baronov, V.Ju., Uljanov, K.N., Sovj.Phys.Techn.Phys. 14, 183 (1969).
(12) Mouwen, C.A.M., Claassens, J.M.M., Phys. Lett. A 31, 123 (1970).
(13) Mouwen, C.A.M., Journ.Sci.Instr. 3, 27 (1970).

CHAPTER II EXPERIMENTAL METHODS

INTRODUCTION

In the foregoing chapter it was outlined that there are only a few diagnostic methods which can be applied to the experimental investigation of the high pressure positive column. The most important of these are line broadening experiments and thermocouple measurements. The line broadening experiments performed in the actual investigation concerned mainly the resonance broadening of one specific line of the visible neon spectrum (λ = 5852 Å). The line profile of this spectrum line has been determined with the aid of a Fabry-Perot interferometer of the order-scanning type. The details of this method and the subsequent analysis of the experimental line profiles are treated in sections 4 and 5 of this chapter. The specific technical problems related to the construction of the thermocouples will be discussed in section 2. In section 1 some construction details of the discharge tube are given, whereas in section 3 the experimental set up for the gas pressure measurements is described. Finally in section 6 miscellaneous experimental methods are discussed which have been applied incidentally in this investigation.

2.1 The discharge tube.

The measurements presented in this thesis were performed mainly with two types of tipped-off discharge tubes. The construction of these tubes is schematically shown in Fig.2.1. Although an optimal unity in the construction of the various discharge tubes of the same type was aimed at , it could not be avoided that incidentally slight differences in minor construction details had to be admitted. From an experimental point of view it is important to notice that this resulted in some extra scattering in the results. The discharge tubes referred to as type (a), were made of pyrex and had a total length of about 150 mm. The distance between the electrodes was 110 mm and the inner diameter 12 mm. The cathode was a hollow tantalum cylinder whereas the ring-

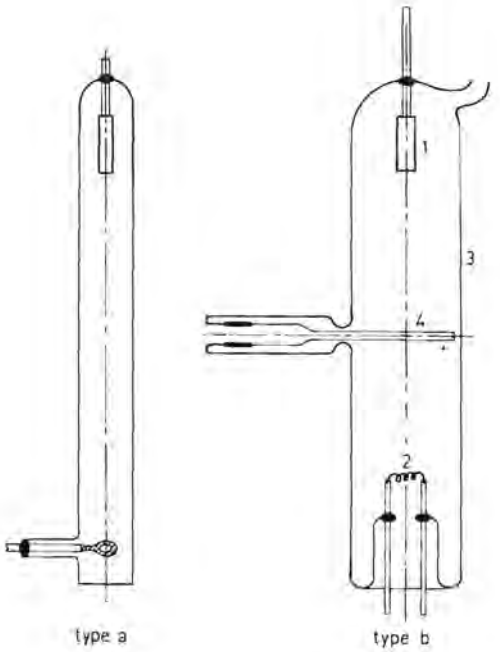

Fig. 2.1a Schematic representation of discharge type (a).

Fig. 2.1b Schematic representation of discharge type (b).

In Fig. 2.1b the various numbers indicate the following construction details.

1 = anode; massive nickel cylinder .

2 = cathode; wolfram with barium oxide layer.

3 = pyrex tube;

inner diameter 27 mm,
outer diameter 30 mm,
total length 290 mm,
electrode distance 210 mm

4 = thermocouple

shaped anode was made of fernico on which a thin layer of enamel was applied. As a consequence of various construction details these discharge tubes could be used for discharge currents up to 250 mA and maximum operating pressures of about 500 torr. With this discharge type both line broadening experiments and spectral radiant flux measurements were performed.

Since the operating range of discharge type (a) was limited to rather low values of both discharge current and operating pressure, discharge tube type (b) was developed. Tubes of this type could be used with maximal operating pressures of 1,5 atm and discharge currents up to 1A. To the discharges obtained in these tubes various plasma diagnostic techniques have been applied simultaneously, namely spectrum line broadening experiments, thermocouple measurements, radiant flux measurements and gas pressure measurements.

2.2 Thermocouple measurements

The thermocouple constructions used in the various experiments were slightly different. The common and essential parts of the constructions are shown in Fig.2.2. Apart from the construction shown in this figure, where the junction of the thermocouple wires is fixed to the top of the fused silica capillary, also a slightly different construction was used in which the thermocouple as such could be slipped to and fro in the capillary. Assuming an ideal thermal contact between the capillary and the junction of the thermocouple, it is possible to determine in this way the temperature distribution in the axis of the capillary. As will be shown this temperature distribution $T_t(r)$ is a first approximation for the radial gas temperature distribution $T_a(r)$ in the discharge tube.

The thermocouples as such were constructed of 50 μm platinum; platinum-rhodium (10%) (Pt-PtRh^{10}) wires which were joined by the argon-arc welding process. The thickness of such a junction was less than 150 μm. The two wires were isolated electrically by enclosing one of them in a fused-silica capillary having a diameter of about 250 μm. These Pt-PtRh^{10} thermocouples may be used in principle in the temperature range between

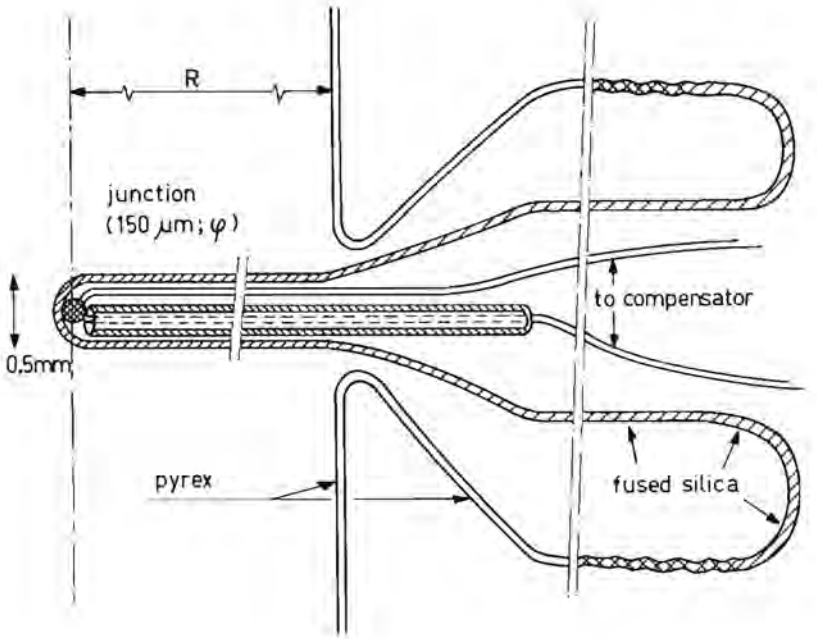

Fig. 2.2 Schematic diagram of the thermocouple configuration used in the experiments.

300 and 1800 K. Since the thermoelectric power of Pt-PtRh^{10} is only small (≈ 10 µV/K), in part of our experiments chromel-alumel thermocoax was used. These industrial thermocouples consist of a thin chromel and a thin alumel wire, enclosed in a cover of inconel. The components of these thermocoax thermocouples are electrically isolated by magnesia. This thermocoax has an outer diameter of about 250 µm, a thermoelectric power of about 40 µV/K and may be used in the temperature range between 300 and 1300 K. In the temperature range in which they were used the various thermocouples were calibrated to an absolute accuracy better than 0.5 K. The thermoelectric e.m.f. was measured with the help of a

current compensation method. The absolute inaccuracy in this method was about 3 μV, which, depending on the thermocouple components corresponds to 0,1 to 0,5 K. In the experiments performed with the movable thermocouples the position of the thermocouples was determined with the aid of a microscope. The absolute error in these position measurements was about 5 μm.

In general the discharge plasma will be distorted noticeably by the presence of the thermocouple. In the constricted positive column the discharge plasma proper is concentrated completely in a small channel surrounding the discharge axis. In the actual experiments the presence of the thermocouple in the direct neighbourhood of the discharge axis resulted in a slight asymmetry in the light emitting part of the discharge. This distortion of the discharge filament was compensated visually by applying a small magnetic field. The maximum variation of the e.m.f., due to the application of the magnetic field, is very closely related to the difference between the thermocouple temperatures in the distorted and the undistorted plasma. To obtain a good estimation of the e.m.f. in the undistorted plasma this maximum variation of the e.m.f. was added to the e.m.f. measured in the distorted plasma.
Although by this correction the systematic error due to the distortion of the plasma is considerably reduced, this reduction was not completely. However, from a comparison of the axis temperatures determined with the aid of thermocouples with the temperatures obtained from simultaneous gas pressure and line broadening measurements the conclusion could be drawn that the influence of the remaining distortion on the results was less than 5 per cent.

2.3 Gas pressure measurements.

In order to compare the results of the thermocouple measurements with those of the line broadening experiments, in part of our investigation the operating pressure in the discharge tube was measured. For that purpose a small hollow fused-silica spiral was connected to the discharge tube. Since by an appropriate construction of this spiral a variation of the gas pressure in the discharge tube resulted in an angular displace-

ment of the spiral, this device could be used to determine the gas pressure in the discharge tube. The rotation of the spiral was detected by measuring the linear displacement of a light spot obtained by focussing a laser beam which was reflected by a small mirror mounted on top of the spiral. In order to avoid non-linear effects the spiral was used as an indicator in a pressure compensation method. For that purpose the spiral was enclosed in a pyrex tube that could be evacuated and was connected to a U-tube mercury manometer.

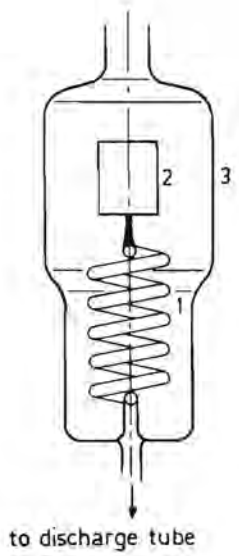

Fig. 2.3.
The fused silica spiral manometer.

1 = fused silica spiral.

2 = mirror.

3 = pyrex tube.

Before the ignition of the discharge the pyrex tube was evacuated. Starting from this condition a zero-position of the mirror was defined by focussing the laser beam on a small pinhole, 1 mm in diameter, behind which a photodiode was mounted. The adjustment of this starting position was visualised by a signal lamp which was steered by the photodiode. After ignition of the discharge the increase of the gas pressure in the discharge tube was compensated by letting gas into the pyrex tube. The

moment the difference of the gas pressures in and outside the spiral was equal to the cold filling pressure was indicated by the signal lamp. At that moment the gas inlet was stopped and the total pressure increase was read from the manometer. By adding this pressure to the known filling pressure of the discharge tube, the operating pressure in the discharge tube was obtained.

In order to increase the sensitivity of the equipment the laser beam was reflected several times by fixed mirrors. In that way an optical path of about 20 m was obtained.

Due to thermal radiation of the plasma and heat conduction through the connection pipe the fused-silica spiral was slightly heated. The thermal expansion following from this increase in temperature also resulted in a small rotation of the mirror. If this effect was taken into account the remaining systematic error in the method was estimated to be less than 5 torr. At operating pressures of about 1 atm this corresponds to a relative error of about 1 per cent.

2.4 The order scanning Fabry-Perot interferometer.

In the past, a number of methods have been developed for scanning the interference pattern of a Fabry-Perot interferometer. The method most frequently used is pressure scanning as described by Jacquinot and Dufour[1], Kuhn[2] et al, but in time resolved spectroscopy, several other scanning methods are widely used (Cooper and Greig[3], Bradley[4], Auth[5]). In these methods, the optical path within the interferometer is changed by varying the refractive index of the medium between the interferometer plates (pressure scanning), or by changing the distance between them (thermal, piezoelectric or mechanical scanning).

In order scanning, however, the optical path between the interferometer plates is kept constant and the different orders of the fixed interference pattern are scanned with a movable detector (Mewe and de Vries[6]). The principle of order scanning has some advantages with respect to other methods.

a) The method is simple from an experimental point of view.

b) The time of the scanning period can easily be varied from a few

milli-seconds to a few hours.

c) It is possible to attain a great accuracy.

Alternatively, however, there are some disadvantages of which the most important are:

d) It is difficult to determine the dispersion function.

e) Since the shape of the detector slit is not adapted to the curvature of each separate interference fringe, the measured spectral line profile is distorted with respect to the original line profile.

In the present section it is shown in what way these latter effects can be anticipated. In sections 2.4.1 and 2.4.2 a simple but accurate method for the determination of the dispersion function is given. In reference (16) the influence of the dimensions of a rectangular detector slit on the shape of the measured spectral line profile is discussed.

2.4.1 Determination of the dispersion function.

In Fig. 2.4 an order scanning Fabry-Perot spectrometer is schematically drawn.

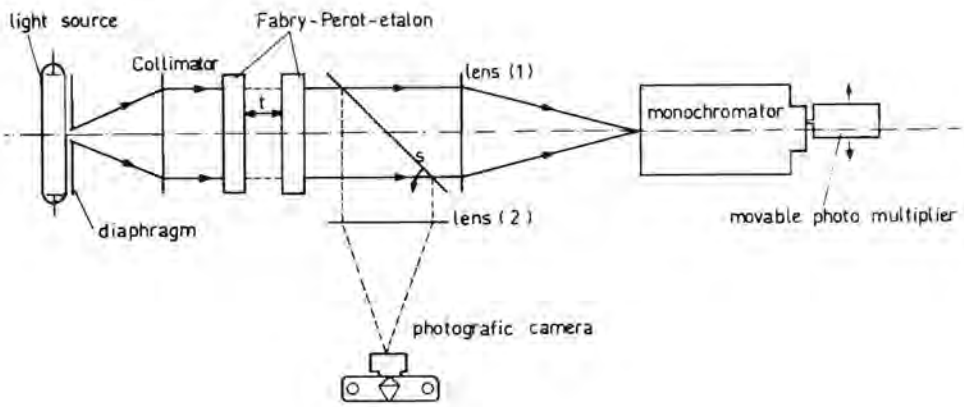

Fig.2.4 Simplified diagram of the optical arrangement.

The dispersion function $D_k(\lambda) = \frac{d\lambda}{dr}$, is given by

$$D_k(\lambda) = \frac{\lambda}{f}\sqrt{\frac{\lambda}{t}\,(k-1+e(\lambda))} \qquad (2.1)$$

where:

λ = the wavelength,
f = the focal distance of lens (1),
t = the etalon distance,
$e(\lambda)$ = the fractional order of the centre
k = the fringe number.

The difficulty in determining $D_k(\lambda)$ lies in the accurate determination of $e(\lambda)$. Usually the radii r_k of a number of successive fringes are measured and $e(\lambda)$ is determined by applying a least squares method to r_k^2 plotted as a function of k. This method, however, gives rise to some difficulties. To measure the radii of several successive fringes it is necessary to scan over a long distance in the focal plane of the monochromator. This leads to a systematic error in the measured values of r_k because of the curvature of the focal plane. Spherical aberration in the lenses of the optical system causes the central rays to have a greater focal distance than the outer rays. This results in a systematic decrease of $e_k(\lambda)$ with increasing k. When a simple monochromator is used, the entrance slit is projected on the exit slit as a curved line. Since detection usually occurs at the exit slit, the mutual proportions of the fringes are affected by this curvature. In the method presented here, the objections mentioned in the preceding section are largely eliminated whereas the analysis of the interference pattern is strongly simplified.

2.4.2 New method.

Formula (1) can be written as

$$D_k(\lambda) = 2\beta(\lambda)\Delta\lambda_s\cdot\{k-1+e(\lambda)\}^{\frac{1}{2}} \qquad (2.2)$$

where:

$$\beta(\lambda) = \frac{1}{f}\left(\frac{t}{\lambda}\right)^{\frac{1}{2}} ,$$

and

$\Delta\lambda_s$ is the free spectral range expressed by

$$\Delta\lambda_s = \lambda^2/2t.$$

In order to determine $e(\lambda)$, now the quantity $B_k(\lambda)$ is measured where

$$B_k(\lambda) = r_{k+1}(\lambda) - r_k(\lambda).$$

Using the well-known formula for r_k,

$$r_k = f\left(\frac{\lambda}{t}(k-1+e(\lambda))\right)^{\frac{1}{2}}$$

$e(\lambda)$ can be written as

$$e(\lambda) = -k + \left\{\frac{1+\beta^2(\lambda)B_k^2(\lambda)}{2B_k(\lambda)\,\beta(\lambda)}\right\}^2$$

Substitution of this expression for $e(\lambda)$ in (2) yields

$$D_k(\lambda) = \Delta\lambda_s \frac{1-\beta^2(\lambda)B_k^2(\lambda)}{B_k(\lambda)} \qquad (2.3)$$

Now the light source to be measured is replaced by a spectral light source e.g. laser or spectral lamp. Using a photographic camera instead of the monochromator a negative is made of the interference pattern caused by a spectral line with wavelength λ_o close to λ. (Fig.2.4) . If the camera lens is of good quality, the disturbing influence mentioned can be neglected. From the negative, with the aid of an ordinary magnifier, it is possible to determine $e(\lambda_o)$ in the usual way. Once the negative has been made, the mirror S in Fig.(2.4) is turned away and in full analogy with $B_k(\lambda)$ the quantity $B_k(\lambda_o)$ is determined. Then $\beta(\lambda_o)$ can be calculated from:

$$\beta(\lambda_o) = \frac{\{(k'+e(\lambda_o)\}^{\frac{1}{2}} - (k'-1+e(\lambda_o)\}^{\frac{1}{2}}\}}{B_{k'}(\lambda_o)} \qquad (2.4)$$

In relation (4), $\beta(\lambda_o)$ is expressed in terms of the easily measurable quantities $e(\lambda_o)$ and $B_{k'}(\lambda_o)$. Once the quantity $\beta(\lambda_o)$ has been determined, $\beta(\lambda)$ can be calculated

$$\beta(\lambda) = \{ \frac{\lambda_o}{\lambda} \}^{\frac{1}{2}} \beta(\lambda_o)$$

Now $\beta(\lambda)$ and $B_k(\lambda)$ are known, so that $D_k(\lambda)$ can be calculated. Usually the light intensity in the inner fringes is measured because in these fringes the dispersion is optimal. Suppose for that reason, that we are only interested in the first and second fringe. As a consequency of this only $B_1(\lambda)$ have to be measured. Once $B_1(\lambda)$ and $\beta(\lambda)$ are determined, we may write for the dispersion in the first and second fringe

$$D_1(\lambda) = \Delta\lambda_s \frac{1-\beta^2(\lambda)\ B_1^2(\lambda)}{B_1(\lambda)} \qquad (2.5)$$

$$D_2(\lambda) = \Delta\lambda_s \frac{1+\beta^2(\lambda)\ B_1^2(\lambda)}{B_1(\lambda)} \qquad (2.6)$$

The method described, proved to be very suitable for plasma spectroscopic purposes. Although the transmitted luminous flux is smaller than in methods using an on-axis pinhole, the luminous flux available is largely sufficient. By using a Fabry-Perot interferometer with a plate separation varying from 3 to 15 mm we determined halfwidths in the range from 0.03 to 0.4 cm^{-1}, with a relative inaccuracy of about 1 per cent.

2.4.3 Distortion of the measured line profile.

When the circular interference pattern is scanned with a rectangular slit, the measured line shape is a distorted image of the real shape. The same situation occurs when a negative is made of the interference

pattern and the line shape is determined with the aid of a densito - meter. In reference (16) the distortion of the line shape is calculated for the case that the original line profile is a Lorentzian one, as well as for a Gaussian original profile.

2.5 Analysis of the experimental spectrum line profiles.

With the aid of the order scanning Fabry-Perot spectrometer described in the preceding section, on a recorder a representation of the line profile was obtained which is related very closely to the real line shape. In general an observed line profile is the result of several line broadening mechanisms acting simultaneously. As a consequence the diagram obtained from the recorder is a very complex composition of the various broadening mechanisms. Thus from the point of view of one particular cause of spectrum line broadening the experimental line profile appears to be distorted by other broadening mechanisms and should be corrected for these disturbing influences before a comparison with theoretical results is undertaken. The following is a discussion of how an observed spectrum line profile may be corrected for the various disturbing effects.

2.5.1 Unfolding of the observed line profile.

Frequently situations will be encountered where Doppler as well as resonance broadening are significant. Then the observed line profile must be corrected for the non relevant broadening mechanism or, in short, it must be unfolded. This is possible since usually the two line broadening causes are independent so that they may be considered as superimposed. Let us suppose that $I_D(\omega)$ describes the profile caused by the Doppler effect and $I_R(\omega)$ is the profile due to resonance broadening; then the measured line shape $I(\omega)$ is given by the "folding" or convolution integral

$$I(\omega') = \int_{-\infty}^{+\infty} I_D(\omega)\ I_R(\omega'-\omega)d\omega$$

In its general form the application of this unfolding process to the correction of line profiles and halfwidths is very laborious. Fortunately one may describe without any significant loss in precision the Doppler as well as the resonance broadening by simple analytical functions namely the well-known Gaussian and Lorentzian distributions. The folding of these two shapes leads to the so-called Voigt-profiles, which are available in tabular as well as in graphical form for a wide range of conditions.[7][8][9][10].

In the foregoing the total broadening caused by two independent broadening mechanisms was discussed. In the actual experiments, however, natural and instrumental broadening also had a noticeable influence on the shape of the line profile. Now it may be shown[11][12], that the instrumental line profile of a Fabry-Perot interferometer as well as the natural broadening may be described by Lorentz functions. So in principle the observed line profile should be described by a convolution integral of four independent broadening mechanisms. Fortunately, it may be shown[6] that the convolution integral of two Lorentz functions yields a new Lorentz function the halfwidth of which equals the sum of the two initial halfwidths. Starting from this mathematical fact, the observed spectrum line profile may be represented by a folding integral of only one Lorentz function, which represents the total broadening effect of resonance, natural and instrumental broadening, and a Gauss function representing the Doppler broadening.

The calculation of the Doppler halfwidths was based on the average gas temperature of the emitting part of the discharge plasma. These average gas temperatures were derived graphically from the gas temperature distributions obtained from the thermocouple measurements. The instrumental line profile was calibrated by measuring the line profile of a narrow spectrum line of which the halfwidth is known. For reasons of simplicity we based the calibration of the interferometer on very accurate measurements of the shape and the halfwidth of the λ = 5852 Å line in neon[12]. Incidentally this procedure was checked by calibrating the interferometer with the aid of the λ = 6439 Å line emitted from a low pressure cadmium spectral lamp[13]. Within the limits of error both calibation methods gave the same result.

2.5.2 Determination of the resonance halfwidth.

Since there were no grounds to expect significant deviations from the theoretical line profiles we followed the usual procedure in line broadening spectroscopy according to which only the halfwidth of the line profile is determined. Incidentally, however, some line profiles were analysed accurately in order to find out if any deviation from the theoretical line profiles could be observed.

From the foregoing it follows that the resonance halfwidth may be calculated as follows. The observed halfwidth was corrected for Doppler broadening with the aid of correction tables given by Davies and Vaughan[7]. Then the remaining Lorentz halfwidth was corrected for natural and instrumental broadening. The corresponding gas density was obtained by dividing the remaining resonance halfwidth by the appropriate broadening constant. The broadening constant of the λ = 5852 Å line ($C = 6.37.10^{-20}$ $cm^{-1}/at.cm^3$) was taken from Kuhn[12].

2.6 Miscellaneous experimental methods.

Apart from the experimental methods discussed in the foregoing, incidentally some more common plasma diagnostic methods have been applied. Since the principles and the experimental set up of these methods can be found in detail in various handbooks[14], only some characteristic details will be reviewed briefly below.

2.6.1 Microwave measurements.

For a minor part of the measurements presented in the following chapters, estimations of the electron densities were made from phase shift measurements with a 4 mm microwave interferometer. Since the spatial resolution of this method is of the same order of magnitude as the effective diameter of the active plasma column, the results obtained in this way should be considered as a rough estimation of the average electron density. The possible systematic error in these measurements was about 100 per cent.

2.6.2 Spectrum line intensity measurements.

In some of the constriction models discussed in chapter 1 the assumption was made that the plasma is in L.T.E.. Since this basic assumption is of utmost importance for the concept of the high pressure column as such, the validity of this assumption was checked experimentally with the aid of line intensity measurements. These measurements were performed mainly on discharges of the type (b).

With the aid of a 1.0 m. Jarrel-Ash grating double monochromator the relative intensities of 8 visible neon lines (2p-1s transitions) were determined. In order to compare the various intensities the transmission function of the optical equipment was determined with the aid of a calibrated tungsten ribbon lamp.

2.6.3 Optical absorption measurements.

The model of the high pressure positive column presented in chapter 5 predicts a very low concentration of metastable atoms in the axis of the discharge tube. This theoretical prediction was verified experimentally by measuring the absorption of various visible neon lines. For that purpose a special discharge tube was developed in which the cathode as well as the anode were cone-shaped. Both electrodes were provided with a narrow slit in the axial direction. The dimensions of these slits were 1.0 x 8 mm. Moreover, the ends of the discharge tube were provided with optically flat pyrex windows. This construction enabled us to do end-on measurements. For the emitter tube also a high pressure neon discharge was used. With the aid of an appropriate optical system from the total radiance of this discharge a narrow parallel beam of light was isolated. The effective diameter of this beam was 0.5 mm. The beam was send through the absorbing tube in a direction parallel to the tube axis. The absorption of this beam in the discharge was determined as a function of the radius r. In this way a good estimation of the radial distribution of metastable atoms could be obtained.

2.6.4 Radiant flux measurements.

To calculate the shape of a line profile emitted from an inhomogeneous plasma the knowledge of the radial distribution of radiant flux per unit volume of that spectrum line is needed[15]. This distribution was obtained from lateral line intensity measurements. The spectroscopic equipment applied in these measurements was nearly identical to that used for the relative line intensity measurements. The only difference was that now the discharge tube could be moved to and fro in a direction perpendicular to the tube axis as well as to the viewing direction of the optical system. With the aid of the optical system the radiation accepted by the monochromator was reduced to that emitted from a small volume having the shape of a diabolo. The effective width of this diabolo shaped plasma volume was about 0.3 mm. By moving the discharge tube with respect to the fixed optical system a lateral spectrum line intensity distribution was obtained. These experimental distribution functions were fitted by a digital computer to a sum of two Gauss functions. These Gauss functions had a different height and a fixed ratio of their halfwidths. With the aid of the computer these relative intensities and halfwidths were determined. Then the resulting sum-function was subjected to an analytical Abel-transformation. In this way the radial distribution of spectral radiant flux could be calculated.

References.

1) Jacquinot, P., Dufour, C.H. J.Rech.C.N.R.S. 6, 91 (1948).
2) Kuhn, H.G, Lewis, F.L, Stacey, D.N and Vaughan, J.M., Rev.Sci. Instrum. 39, 86 (1968).
3) Cooper, J. Greigh, J. R., Proc. VIth Conf.Ion.Phen.in Gases (Paris) 1 (1963).
4) Bradley, D.J, Proc.Conf.Opt.Instr.Techn.(London)31 (1961).
5) Auth, D.C., Phys.Letters. 27 (A) 536 (1968).
6) Mewe,R.,de Vries, R.F., Jour.Nucl.En.(part C) 6, 591 (1964).
7) Davies, J.T., Vaughan, J.M., Astrophys. Journ. 137 1302 (1963).

8) Armstrong, B.H., J. Quant. Spectr. Radiat. Transfer 7, 61 (1967).
9) Posener, D.W., Austr.Journ.Phys. 12, 184 (1959).
10) De Vries R.F., Rijnhuizen report (65-26) (Euratom-Fom) (1965).
11) Traving, G., Über die Theorie der Druckverbreiterung von Spektrallinien. Braun Verlag Karlsruhe (1960).
12) Kuhn, H.G., Proc. Roy. Soc. (A) 299 423 (1967).
13) Engelhard, N.P.L., Symposium on interferometry. 21 (1959).
14) Huddlestone, R.H., Leonard, S.L., Plasma diagnostic techniques. Academic Press (New York) (1965).
15) Chapter 3 of this thesis.
16) Mouwen, C.A.M., Journ.Sci.Instr. 3, 27 (1970).

CHAPTER III SPECTRUM LINE BROADENING

3.1.1 General theory of resonance broadening.

In most of the theoretical and experimental work done in the field of spectrum line broadening the assumption is made that the emitting plasma is homogeneous.[1][2][3][4] When in such a plasma the line profile of the spectrum line, emitted by a transition from energy level E_n to E_m, is determined by resonance broadening, this line profile may in a very good approximation be represented by a Lorentz function the halfwidth: γ_{nm} of which is given by

$$\gamma_{nm} = C_{nm}\, n_a \tag{3.1}$$

where:

C_{nm} = the broadening constant of the spectrum line with central frequency ω_{nm}.[5][6]

n_a = density of neutral gas atoms.

This broadening constant can be calculated from the relation

$$C_{nm} = k\,\frac{f_{mo} q^2}{m_e\, \omega_{mo}} \tag{3.2}$$

where:

f_{mo} = the oscillator strength of the corresponding resonance line.

k = a numerical factor of the order 1.

ω_{mo} = the central frequency of the corresponding resonance line.

m_e = electronic mass.

q = electronic charge.

In practical spectroscopy, apart from a few exceptions, it is assumed that the theories available now give a sufficiently correct description

of the line broadening to use this mechanism as a plasma diagnostic tool. Especially in this category of experiments, sometimes in direct contradiction with the experimental plasma conditions, the assumption is generally maintained that the emitting plasma is homogeneous.[7][8][9][10]

By this assumption, however, a large systematic error may be introduced. In the present work, the influence of gradients in both the gas temperature and the spatial distribution of emitting atoms on the shape and the halfwidth of a resonance broadened spectrum line profile is calculated for various cases of practical interest. Moreover, a new method is presented to determine the density and the temperature of neutral atoms in the axis of a gas discharge by measuring the halfwidth of a resonance broadened spectrum line emitted by that discharge.

We consider now an optically thin plasma which is supposed to be inhomogeneous but radially symmetric, whereas axial variations of the various plasma parameters are neglected. The density of neutral atoms as a function of the distance r to the tube axis is given by $n_a(r)$, whereas the energy emitted in a spectrum line with central frequency ω_{nm} per second per unit volume is denoted by $P_{nm}(r)$. The shape of a resonance broadened spectrum line, emitted at the position r, may be represented in a normalised form by

$$I(\omega.r) = \frac{2}{\pi C_{nm} n_a(r)} \quad \frac{1}{1 + \frac{4(\omega-\omega_{nm})^2}{C_{nm}^2 n_a^2(r)}} \tag{3.3}$$

With the aid of an optical system as schematically shown in Fig. 3.1, for a certain spectrum line, which in reduced form is given by $I(\omega.r)$, the radiance in a small frequency band $d\omega$, integrated over the line PQ, is measured as a function of u.
The result is called $dL_{nm}(\omega.u)$ and is related to $P_{nm}(r)$ as:

$$dL_{nm}(\omega.u) = \frac{1}{4\pi} \int_{-d(u)}^{+d(u)} \frac{P_{nm}(r)\ I(\omega.r)\ r\ dr\ d\omega}{\sqrt{r^2 - u^2}} \tag{3.4}$$

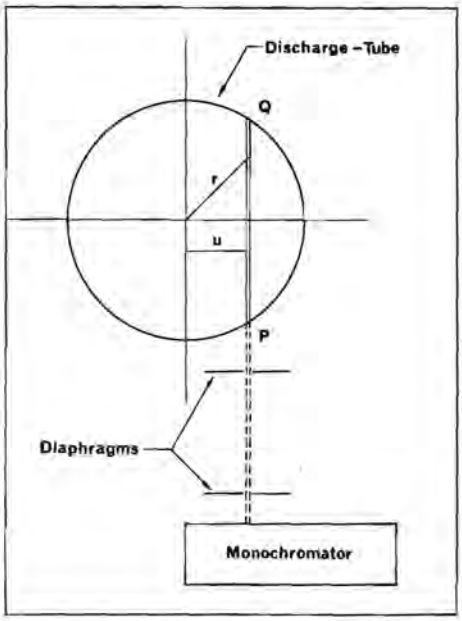

Fig.3.1 Simplified diagram of the optical arrangement.

For the special case that u = 0, the observed spectrum line profile $I_{nm}(\omega.0)$, defined by

$$I_{nm}(\omega.0) = \frac{dL_{nm}(\omega.0)}{d\omega} \tag{3.5}$$

is given by

$$I_{nm}(\omega.0) = \frac{1}{4\pi} \int_{-R}^{+R} P_{nm}(r)\ I(\omega.r)dr \tag{3.6}$$

or in normalised form

$$I^{n}_{nm}(\omega.0) = \frac{\int_{-R}^{+R} P_{nm}(r)\ I(\omega.r)dr}{\int_{-R}^{+R} P_{nm}(r)dr} \qquad (3.7)$$

where:

R = discharge radius.

Both functions $I(\omega.r)$ and $I^{n}_{nm}(\omega.0)$ obey the normalisation condition

$$\int_{-\infty}^{+\infty} I(\omega)d\omega = 1$$

Expression (3.7), which in a more general form has also been studied by Bartels[11], shows that $I^{n}_{nm}(\omega.0)$ is determined uniquely by the functions $P_{nm}(r)$ and $I(\omega.r)$. Since the latter function only depends on $n_a(r)$, the normalised spectrum line profile may be calculated if only $n_a(r)$ and $P_{nm}(r)$ are known.

3.1.2 Shape of $n_a(r)$ and $P_{nm}(r)$ for some special cases.

In an arbitrary discharge, $n_a(r)$ and $P_{nm}(r)$ are functions of a very complex nature. This implicates that in general it is impossible to calculate $I^{n}_{nm}(\omega.0)$ analytically. In a previous paper[12], however, it was reported that for the special case of a positive column in neon, under certain conditions, $P_{nm}(r)$ and $n_a(r)$ may be approximated very well by simple analytical functions. Three examples will be given below.

Low pressure, low current, positive column.

We consider a positive column in a low pressure ($p < 10$ torr) discharge, with a discharge current below 10 mA. Under these experimental conditions, both $P_{nm}(r)$ and $n_a(r)$ are very nearly constant, so that the assumption of a homogeneous plasma holds.

Low pressure, moderate current, positive column.

When in a low pressure discharge the current is increased to a few hundred mA, in a first approximation $P_{nm}(r)$ remains constant over the cross section of the discharge, whereas the gas temperature in the discharge axis raises with respect to the wall-temperature. In this range of discharge conditions, however, the gradient in the gas temperature is only small, so that in a first approximation the gas density distribution may be represented by a parabolic function.

$$n_a(r) = n_a(0) + \{n_a(R) - n_a(0)\} \frac{r^2}{R^2} \tag{3.8}$$

High pressure constricted positive column.

When in a positive column the gas pressure is increased above a few hundred torr, a constriction of the positive column takes place[13]; the emission of light in the column is confined to a small channel around the tube axis. The space between this radiating cylinder and the tube wall remains completely dark. These phenomena may illustrate that in this case the following functions appeared to be reasonable approximations.

$$n_a(r) = n_a(0) + \{n_a(R) - n_a(0)\} \frac{r^2}{R^2} \tag{3.9}$$

$$P_{nm}(r) = \begin{cases} P_{nm}(0), & \text{for } 0 \leq r \leq a \\ 0, & \text{for } a < r < R \end{cases} \tag{3.10}$$

With the aid of these simple mathematical functions it was possible to calculate $I^n_{nm}(\omega.0)$ and γ_{nm} analytically[12]. Although the expressions for $I^n_{nm}(\omega.0)$ and γ_{nm}, obtained in this way, are only first order approximations, the numerical results calculated from them are in reasonable agreement with the experimental results. The agreement is illustrated in Fig.3.2.

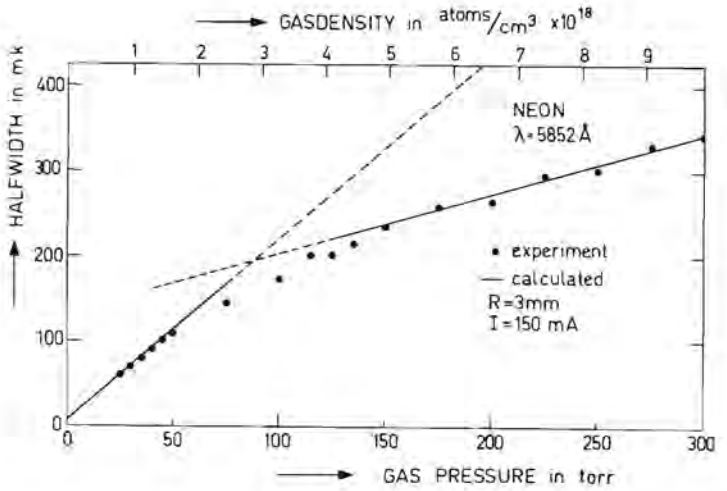

Fig.3.2 Some experimental halfwidths as a function of the filling pressure at room temperature. On the upper scale the corresponding gas densities at room temperature are plotted.

In this figure, the halfwidth of the resonance broadened λ = 5852 Å neon line, emitted from a positive column and measured with a Fabry-Perot interferometer, is compared with the halfwidth calculated from eqs.(3.3) through (3.10).The values for $n_a(0)$ and $n_a(R)$ used in these calculations were derived from gas temperature measurements with the aid of thermocouples[14], whereas for the value of a in (3.10) the halfwidth of the experimental $P_{nm}(r)$ curve was used. The value for C_{5852} was taken from Kuhn[15]. For pressures up to 80 torr (3.9) was used; (3.10) for the higher pressures.

Although Fig. 3.2 suggests a reasonable agreement between theory and experiment, it must be kept in mind that the choice of a, which seems to be a reasonable approximation, in fact is quite arbitrary. Moreover, in the pressure range from 50 to 150 torr none of the simple models

discussed above yields a satisfactory agreement with the experimental results. Considerations of this kind, clearly show the need for more adequate approximation functions for $P_{nm}(r)$ and $n_a(r)$ than those introduced before. In general, the precise shape of the distribution functions $P_{nm}(r)$ and $n_a(r)$ cannot be calculated theoretically without an exact knowledge of the basic discharge processes. Fortunately, it follows both from theoretical and experimental investigations[13][14], that for a great number of cylindrically symmetric discharges, in a large region of discharge conditions, the experimental functions $P_{nm}(r)$ and $n_a(r)$ may be fitted very well by a two parameter representation of a rather simple mathematical form. In the next paragraph the specific shape of both representations will be discussed for the special case of a high pressure constricted positive column. It must be kept in mind, however, that the representations introduced, hold in a much wider region than that discussed here.

3.1.3 General representation of $n_a(r)$ and $P_{nm}(r)$.

Starting from a new model for the high pressure positive column, as described in an earlier paper[18], it is possible to express the functions $P_{nm}(r)$ and $n_a(r)$ in a number of directly measurable macroscopic parameters. Both from thermocouple measurements[14] and theoretical calculations[13] it followed that in the positive column, for a great variety of discharge conditions, the gas temperature distribution may be represented by the following empirical relation:

$$\frac{T_a(r)}{T_a(o)} = \theta + \frac{(1 - \theta)}{1 + \frac{r^2}{\beta^2}} \qquad (3.11)$$

Under the assumption that the ideal gas law holds the gas density distribution may then be written as:

$$\frac{n_a(r)}{n_a(0)} = \frac{(1 + \frac{r^2}{\beta^2})}{(1 + \theta \frac{r^2}{\beta^2})} \qquad (3.12)$$

where θ and β are parameters directly following from the thermocouple measurements mentioned. The relative systematic error introduced by assuming an empirical relation according to (3.12) for the gas density distribution is discussed in an earlier paper and amounts only a few percent. From lateral spectrum line intensity measurements and recent calculations[13][14] it followed that for nearly the same variety of discharge conditions for which (3.12) holds, the function $P_{nm}(r)$ can be represented with a relative error of less than a few percent by an empirical relation of the form:

$$P_{nm}(r) = P_{nm}(0) \exp\left[-\frac{r^2}{\chi^2_{nm}}\right] \qquad (3.13)$$

where χ_{nm} is a parameter directly depending on the discharge conditions and also following from the experiment. Although we succeeded in representing $P_{nm}(r)$ and $n_a(r)$ by rather simple mathematical functions, unfortunately this simplification was not radical enough to calculate expression (3.6) with the aid of (3.12) and (3.13) analytically. Since a further simplification of the representations for $P_{nm}(r)$ and $n_a(r)$ is not possible without the introduction of a considerable systematic error, we shall calculate an approximate expression for $I_{nm}(\omega.0)$ which yields, apart from the relative systematic errors introduced by the functions (3.12) and (3.13) , a relative inaccuracy of less than one per mil.

3.1.4 Normalised spectrum line profile.

In most inhomogeneous discharges of cylindrical symmetry, of which the constricted column is a striking example, the greater part of the light is emitted in the direct neighbourhood of the discharge axis. Consequently

the shape of the spectrum line in question is largely determined by the behaviour of $n_a(r)$ for small values of $\frac{r}{R}$. Realising this, we expand the function $I(\omega.r)$, given in (3.3), in a Taylor series near $r = 0$. After substitution of this series expansion in (3.6) we obtain the following expression for $I_{nm}(\omega.0)$.

$$I_{nm}(\omega.0) = \frac{1}{2\pi} \sum_{j=0}^{\infty} \frac{1}{j!} \left[\frac{\partial^j I(\omega.r)}{\partial r^j} \right]_{r=0} \int_0^R P_{nm}(r) r^j \, dr. \qquad (3.14)$$

This complex relation can be simplified greatly by remarking that $I(\omega.r)$ is an even function of r, so that all odd derivatives drop out. Moreover, a simple calculation shows that the influence of all terms for which $j \geq 6$, is far less than one per mil. These terms neglecting reduces expression (3.14) to:

$$I_{nm}(\omega.0) = \frac{1}{2\pi} \left[I(\omega.0) \int_0^R P_{nm}(r) dr + \frac{1}{2} \left[\frac{\partial^2 I}{\partial r^2} (\omega.r) \right]_{r=0} \times \right.$$

$$\left. \times \int_0^R P_{nm}(r) \, r^2 dr + \frac{1}{24} \left[\frac{\partial^4 I(\omega.r)}{\partial r^4} \right]_{r=0} \int_0^R P_{nm}(r) \, r^4 dr \right] \qquad (3.15)$$

Because the gas density distribution is an even function of r, the derivatives in expression (3.15) can be written for $r = 0$ as:

$$\left[\frac{\partial^2 I(\omega.r)}{\partial r^2} \right]_{r=0} = \left[\frac{\partial^2 n_a(r)}{\partial^2 r} K(\omega.r) \right]_{r=0}$$

and

$$\left[\frac{\partial^4 I(\omega.r)}{\partial r^4} \right]_{r=0} = \left[\frac{\partial^4 n_a(r)}{\partial r^4} K(\omega.r) + 3 \frac{\partial^2 n_a(r)}{\partial r^2} \frac{\partial^2 K(\omega.r)}{\partial r^2} \right]_{r=0}$$

where

$$\left[K(\omega.r) \right]_{r=0} = \frac{2 C_{nm}}{\pi} \left[\frac{4(\omega-\omega_{nm})^2 - C_{nm}^2 n_a^2(r)}{(4(\omega-\omega_{nm})^2 + C_{nm}^2 n_a^2(r))^2} \right]_{r=0}$$

Strictly speaking, the function $P_{nm}(r)$ defined by (3.13) is not a realistic one since it does not obey the boundary condition:

$$P_{nm}(R) = 0 \ .$$

Under the actual experimental conditions, however, $P_{nm}(R)/P_{nm}(0)$ is smaller than one per mil, the limit of error of this calculation. Therefore the upper integration limit in (3.15) may be replaced by ∞. Then the integration in (3.15) may be carried out and inserting (3.12) and (3.13) we obtain for $I_{nm}(\omega.0)$ after some laborious but elementary calculus, the expression

$$I_{nm}(\omega.0) = \frac{P_{nm}(0)}{4\sqrt{\pi}} \chi_{nm} \left[I(\omega.0) + \frac{1}{2}(1-\theta) \frac{\chi_{nm}^2}{\beta^2} n_a(0) K(\omega.0) + \ldots \right.$$

$$\left. \ldots R(\theta^2, \frac{\chi_{nm}^4}{\beta^4}) + \ldots\ldots \right] \qquad (3.16)$$

where:

$R(\theta^2, \frac{\chi_{nm}^4}{\beta^4})$ is a rest term of the order $(\theta^2 \frac{\chi_{nm}^4}{\beta^4})$.

For the actual experimental conditions, the various dimensionless parameters have approximately the following values: $\frac{\chi}{\beta} \approx \frac{1}{3}$ and $\theta \approx \frac{1}{2}$ and substitution of these values in the rest term showed that if a relative inaccuracy less than 1% is wanted, this term may be neglected. Then the line profile $I^0_{nm}(\omega.0)$, reduced to a top value one may be represented by:

$$I^0_{nm}(\omega.0) = \left[\frac{1+\mu_{nm}}{1-\mu_{nm}} \right] I_{nm}(\omega.) - \left[\frac{2\mu_{nm}}{1-\mu_{nm}} \right] I^2_{nm}(\omega) \qquad (3.17)$$

where:

$$I_{nm}(\omega) = \frac{1}{1 + \frac{4(\omega-\omega_{nm})^2}{\gamma^2_{nm}(0)}}$$

$$\mu_{nm} = \frac{1}{2}(1 - \theta) \frac{\chi_{nm}^2}{\beta^2}$$

$$\gamma_{nm}(0) = C_{nm}\, n_a(0).$$

Since $I_{nm}(\omega)$ only depends on $n_a(0)$, it follows from expression (3.17) that the profile of a spectrum line emitted from an inhomogeneous plasma of cylindrical symmetry is uniquely determined by the quantities $n_a(0)$ and μ_{nm}. The importance of the dimensionless parameter μ_{nm} in these calculations may be illustrated by a calculation of the halfwidth of the function $I_{nm}(\omega.0)$. This halfwidth γ_{nm} is defined by the relation

$$\gamma_{nm} = 2 \mid \omega_{\frac{1}{2}} - \omega_{nm} \mid$$

where $\omega_{\frac{1}{2}}$ is a solution of the equation:

$$I^0_{nm}(\omega.0) = \frac{1}{2} I^0_{nm}(\omega_{nm}.0)$$

If $I^0_{nm}(\omega.0)$ is given by (3.17), γ_{nm} can be calculated directly. The result is

$$\gamma_{nm} = \gamma_{nm}(0)\ (1 + \mu_{nm} + \frac{1}{2}\mu^2_{nm} + \ldots) \qquad (3.18)$$

When in a first order approximation this expression is rewritten in the form

$$\mu_{nm} \simeq \frac{\gamma_{nm} - \gamma_{nm}(0)}{\gamma_{nm}(0)},$$

the significance of μ_{nm} is obvious. It expresses the relative increase of the observed halfwidth, due to plasma inhomogeneities, with respect to the halfwidth $\gamma_{nm}(0)$ of a spectrum line emitted at the discharge axis. Although the absolute value of γ_{nm} depends both on $n_a(0)$ and μ_{nm}, it follows from (3.17) that the shape of the spectrum line profile on a scale $\frac{\Delta\omega}{\gamma}$ only depends on the value of μ_{nm}. The influence of a variation in μ_{nm} on the shape of a spectrum line profile is illustrated in Fig.3.3 where the line profile $I^0_{nm}(\omega.0)$ is plotted for three values of μ_{nm} resp: 0, 0.1 and 0.2. Since a variation in μ_{nm} adds a correction to the line profile which is quadratic in ω, the line profile remains symmetric and Lorentz-like, as can be seen from the figure.

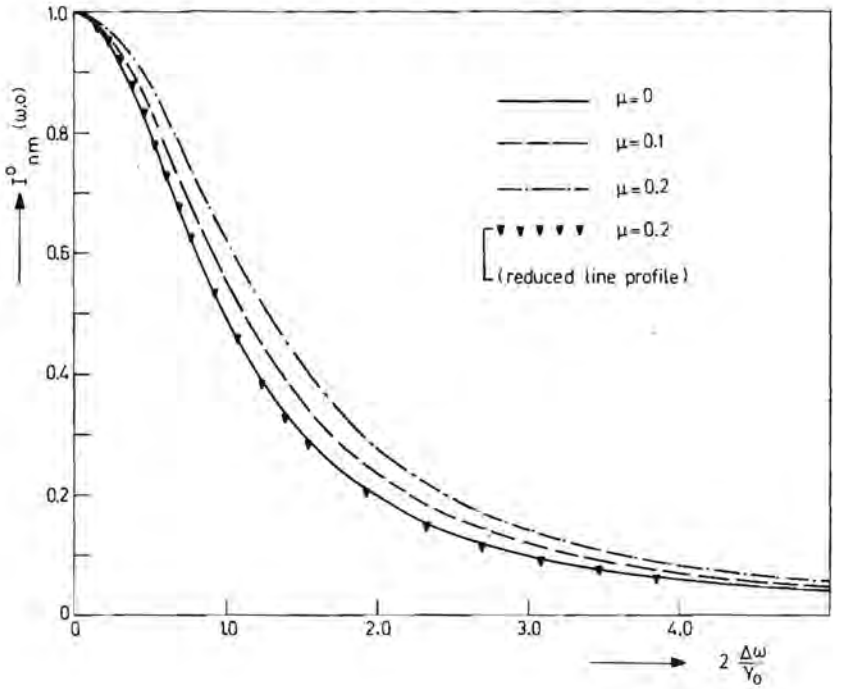

Fig. 3.3 Some calculated spectrum line profiles for various values of the parameter μ.

This is illustrated more in detail in the same figure, where for $\mu_{nm} = 0.2$, (being the maximum value of μ_{nm} considered in our experiments), the line profile is analysed and in reduced form compared with a pure Lorentz-function. It is surprising to see that the deviations of the line profile, in its reduced form, from a Lorentz-function are smaller than the line width of the drawing. This is in agreement, however, with computer calculations in which $I_{nm}(\omega.0)$ was calculated numerically, using the original experimental functions $P_{nm}(r)$ and $n_a(r)$. From these calculations it followed too that for the whole region of plasma parameters investigated, the line profile could be approximated with a relative error of less than one per cent by a pure Lorentz-function. This conclusion, which is of utmost practical importance, may be

formulated as follows:

If in an inhomogeneous plasma of cylindrical symmetry the spectral inhomogeneity, characterised by the parameter μ_{nm}, is small then the observed spectrum line profile may be represented to a very good approximation by a pure Lorentz function.

From the foregoing it is clear that the quantity μ_{nm}, introduced in the preceeding section as a dimensionless parameter, plays an important part in the description of the line broadening in inhomogeneous plasmas. For that reason it seems usefull to define μ_{nm} as a new spectroscopic variable called: "spectral inhomogeneity". The definition of μ_{nm} introduced here for the special case of a resonance broadened spectrum line, emitted from a cylindrically symmetric plasma,can be adapted easily to other line broadening mechanisms or other symmetries. These extensions or modifications, however, will not affect the fundamental meaning of this quantity. The great advantage of this concept is the possibility to characterise the influence of plasma inhomogeneities on the spectrum line profile with only one representative parameter. That, apart from this typical line broadening interpretation, there exists a clear plasma dynamical sense of μ_{nm} is illustrated by the fact that, apart from a numerical factor of the order one, μ_{nm} is equal to the parameter K, which will be defined in chapter 5[13] as the Joule dissipation in Watts per unit volume. As a consequence a large Joule dissipation implicated a large μ_{nm} value and of course a strongly inhomogeneous plasma, whereas a small Joule dissipation will result in a nearly homogeneous plasma.

3.1.5 Influence of other line broadening mechanisms.

Apart from the resonance broadening discussed in the preceding sections, there are a number of line broadening mechanisms which may influence the shape of the spectrum line profile essentially.

3.1.5.1 Natural line broadening.

The profile of a spectrum line which is exclusively determined by natural broadening may be described by a pure Lorentz-function. The halfwidth of this function, called the natural or radiation width, is only a few milli-Kaiser so in the vast majority of practical line broadening experiments its influence is of only minor importance. Nevertheless, in the actual experiments, reported in this thesis, the influence of the natural broadening both on the line shape and on the halfwidth was accounted for. Following Kuhn[15], 3,66 milli-Kaiser was taken for the radiation width of the λ = 5852 Å neon spectrum line.

3.1.5.2 Doppler broadening.

This broadening mechanism, which is essentially caused by the thermal motion of the emitting atoms, may be described by the following Gauss function[5]

$$I_{nm_D}(\omega) = \frac{1}{\sqrt{\pi}.\Delta\omega_D} \cdot \exp\left[- \frac{(\omega-\omega_{nm})^2}{\Delta\omega_D^2} \right] \qquad (3.19)$$

The halfwidth γ_{nm_D} of this function if given in frequency units by

$$\gamma_{nm_D} = 2\sqrt{\ln 2}.\Delta\omega_D = 7.16\ 10^{-7}\ \omega_{nm}.\sqrt{\frac{T_a}{M}} \qquad (3.20)$$

where:

M = atomic weight of the emitting atoms.

In our experiments the Doppler halfwidth amounted to only a few per cent of the observed halfwidth. As a consequence the radial dependence of the Doppler broadening was neglected. When calculating the resonance halfwidth, however, the observed halfwidths were corrected for this Doppler broadening. For T_a the average gas temperature of the emitting part of the discharge plasma was substituted. The details of this rather complicated procedure are discussed extensively in chapter 2 of this thesis.

3.1.5.3 Isotope effects.

Natural neon consists of three isotopes with the following relative abundances: Ne_{20}(90,8%); Ne_{21}(0,03%); Ne_{22}(8,9%). If the influence of the Ne_{21} component is neglected, the observed spectrum line profile will exhibit a hyperfine structure consisting of two peaks with approximately the same halfwidth and relative heights directly proportional to the relative isotope abundances. In general the presence of isotopes may lead to a noticeable distortion of the original spectrum line profile which in its turn may result in a considerable increase of the observed halfwidth as illustrated in Fig.3.4a. This relative increase

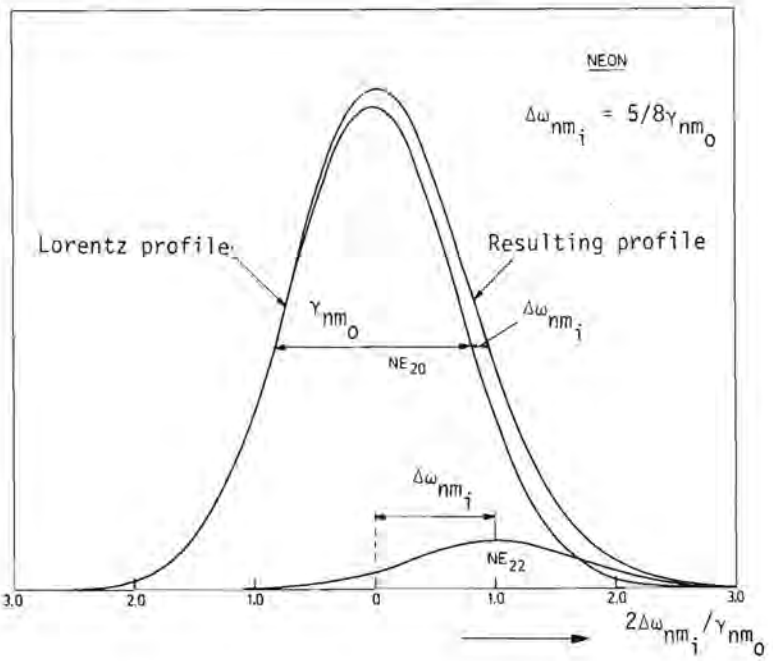

Fig. 3.4a Influence of the isotope Ne_{22} on the profile of a neon spectrum line (calculated)

of the observed halfwidth depends on the ratio of the original halfwidth γ_{nm_o} to the isotope splitting: $\Delta\omega_{nm_i}$. A first order calculation shows that the asymptotic behaviour of the relative increase of the observed halfwidth of a Lorentz-line profile, due to the presence of an isotope, may be characterised by the approximate expressions given in tabel I.

Table I. Asymptotic values for the increase of the halfwidth, due to an isotope having the same halfwidth γ_{nm_o} as the original line profile and a relative abundance k. The isotope splitting is $\Delta\omega_{nm_i}$.

$\frac{\Delta\omega_{nm_i}}{\gamma_{nm_o}}$	$\frac{\Delta\gamma}{\gamma_{nm_o}}$
$\frac{\Delta\omega_{nm_i}}{\gamma_{nm_o}} >> 1$	$= k \frac{\gamma^2_{nm_o}}{\Delta\omega^2_{nm_i}}$
$\frac{\Delta\omega_{nm_i}}{\gamma_{nm_o}} \approx 1$	$= \frac{3}{4} k$
$\frac{\Delta\omega_{nm_i}}{\gamma_{nm_o}} << 1$	$= 4k \frac{\Delta\omega^2_{nm_i}}{\gamma^2_{nm_o}}$

For the special case of Neon this effect is illustrated in Fig.3.4b, where the relative increase in the observed halfwidth of the λ = 5852 Å line is plotted versus the dimensionless parameter $[\frac{\Delta\omega_{nm_i}}{\gamma_{nm_o}}]$. From this

figure it can be seen that the relative increase of the halfwidth reaches a maximum value for $\Delta\omega_{nm_i} \approx \gamma_{nm_o}$, whereas both for large and for small values of this parameter is approaches zero.

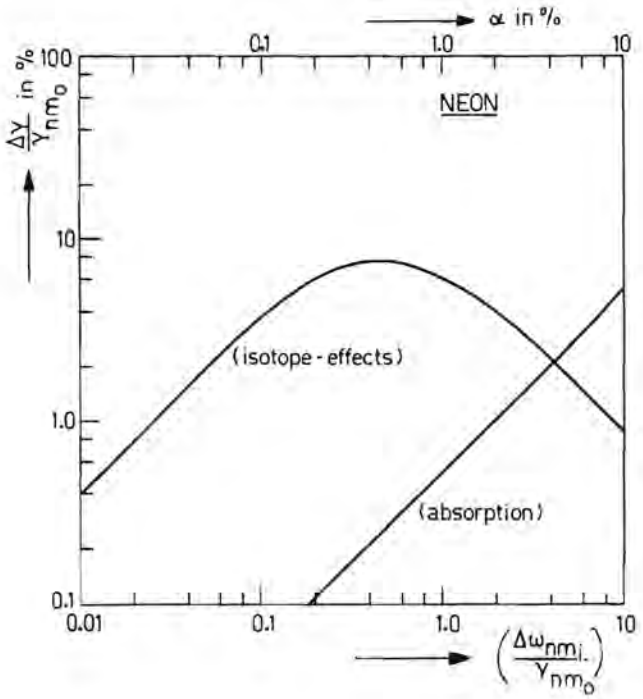

Fig. 3.4b Relative increase of the halfwidth due to isotope effects (lower scale) and self-absorption (upper scale).

3.1.5.4 Self-absorption

The mechanism of self-absorption too may lead to a considerable distortion of the original line profile. In the actual experiments, however, self-absorption was observed only at low gas pressures and high discharge currents and amounted in those cases to only a few per cent. It may easily be shown that the shape of a Lorentz spectrum line profile affected by a small amount of self-absorption may be written in a first order approximation as:

$$I_{nm}(\omega) = I'_{nm}(\omega) \left[1 + \frac{\alpha_{nm}}{2} I'_{nm}(\omega) + \ldots\right] \qquad (3.21)$$

where:

$I'_{nm}(\omega)$ = a pure Lorentz function

α_{nm} = absorption factor defined by:

$$\alpha_{nm} = 1 - \exp\left[-\int_{-d/2}^{+d/2} k_\omega(x)dx.\right]$$

$k_\omega(x)$ = spectral absorption coefficient

d = discharge diameter

A calculation of the halfwidth of this function results in the following approximate expression for the relative increase in the observed halfwidth due to self absorption.

$$\frac{\Delta\gamma}{\gamma_{nm_o}} = \frac{\gamma_{eff} - \gamma_{nm_o}}{\gamma_{nm_o}} \approx \frac{\alpha_{nm}}{2} + \ldots. \qquad (3.22)$$

This relative correction is presented in Fig. 3.4b.

3.1.5.5 Stark broadening.

Apart from the spectrum line broadening caused by neutral particles a line broadening mechanism exists which finds its origin in the interaction between the emitting atoms and the charged particles of the plasma e.g. electrons and ions. Since, in general, the line broadening caused by electrons is an order of magnitude larger than the broadening caused by ions, only the former is considered here. In the case of a spectrum line which exhibits quadratic Stark effect, Lindholm[16] showed that the halfwidth due to electron broadening is given by

$$\gamma_{nm} = \frac{4.5.10^{-3}}{C} C_{nm}.V_e^{1/3}.n_e$$

where:

C_{nm} = quadratic Stark effect constant.
n_e = electron density (per cc).
C = velocity of light.
V_e = mean velocity of the electrons.

With a quadractic Stark effect constant taken from Murakawa [17] et.al., the halfwidth of the λ = 5852 Å neon line may be expressed as:

$$\gamma_{nm} = 7{,}18.10^{-19}.T_e^{1/6}.n_e \qquad (cm^{-1})$$

where:

T_e = electron temperature in Kelvin.

Since in our experiments the electron density does not exceed 10^{14} el/cm^3 and the electron temperature is estimated to be less than 2 electron-Volt, the halfwidth due to the Stark-broadening by the electrons does not exceed a few milli-Kaiser. As a consequence the influence of Stark-broadening on the halfwidths of the observed spectrum line profiles may be neglected.

3.2 Experimental results.

With the aid of an order-scanning Fabry-Perot interferometer, the principle of which is discussed extensively in chapter 2, the halfwidth of the resonance broadened λ = 5852 Å neon spectrum line has been determined for a large region of plasma parameters. The relative systematic error in these experimental halfwidths was estimated to be about one per cent. In the actual experiments the filling pressure at room temperature and the discharge current varied from 1 to 400 torr and 10 to 500 mA, respectively. Tipped off discharge tubes were used with diameters varying from 4 to 40 mm. The typical constructions of the various discharge tubes used in the experiments are discussed in chapter 2, section 1. To give an impression of the influence of the various plasma parameters on the observed halfwidths, some experimental results are shown in Fig. 3.5, where the experimental halfwidth of the λ = 5852 Å line, corrected for Doppler, natural and

instrumental broadening, is plotted versus the filling pressure p_f with the discharge current and the tube diameter as parameters.

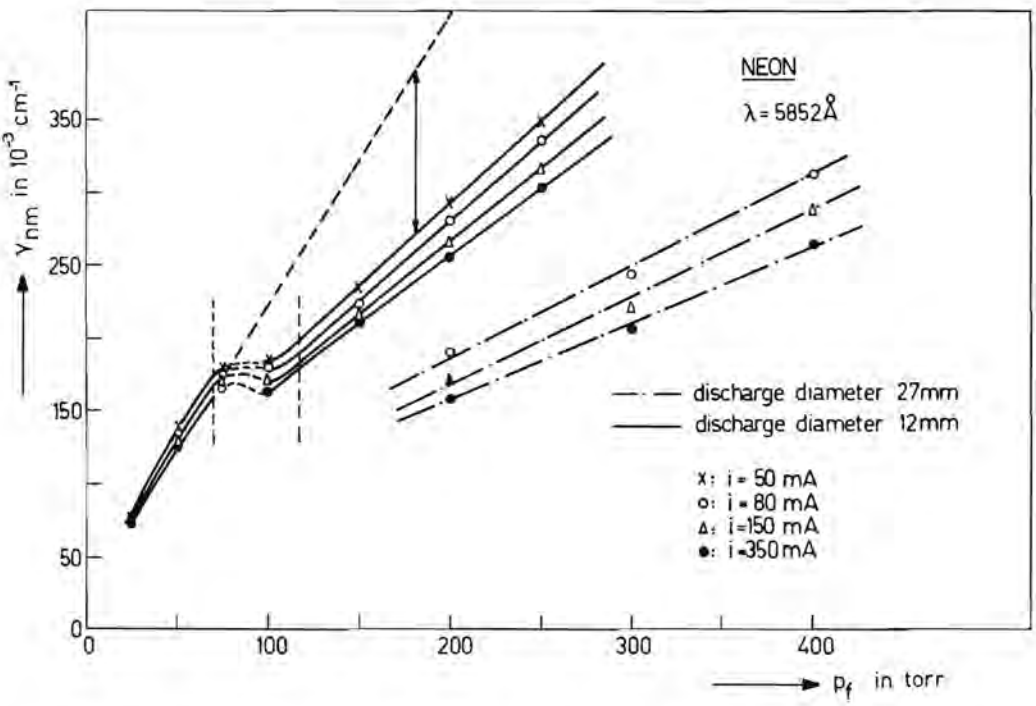

Fig. 3.5 The resonance halfwidth as a function of the filling pressure at room temperature with the discharge current and the tube diameter as parameters.

The dotted line represents the halfwidth of the same spectrum line now emitted from a homogeneous plasma with the same filling pressure. Moreover, these halfwidths together with the corresponding values of the various plasma parameters are given in table II. A first glance at figure 3.5 and at table II shows immediately the large systematic error which may be introduced by assuming that the emitting plasma is homogeneous. By further examination, attention is drawn to the fact that there are apparently three pressure ranges in each of which a specific broadening mechanism dominates over the other one's. For that reason the discussion of the experimental results will be divided into

Table II

Resonance halfwidth γ in a neon positive column for various gas filling pressures (p_f), discharge currents (i) and tube diameters (d).

filling-pressure p_f	discharge current i	resonance halfwidth γ	filling pressure p_f	discharge current i	resonance halfwidth γ
(mmHg)	(mA)	$10^{-3}cm^{-1}$	(mmHg)	(mA)	$10^{-3}cm^{-1}$
25	40	72	200	82	189
25	100	74	200	101	185
25	150	76	200	149	171
25	250	77	200	199	163
50	50	140	200	250	159
50	150	131	200	302	157
50	250	133	200	355	158
75	100	176	300	82	241
75	150	174	300	100	229
75	250	169	300	148	219
100	50	185	300	200	211
100	200	165	300	250	210
100	350	163	300	301	207
150	50	235	300	355	208
150	100	219	400	82	306
150	300	216	400	100	307
200	200	266	400	149	291
200	200	266	400	200	272
200	300	260	400	250	270
250	55	347	400	302	267
250	100	320			
250	300	309			
300	75	374			
300	200	349			
300	300	344			
d = 12 mm			d = 27 mm.		

three parts in which the low pressure, the moderate pressure and the high pressure positive columns are considered respectively.

3.2.1 Spectrum line broadening in the low pressure positive column.

In Fig. 3.6, the experimental halfwidth of the 5852 Å line, corrected for Doppler, natural and instrumental broadening is presented as a function of the gas filling pressure at room temperature (296 K) for one value of the discharge current (150 mA) and the tube diameter (6 mm).

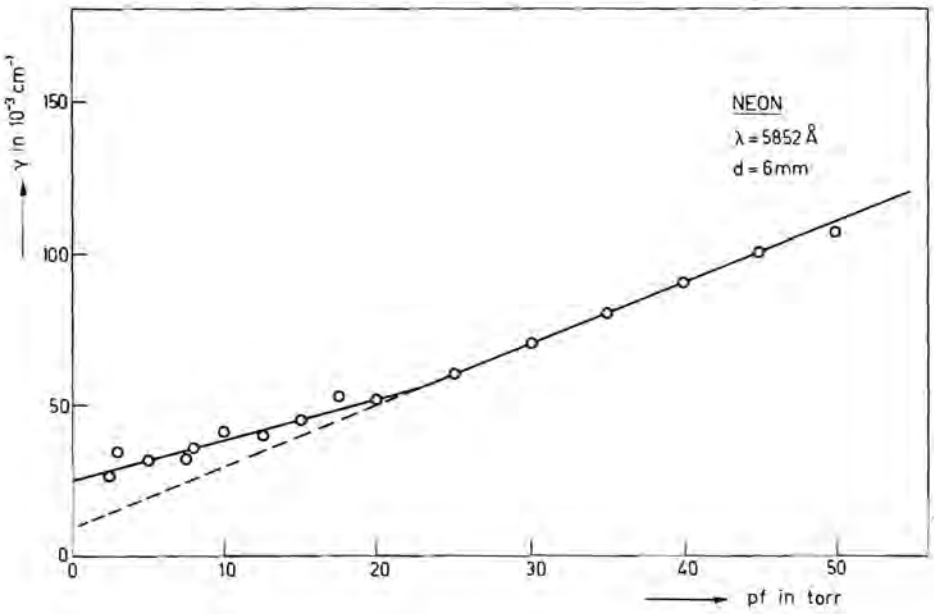

Fig. 3.6 The resonance halfwidth as a function of the filling pressure at room temperature with the discharge current as parameter.

Now from gas temperature measurements as well as from radial line intensity measurements it followed that in this pressure range the spectral inhomogeneity μ is far less than one, so that to a first approximation the emitting plasma can be considered to be homogeneous. From a theoretical point of view one should expect then that the observed halfwidth is proportional to the gas pressure as expressed by relation 3.1. However, from Fig.3.6 it follows that, although the relationship between halfwidth and gas pressure is essentially linear, the broadening constants corresponding with the pressure ranges 0-25 torr and 25-50 torr respectively, are different. The value of the broadening constant calculated from the higher pressure range (C_{5852} = 6,5 $\pm$ 0,15.10^{-20} $cm^{-1}/at.cm^3$) is in good agreement with the value reported by Kuhn[15] et.al. (C_{5852} = 6,37 $\pm$ 0,15.10^{-20} $cm^{-1}/at.cm^3$). In order to ascertain which extra broadening mechanism could be responsible for the deviations appearing in the low pressure region, the influence of the discharge current on the observed halfwidth was determined. The result is presented in Fig.3.7 where the observed halfwidth is plotted versus the discharge current for a filling pressure of three torr and a discharge diameter of 10 mm.
Since on the one hand the halfwidth strongly depends on the discharge current but on the other hand the electron density is too low ($n_e \leq 10^{11}$ el/cm^3) to bring about a noticeable Stark-broadening, the conclusion was drawn that the extra line broadening is caused by self-absorption and isotope effects. In order to verify this conclusion for a filling pressure of 3 torr and the same discharge diameter the line absorption coefficient was determined as a function of the discharge current. With the aid of this absorption coefficient and the relations discussed in sections 1.5.3 and 1.5.4 of this chapter, the halfwidth of the λ = 5852 Å including self absorption and isotope effects was calculated as a function of the discharge current. The calculated variation in the halfwidth caused by an increase of the discharge current from 1 to 150 mA amounts to 20.$10^{-3}cm^{-1}$, which is in good agreement with the variation in the halfwidth observed in the experiment. In the pressure range 25-50 torr, within the limits of error no significant variation of the halfwidth with tube diameter or discharge current was observed. This indicates that in this pressure range the

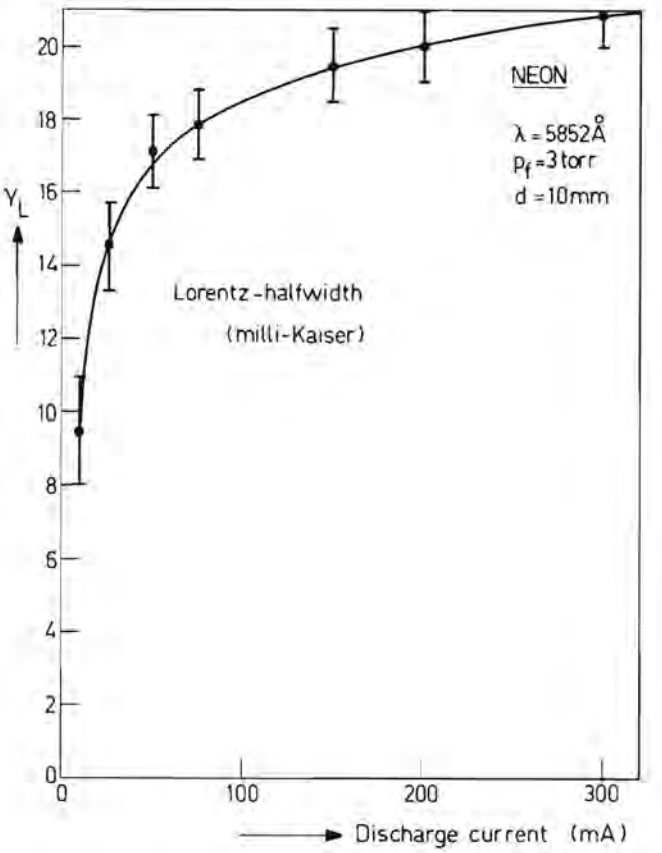

Fig. 3.7 Observed halfwidth as a function of the discharge current.

halfwidths presented in Fig.3.6, characterise the resonance broadening only. Therefore in this pressure region the broadening constant calculated from the experiments has a well-defined meaning.

3.2.2 Spectrum line broadening in the moderate pressure positive column.

The gas pressure range from 50 to 150 torr should be considered as a transition range, since in this region a constriction of the positive column occurs. As soon as this constriction sets in, the functions $n_a(r)$ and $P_{nm}(r)$ may reasonably well be described by the empirical relations (3.12) and (3.13). The values of the halfwidth calculated

with the aid of these experimental functions $n_a(r)$ and $P_{nm}(r)$ are in good agreement with the experimental values.
However, in this range of plasma parameters, the mathematical description of the plasma is so complicated that it is not possible to include the various plasma phenomena in a simple model. As a consequence it is impossible to relate the various parameters characterising the functions $P_{nm}(r)$ and $n_a(r)$ directly to the basic discharge phenomena. So, apart from a relative decrease of the observed halfwidth at the moment of constriction, only little plasma dynamical information can be obtained from halfwidth measurements in this pressure range.

3.2.3. Spectrum line broadening in the constricted high pressure positive column.

In section 1 of this chapter, approximate expressions have been derived for both the line shape and the halfwidth of a spectrum line emitted from a constricted positive column. In these calculations $I^o_{nm}(\omega.0)$ was expressed in terms of the spectral inhomogeneity μ_{nm} and the line profile of the spectrum line emitted at the discharge axis $I_{nm}(\omega)$. For a resonance broadened spectrum line, this profile is fully determined by the neutral atom density at the discharge axis $n_a(0)$, which in its turn is uniquely defined by the gas temperature distribution in the discharge tube.

3.2.3.1 Calculation of $n_a(0)$.

In the following a plasma in a tipped-off discharge tube is considered. At operating conditions the space within this discharge tube consists of two essentially different parts:

(1) The proper discharge plasma which is inhomogeneous but radially symmetric. The gas density distribution in this plasma with volume V_p is given by $n_a(r)$.

(2) The dummy space with volume V_D, defined as the space belonging to the discharge tube but not to the plasma as

such e.g. the space behind cathode and anode. Since in this space the temperature gradients are small, it will be characterised by an average gas temperature $\bar{T}_D$.

At operating conditions the relation between filling density n_f and the average gas density in the plasma column $\bar{n}_p$ is given by

$$\bar{n}_p = n_f \frac{1 + \frac{V_D}{V_p}}{1 + \frac{\bar{T}_p}{\bar{T}_D}\frac{V_D}{V_p}} \tag{3.23}$$

where:

$\bar{T}_p$ = average gas temperature in the plasma column.

With the aid of the empirical distributions (3.11) and (3.12) $n_a(0)$ may be expressed terms of $n_f, \bar{T}_p, T_a(0), \bar{T}_D, V_p$ and V_D

$$n_a(0) = n_f \frac{\bar{T}_p}{T_a(0)} \frac{1 + \frac{V_D}{V_p}}{1 + \frac{\bar{T}_p}{\bar{T}_D}\frac{V_D}{V_p}} \tag{3.24}$$

3.2.3.2 The effective broadening constant $C_{nm_{eff}}$.

Substitution of this expression in relation (3.18) yields, under the condition that $u_{nm} << 1$, a general relation for the halfwidth of a spectrum line profile emitted from a constricted high pressure positive column

$$\gamma_{nm} = C_{nm}\, n_f\, (1 + u_{nm}) \frac{\bar{T}_p}{T_a(0)} \frac{1 + \frac{V_D}{V_p}}{1 + \frac{\bar{T}_p}{\bar{T}_D}\frac{V_D}{V_p}} \tag{3.25}$$

The effective broadening constant $C_{nm_{eff}}$, defined as:

$$C_{nm_{eff}} = \frac{\gamma_{nm}}{n_f} ,$$

may then be written as

$$C_{nm_{eff}} = C_{nm}(1 + \mu_{nm}) \frac{\bar{T}_p}{T_a(0)} \frac{1 + \frac{V_D}{V_p}}{1 + \frac{\bar{T}_p}{\bar{T}_D} \frac{V_D}{V_p}} \qquad (3.26)$$

From this relation it follows that, apart from the small influence of μ_{nm}, $C_{nm_{eff}}$ is completely determined by the gas temperature distributions both in the plasma column and in the dummy space. In Fig.3.8 for a number of discharge conditions in neon, the effective C-values of the λ = 5852 Å line are plotted versus the parameter θ. The corresponding values of discharge radius, discharge current and filling pressure are presented in table III.
From this figure it follows that for the λ = 5852 Å line , the effective broadening constant is independent of the relevant discharge parameters. It may in a first approximation be representated by an empirical relation of the form.

$$C_{eff} = C_o + k.\theta. \qquad (3.27)$$

3.2.3.3 Comparison of experimental and theoretical halfwidths.

Using thermocouples to measure the gas temperature it has been possible to determine $T_a(r)$ and $\bar{T}_D$. The experimental $T_a(r)$ curves were fitted to the empirical relation (3.11) with the aid of a computer which calculated the parameters $T_a(0)$, $\bar{T}_p$, θ and β.
The average temperature in the dummy space was evaluated graphically. The values of μ_{nm} were obtained from spectrum line intensity measurements as discussed in chapter 2, section 5. Substitution of these experimental values in the general expression for γ_{nm} (3.25) yields a number of calculated halfwidths which are compared with the corresponding

Table III

p_f (torr)	i(mA)	R(mm)	θ	β(mm)	x(mm)	$\bar{T}_p$(K)	$\bar{T}_D$(K)	$\frac{V_D}{V_p}$	C_{eff}	γ(exp) mK	γ(calc) mK
200	80	13.5	0.32	7.2	1.55	525	305	0.32	0.48	190	190
200	150	13.5	0.28	6.3	2.15	575	310	0.32	0.43	171	171
200	200	13.5	0.25	6.1	2.50	590	312	0.32	0.41	164	164
200	250	13.5	0.23	6.0	2.77	600	315	0.32	0.40	159	160
200	300	13.5	0.22	6.0	2.92	625	317	0.32	0.40	157	158
200	350	13.5	0.21	6.0	3.06	650	320	0.32	0.39	159	157
300	80	13.5	0.28	6.1	1.83	550	310	0.32	0.40	241	241
300	150	13.5	0.23	5.8	2.32	620	315	0.32	0.36	218	219
300	200	13.5	0.21	6.0	2.78	690	317	0.32	0.35	211	212
300	250	13.5	0.19	6.0	2.98	740	320	0.32	0.35	211	211
300	300	13.5	0.18	6.3	3.24	760	322	0.32	0.35	207	208
300	350	13.5	0.18	6.5	3.48	780	325	0.32	0.34	209	207
400	80	13.5	0.22	7.0	1.97	625	315	0.32	0.39	306	315
400	150	13.5	0.18	7.0	2.82	725	320	0.32	0.34	292	275
400	200	13.5	0.17	7.1	3.21	800	322	0.32	0.34	272	272
400	250	13.5	0.16	7.1	3.50	870	325	0.32	0.34	271	270
400	300	13.5	0.15	7.3	3.84	920	327	0.32	0.33	267	267
400	350	13.5	0.15	7.4	4.12	950	330	0.32	0.33	-	267
150	300	6.0	0.53	6.3	2.7	600	330	0.25	0.78	216	215
150	150	6.0	0.58	6.2	2.2	530	315	0.25	0.72	218	217
200	300	6.0	0.50	7.0	3.40	650	350	0.25	0.64	261	258
250	250	6.0	0.46	6.1	2.7	650	350	0.25	0.62	315	310

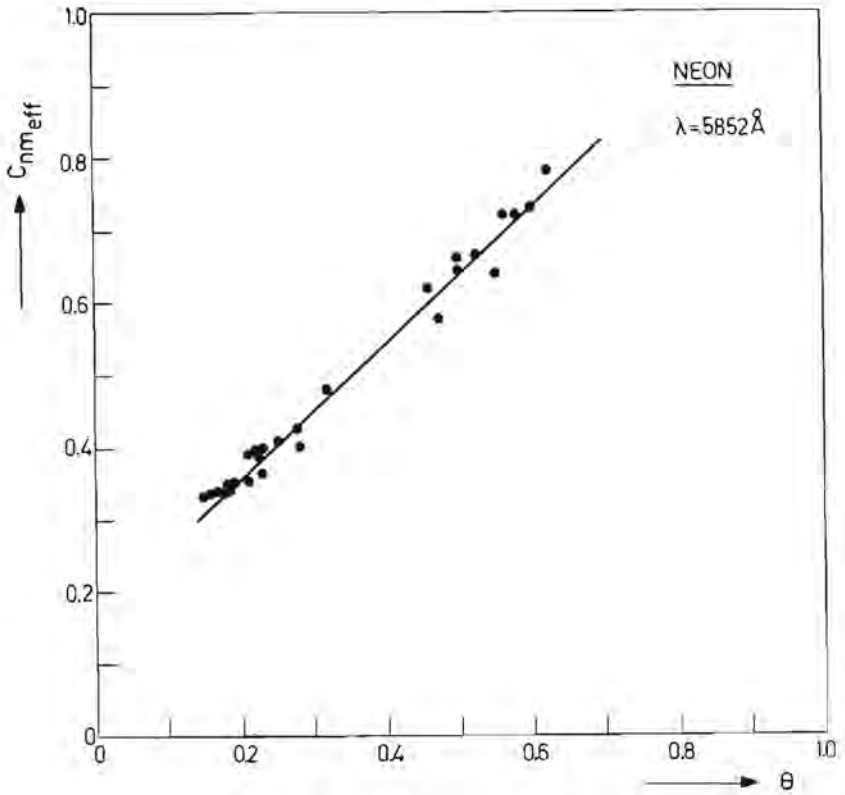

Fig. 3.8 Some experimental values for $C_{nm_{eff}}$ as a function of the parameter θ.

experimental values in Fig.3.9. Moreover, all the relevant parameters describing the discharge tube and the functions $P_{nm}(r)$ and $n_a(r)$ are tabulated also in Table III.
From Fig.3.9, in which the resonance broadening halfwidth is plotted versus the discharge current with the filling pressure as a parameter, it follows that there is a good agreement between experimental and calculated halfwidths.

3.3 New method for the determination of gas temperatures.

In the foregoing a general expression has been derived for the halfwidth of a resonance broadened spectrum line, emitted from a plasma of cylindrical symmetry, enclosed in a tipped-off discharge tube the

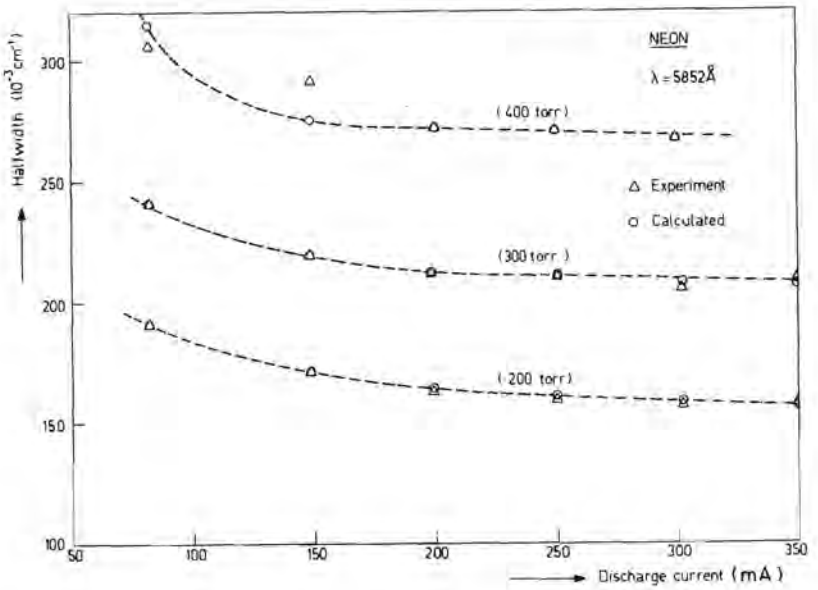

Fig. 3.9 Comparison of the experimental and calculated resonance halfwidths as a function of the discharge current with the filling pressure at room temperature as parameter.

filling pressure of which is known. In practice on the contrary there are used a lot of open plasma systems in which not the filling pressure but the operating pressure is known[8] e.g.: free burning arcs, plasmas in which a certain operating pressure is maintained externally, or plasmas in which the operating pressure is determined with the aid of a pressure probe. For plasmas of this type, for which in broad outlines the theories developed in section 1 hold, the complex expression (3.25) for the halfwidth of a resonance broadened spectrum line reduces to the simple form

$$\gamma_{nm} = C_{nm} \cdot \frac{p_0}{k.T_a(0)} (1 + \mu_{nm}) \qquad (3.28)$$

where:

p_o = operating pressure.

Unfortunately this expression still contains two unknown parameters, namely μ_{nm} and $T_a(0)$. So it seems impossible to calculate $T_a(0)$ from a line broadening experiment only. In section 1, however, it was shown that in general $\mu_{nm} << 1$. And it is this condition which enables us to calculate $T_a(0)$ indirectly with the aid of the following itteration routine. Let us first assume that $\mu_{nm} = 0$. Then $T_a(0)_1$ is defined by

$$T_a(0)_1 = \frac{p_o C_{nm}}{k.\gamma_{nm}} \tag{3.29}$$

Now a simple calculation shows that for a great number of experimental conditions μ_{nm} may be approximated by the following expression.

$$\mu_{nm} \simeq (T_a(0)_1 - T_R)\left[\frac{T_a(0)_1 - T_a(R)}{T_R - T_a(R)}\right]\frac{x^2_{nm}}{R^2} \tag{3.30}$$

where:

T_R = room temperature.

Substitution of the value of μ_{nm}, calculated in this way, in (3.28) yields a new approximate value of the axis gas temperature $T_a(0)_2$ which in its turn after substitution in (3.30) yields a better approximate value for μ_{nm} etc.... This itteration routine, already after two cycles yields reasonable approximate values both for $T_a(0)$ and μ_{nm}. As a consequence it enables us to determine the gas temperature in the axis of the discharge tube from a halfwidth measurement combined with a measurement of the radial spectrum line intensity distribution.

3.3.1 Experimental verification of the new method.

In a number of tipped-off discharge tubes in neon, the operating pressure p_o for a great many discharge conditions was determined with the aid of a pyrex spiral manometer. For the same discharge conditions and in the same discharge tubes, the gas temperature distributions

were determined with thermocouples; the halfwidths of the λ = 5852 Å neon line were obtained from measurements performed with a Fabry-Perot interferometer. The corresponding values of χ_{5852} were derived from radial spectrum line intensity measurements. The gas temperatures in the axis of the discharge tube, calculated from the experimental values of p_o, χ_{5852} and γ_{5852} according to the itteration method outlined in section 3.3, are compared in Table IV with the corresponding values derived from thermocouple measurements. These measurements were corrected for thermal radiation effects.

From Table IV it follows that within the limits of error there exists a reasonable agreement between the results of the two methods. Consequently it is expected that for many practical purposes where only an approximate value of $T_a(0)$ is wanted, the new method presented here will do well enough.

p_f (torr)	i (mA)	p_o (torr)	γ_{5852} (10^{-3}cm^{-1})	$T_a(0)$ calc. Kelvin	$T_a(0)$ therm. Kelvin
400	350	905	267	2140	2070
400	300	865	267	2020	1975
400	250	837	271	1930	1890
400	150	750	290	1640	1610
300	350	615	208	1830	1780

Table IV A comparison of some experimental thermocouple temperatures with those obtained from combined line broadening and gas pressure measurements.

3.4 Conclusion

In the foregoing sections a first attempt has been made to describe the spectrum line broadening in inhomogeneous plasmas of cylindrical symmetry. It has been shown that for a resonance broadened spectrum line the line profile is completely determined by the radial gas temperature distribution $T_a(r)$ and the radial distribution of spectrum line radiation $P_{nm}(r)$. By a systematic theoretical and experimental investigation of the shape of these functions, it has been possible to develope for both an empirical representation holding in a vast region of plasma conditions especially for the constricted high pressure positive column. Starting from these empirical representations, general approximate expressions were derived for both the line shape and the halfwidth of a resonance broadened spectrum line emitted from an inhomogeneous plasma of cylindrical symmetry. For the special case of a constricted positive column in neon these calculated line profiles and halfwidths were in agreement with the experimental results within the limits of error.

These calculations were in first instance developed for the typical plasma conditions of the constricted high pressure positive column. Thanks to the large region of validity of both empirical functions it is expected that the theory presented here may be applied in a first approximation to very many of other plasmas which are not typically constricted. In these cases systematic errors may be introduced. These difficulties, however, may be overcome on the one hand by completing or extending the theory presented here by more adequate representations for $n_a(r)$ and $P_{nm}(r)$ and on the other hand by taking into account more terms in the series representations for both the line profile and the halfwidth. This procedure will be discussed in a paper, to be published shortly, in which the spectrum line broadening in a high pressure (1 atm) high current (6A) mercury discharge is considered.

Since the expression for the halfwidth of a resonance broadened spectrum line, presented here, has been shown to be in good agreement with the results of independent gas temperature measurements, the method given may be used in the opposite direction to determine approximate values for the gas temperature and gas density.

References

1) Foley, H.M., Phys. Rev. 69, 616 (1946).
2) Hindmarsh, W.R., Thomas, K.A., Proc.Phys.Soc.A, 77, 1193 (1961).
3) Kuhn, H.G., Vaughan, J.M., Proc.Roy.Soc. A, 277, 297 (1963)
4) Vaughan, J.M., Proc.Roy.Soc. A,295, 164 (1966).
5) Breene, R.G., The Shift and Shape of Spectral Lines. Pergamon Press. Oxford (1961).
6) Traving, G., Uber die Theorie der Druckverbreiterung von Spektrallinien. Braun Verlag. Karlsruhe (1960).
7) Lang, K., Acta.Phys.Austria. 5, 376 (1951).
8) Krämer, K., Phys.Z. 40, 81 (1939).
9) Massey, J.T., Cannon, S.M.,J.Appl.Phys. 36, 361 (1965).
10) Edwin, R.P., Turner, R., Journ.Opt.Soc.Am. 60, 448 (1970).
11) Bartels, H., Z.Phys. 126, 108 (1949).
12) Mouwen, C.A.M., Proc. 9th Conf.Ion.Phen.in Gases, Bucharest 589 (1969).
13) Chapter V of this thesis.
14) Chapter IV of this thesis.
15) Kuhn, H.G., Lewis, E.L., Proc.Roy.Soc. A,299, 423 (1966).
16) Lindholm, E., Arkiv.f.Math.Astr.Phys. 28, B, 3 (1941).
17) Murakawa, K., Mizuno, S., J.Phys.Soc.Jap. 14, 1235 (1959).
18) Mouwen C.A.M., Claassens J.M.M., Phys.Lett. 31A, 123 (1970).

CHAPTER IV THERMOCOUPLE MEASUREMENTS

4.1 Introduction.

One of the oldest methods to determine gas temperatures in plasmas is the use of thermocouples[1][2][3]. Unfortunately, up to now, no satisfactory answer has been given to the following fundamental question: How great is the total systematic error in such thermocouple measurements caused by the following physical processes: recombination, deexcitation, conduction and radiation? Moreover, it is not clear at all to what extent the plasma as such is distorted by the presence of the thermocouple. Doubts of this kind have brought about that the measurement of gas temperatures with the aid of thermocouples is a scarcely used diagnostic tool in plasma physics.

In the present work, however, an attempt has been made to answer this fundamental question by comparing the experimental results of a number of thermocouple measurements with the results obtained from independent line broadening experiments performed in the same discharge plasma.

4.2 Experimental results.

The purpose of the experiments was to determine the gas temperature distribution in a constricted positive column in neon. As will be shown in section 4.3., the thermocouple measurements yield only a first order approximation of this gas temperature distribution. The deviation between real and experimental gas temperature finds its origin in the various physical processes mentioned in the introduction. The effect of most of them is related directly to the presence and the dimensions of the thermocouple. For that reason, the radial gas temperature distributions were determined in two different ways, in each of which the dimensions as well as the presence of the thermocouple as such played an essentially different part. For the first method, at three positions in the discharge tube, lying at different distances from the discharge axis, a fused

silica capillary was mounted. The temperature at the top of such a capillary was determined with the aid of a thermocouple, mounted in top of the capillary. According to the second method, only one capillary was mounted in which the gas temperature was determined at about 15 different positions, with the aid of a movable thermocouple. Experiments according to both methods were performed in the same range of plasma parameters, and within the limits of error, the two methods yielded the same results. As the experimental values obtained from the experiments with the movable thermocouples were more accurate, they were used for further investigations.

With the help of a computer and using a least squares method the experimental values for the thermocouple temperature $T_t(r)$ were fitted to the following empirical relation

$$\frac{T_t(r)}{T_t(0)} = \theta + \frac{(1-\theta)}{1 + \frac{r^2}{\beta^2}} \qquad (4.1)$$

where:

$T_t(0)$ = thermocouple temperature at the axis of the discharge

r = distance from the axis of the discharge

θ = parameter defined by $\theta = \frac{T_t(\infty)}{T_t(0)}$

2β = halfwidth of the Lorentz function: $F(r) = \frac{1}{1 + \frac{r^2}{\beta^2}}$

An experimental temperature distribution is shown in Fig.4.1, where the temperatures found from these thermocouple measurements were plotted for p = 415 torr and I = 300 mA. This experimental curve is fitted by means of a least squares method to relation (4.1). The best fit is also shown in the figure.

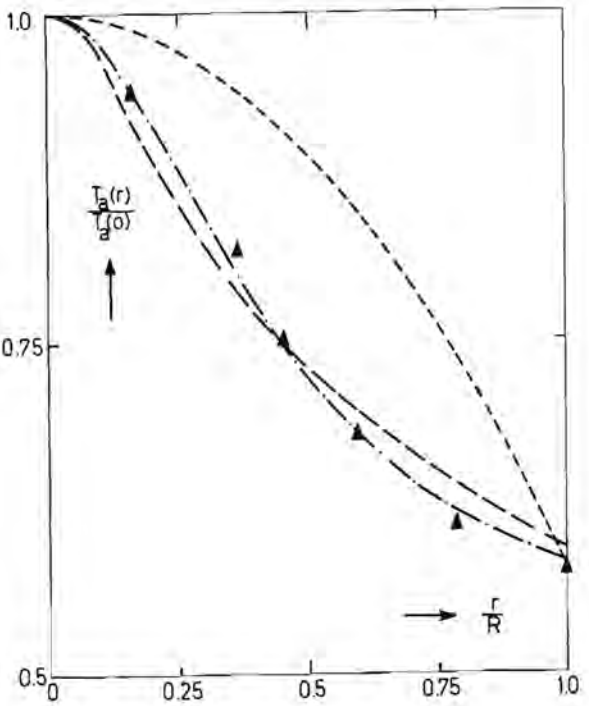

Fig. 4.1 Experimental gas temperature distribution for a constricted discharge in neon. The filling pressure at room temperature was 415 torr and the discharge current 300 mA.

It appeared that for all our experimental results the relative deviations from relation (4.1) amounted to only a few per cent. With the aid of the computer, for each experimental temperature distribution the values of the following characteristic parameters were calculated:

$$T_t(0), \theta, \beta, \overline{T}_t(r) \text{ and } \frac{T_t(R)}{T_t(0)}$$

where:

$\overline{T}_t(r)$ = average thermocouple temperature in the positive column.

$T_t(R)$ = thermocouple temperature at the wall

For a constricted positive column in neon with an inner diameter of 12 mm in which the filling pressure and the discharge current varied from

10 to 400 torr and from 50 to 400 mA respectively, the following results were obtained

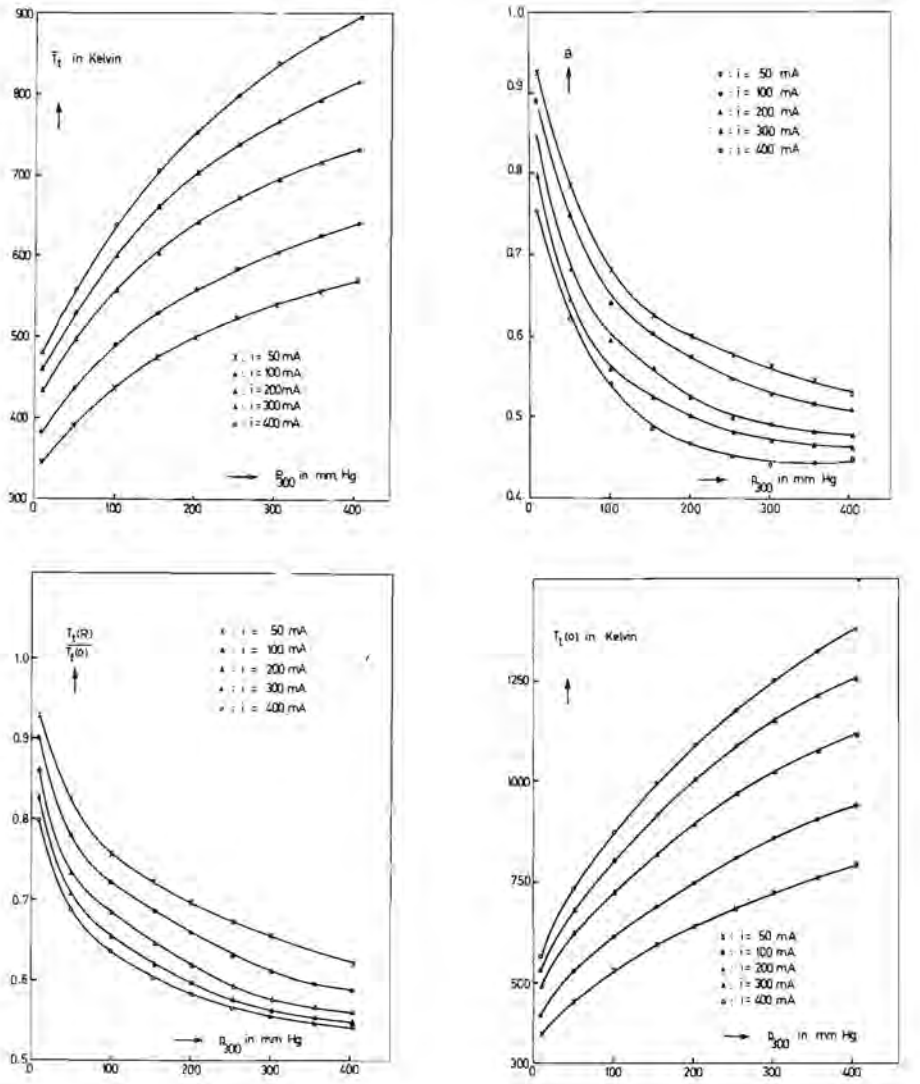

Fig. 4.2-4.5 Some experimental results of the thermocouple measurements plotted as a function of the filling pressure at 300 K with the discharge current as parameter.

p_f (torr)	I (mA)	p_o (torr)	$T_a(0)$ (K)	$T_t(0)$ (K)	$T_t(R)$ (K)	δT_a (K)	$\delta T_a / T_a(0)$ (%)
400	350	893	2105	1460	495	645	30.6
400	150	755	1625	1190	420	435	26.8
400	300	857	1997	1415	490	573	28.6
400	250	828	1910	1347	483	563	29.4
300	350	608	1805	1330	478	475	26.3
300	100	498	1340	993	390	347	25.9
300	200	545	1593	1180	423	413	26.0
200	350	393	1520	1195	435	325	21.4
200	80	315	1025	805	375	220	21.3
200	100	315	1058	845	385	213	20.1
200	200	348	1318	1040	410	278	21.0

Table I. Some experimental temperatures obtained from thermocouple measurements and combined gas pressure and line broadening experiments.

From a combination of a few number of measurements of the halfwidth of the resonance broadened λ = 5852 Å line with a determination of the operating pressure, the conclusion could be drawn that the maximum absolute inaccuracy in the results of these thermocouple measurements does not exceed 250 Kelvin at axis temperatures of about 1250 Kelvin. A more precise discussion of the systematic error in these measurements is presented in the following sections.

4.3 The systematic error in thermocouple measurements.

4.3.1 Experimental

The discharge tubes used in our experiments had an inner diameter of 27 mm and they were used in a vertical position in order to reduce convection effects. Moreover, under the same discharge conditions, both the operating pressure and the halfwidth of the resonance broadened λ = 5852 Å neon spectrum line were determined, each with a relative inaccuracy of about 1 per cent. Following the itteration procedure which is discussed extensively in chapter 3 of this thesis, the real gas temperatures in the axis of the discharge tubes were calculated from the results of these experiments with a relative error which does not exceed 3 per cent. Together with the corresponding values of the relevant parameters, the axis temperatures derived from the thermocouple measurement: $T_t(0)$ and the temperatures obtained from the halfwidth measurements: $T_a(0)$, are given in table I.
In Fig.4.6, the temperature difference:

$$\delta T_a(0) = T_a(0) - T_t(0)$$

is plotted versus $T_t(0)$.
From this figure it follows that there exists a considerable discrepancy between the gas temperature $T_a(0)$ and the thermocouple temperature $T_t(0)$.

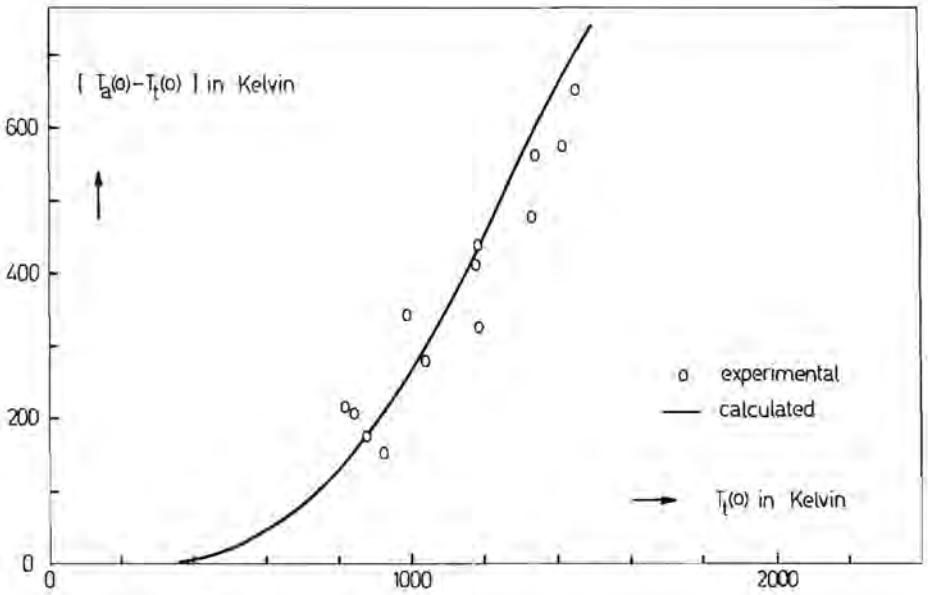

Fig. 4.6 The systematic difference $\delta T_a(0)$ as a function of the thermocouple temperature $T_t(0)$.

4.3.2 Calculation of the systematic difference.

Thanks to the energy transport from the plasma to the thermocouple, the latter will tend to take the temperature of the plasma. This gas temperature can only be reached if no energy transport away from the thermocouple takes place. This may be understood as follows: in the stationary state, any energy transport from the thermocouple must be compensated by an equal energy transport to the thermocouple. Since the latter transport is proportional to: δT_a, it is clear that the situation in which $T_a = T_t$, can only exist if no energy transport to and from the thermocouple takes place. In a real plasma, however, there are a lot of processes transporting energy from the thermocouple to the

plasma or to the wall of the discharge tube. So it must be expected that the temperatures, determined with the aid of thermocouples, are essentially lower than the real gas temperatures of the plasma.
In order to express these considerations in a more quantitative form, we consider now an idealised thermocouple configuration consisting of a thin fused silica capillary of cylindrical symmetry in which the thermocouple as such is situated. The temperature distribution along the

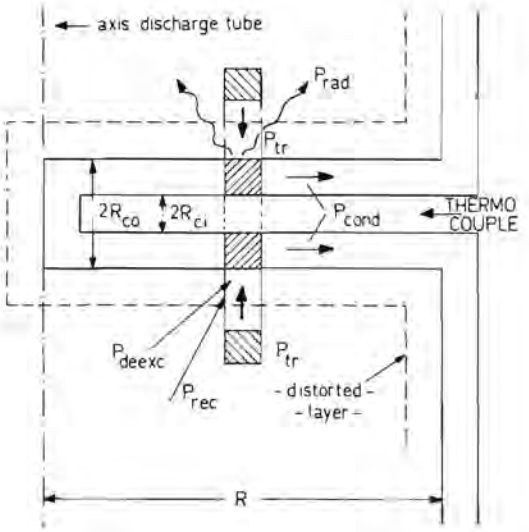

Fig. 4.7 The idealised thermocouple configuration used in the calculation of the systematic difference $\delta T_a(r)$.

capillary equals the temperature distribution measured with the thermocouple if an ideal thermal contact between the thermocouple and the capillary is assumed. The most important processes governing the temperature distribution along the capillary are discussed briefly below.

4.3.2.1 Heat transfer from the plasma to the thermocouple.

If it is assumed that the energy transport from the plasma to the thermocouple takes place in a direction perpendicular to the axis of the thermocouple, the total power transferred to a small cylindrical part of the capillary is given by:

$$dQ_{tr}(r) = 2\pi R_{co} \alpha_{tr} (T_a(r) - T_t(r))dr \qquad (4.2)$$

where:

α_{tr} = heat transfer coefficient from the discharge gas to the capillary.

R_{co} = outer radius of the capillary.

This expression which holds only for an infinitely long capillary may be adapted to the finite length of this capillary by a configuration factor g_c.
If the length of the capillary is large with respect to its diameter $g_c \approx 1$.

4.3.2.2 Heat conduction through the capillary and the thermocouple to the wall.

In the stationary state, the capillary has a temperature distribution, which has a maximum value for $r = 0$ and is minimal for $r = R$.
This temperature distribution causes a continuous heat transfer by conduction in a direction from the discharge axis to the wall of the discharge tube. The total power transported through a small cylindrical part of the thermocouple is given by:

$$dQ_c(r) = \{\pi(R_{co}^2 - R_{ci}^2)\lambda_c + 2\pi R_{to}^2 \lambda_t\} \frac{d^2T_t(r)}{dr^2} dr \qquad (4.3)$$

where:

R = radius of the discharge tube

R_{ci} = inner radius of the capillary.

R_{to} = outer radius of the thermocouple wires
λ_c = thermal conductivity of fused silica,
λ_t = thermal conductivity of the thermocouple wires.

4.3.2.3 Thermal radiation of the capillary.

The capillary as well as the discharge wall are supposed to be diffuse radiators. Then the energy transported to the thermocouple and away from it is proportional to the same configuration factor g_r. The influence of the plasma on the net transport of radiation is neglected. The net power, transported from a small cylindrical part of the capillary in the form of thermal radiation, may then be written as

$$dQ_r(r) = 2\pi g_r R_{co} \sigma \{\varepsilon_c(T_t) T_t^4(r) - \varepsilon_w(T_w) T_w^4\}\, dr. \qquad (4.4)$$

σ = proportionality constant in the Stefan-Boltzmann law.
ε_c = emissivity of fused silica
ε_w = emissivity of pyrex
$T_w = T(R)$ = thermocouple temperature at the discharge wall.

4.3.2.4 Recombination and deexcitation processes at the wall of the capillary.

The total power transferred from the plasma to a small cylindrical part of the capillary by recombination and deexcitation processes is given by:

$$dQ_{dr}(r) = 2\pi R_{co} \{n_i(r) n_e(r) A_i(r) U_i + \sum_{k=1}^{n} n_k(r) B_k(r) U_k\} dr \qquad (4.5)$$

where:

A_i = rate coefficient for recombination of ions and electrons at the wall of the capillary.
B_i = rate coefficient for deexcitation of atoms from the k^{th} excited state to the ground state, occuring at

the wall of the capillary.

U_i = ionization energy of the discharge gas.

U_k = energy of the k^{th} excited level of the discharge gas.

$n_e(r)$ = electron density at position (r)

$n_i(r)$ = ion density at position (r)

$n_k(r)$ = density of atoms in the k^{th} excited state at position (r).

4.3.2.5. The energy balance of the thermocouple.

Since in the stationary state the net power transport to the small cylindrical part of the capillary is zero, the quantities dQ(r) must obey the following equation

$$dQ_{tr}(r) + dQ_{dr}(r) = dQ_c(r) + dQ_r(r)$$

Under the simplifying assumptions mentioned, this energy balance is valid for every small cylindrical part of the capillary. Therefore it may be rewritten in the form of the following second-order differential equation.

$$g_c\alpha_{tr}\left[T_a(r) - T_t(r)\right] + n_i(r)n_e(r)A_i(r)U_i + \sum_{k=1}^{n} n_k(r)B_k(r)U_k =$$

$$\frac{1}{2}\left[\frac{\lambda_c}{R_{co}}\left(R_{co}^2 - R_{ci}^2\right) + \frac{\lambda_t}{R_{co}}R_{to}^2\right]\frac{d^2T_t(r)}{dr^2} + \sigma g_r\left[\varepsilon_c(T_t)T_t^4(r) - \varepsilon_w(T_w)T_w^4\right] \qquad (4.6)$$

The various terms in this equation have the dimension power per unit area.

4.3.3 Approximate solution.

In general, nearly all coefficients in the energy balance of the thermocouple depend on the gas temperature. As a consequence the general solution of this equation is very complex and it only has an analytical

form under very special discharge conditions. For that reason in this section an approximate solution will be presented which is adequate in the whole range of plasma parameters used in our experiments.

From a simple first order estimation it may be concluded that under the actual experimental conditions the influence on the energy balance of heat conduction through both the capillary and the thermocouple wires may be neglected. This can be seen as follows. Let us assume that the exact solution $T_t(r)$ of the balance equation may be approximated by a parabolic function of r.

$$T_t(r) = T_t(0) - (T_t(0) - T_t(R)) \frac{r^2}{R^2} \qquad (4.7)$$

Starting from this approximate expression for $T_t(r)$, the conduction term in (4.6) can be written as

$$P_{cond} = \left[\frac{\lambda_c}{R_{co}} \left(\frac{R_{co}^2 - R_{ci}^2}{R^2} \right) + 2 \frac{\lambda_t}{R_{co}} \frac{R_{to}^2}{R^2} \right] \left[T_t(0) - T_t(R) \right]$$

Inserting the following values for the various quantities (see chapter 2),

$R_{co} = 2.5\ 10^{-4}$m, $\lambda_c = 1.5$ Watt/m.K
$R_{ci} = 1.0\ 10^{-4}$m, $\lambda_t = 50$ Watt/m.K,
$R_{to} = 2.5\ 10^{-5}$m, $T_t(0) = 1000$ K,
$R = 1.0\ 10^{-2}$m, $T_t(R) = 400$ K.

yields for P_{cond} the following approximate value:

$$P_{cond} = 1150 \text{ Watt/m}^2.$$

For the same experimental conditions and the additional approximation

$$\varepsilon_w = \varepsilon_c = g_r = 1,$$

for the radiation term in (4.6) the following estimate value is found.

$$P_{rad} = 5.7\ 10^4 \text{ Watt/m}^2.$$

From a comparison of the estimated values for P_{rad} and P_{cond} it may be concluded that for our experimental conditions the conduction term in eq. (4.6) can be neglected.

Starting from realistic order of magnitude values for A_i and B_k in eq. (4.6), one may conclude that no noticeable contribution of these processes to the energy balance of the thermocouple is to be expected. Consequently, in our further calculations the influence of these processes is neglected.

In order to calculate the value of the heat transfer coefficient α_{tr} some information must be available about the velocity profiles due to convection currents in the direct neighbourhood of the thermocouple. Since on the one hand these velocity profiles depend on a large number of plasma parameters but on the other hand nothing is known about the precise relationship between these velocity profiles and the particular plasma parameters, only an approximate value for α_{tr} can be calculated. For the range of plasma parameters considered in our experiments, the coefficient α_{tr} was estimated to vary between 40 W/m^2K for a low pressure discharge (p_f = 10 torr) and 110 W/m^2K for a high pressure discharge (p_f = 400 torr). Since in this section mainly high pressure discharges are considered, in the further calculation the value α_{tr} = = 100 W/m^2K will be used.

Due to the considerable uncertainty in the precise value of α_{tr} it is not realistic to discuss relative errors of some 10 or 20% in the value of $\frac{g_{tr}}{g_r}$. Consequently this ratio is assumed to be one.

Within the region of validity of the simplifying assumptions discussed in the foregoing the energy balance of the thermocouple may be written as:

$$\alpha_{tr}\left[T_a(r) - T_t(r)\right] = \sigma\left[\varepsilon_c(T_t)T_t^4(r) - \varepsilon_w(T_w)T_w^4\right] \qquad (4.8)$$

For the same region of validity the systematic difference $\delta T_a(r)$ may then be written as

$$\delta T_a(r) = \frac{\sigma}{\alpha_{tr}}\left[\varepsilon_c(T_t)T_t^4(r) - \varepsilon_w(T_w)T_w^4\right] \qquad (4.9)$$

In Fig. 4.6 the systematic difference $\delta T_a(0)$, calculated from expression (4.9), is compared with the corresponding values of $\delta T_a(0)$ obtained from combined thermocouple and line broadening measurements. The temperature dependence of $\varepsilon_c(T_t)$ and $\varepsilon_w(T_w)$ used in the calculations was taken from Wojaczek[4]. For σ the value $\sigma = 5.7\ 10^{-8}$ W/m^{2}K^4 was used. In Fig. (4.8) the systematic difference $\delta T_a(0)$ is given in relative form as a function of the gas temperature $T_a(0)$.

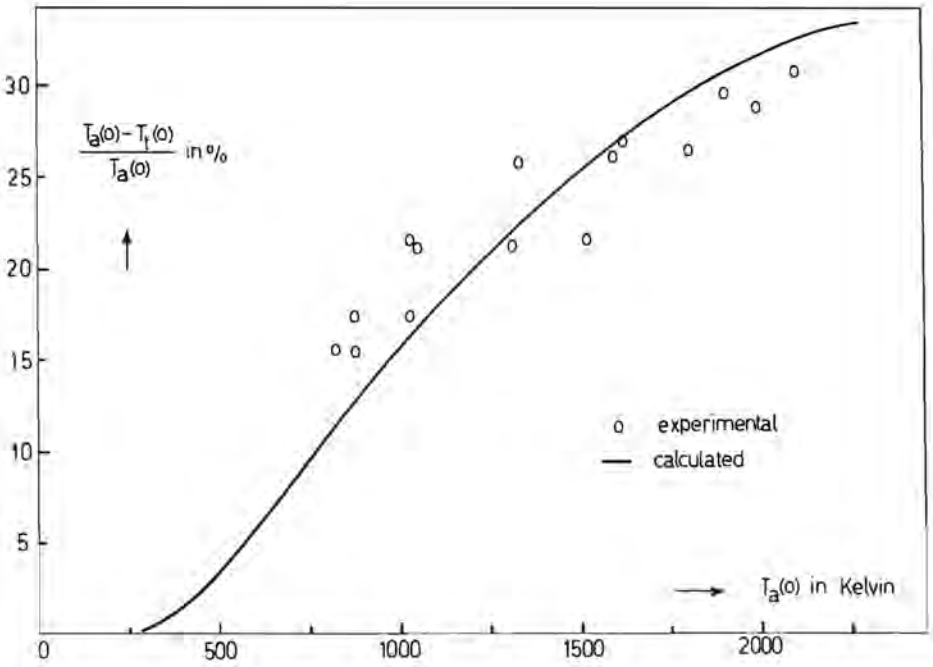

Fig. 4.8 Experimental and calculated relative systematic difference in the thermocouple measurements as a function of the gas temperature.

From these figures it follows that the values of $\delta T_a(0)$ calculated from the simplified balance equation (4.9) are in reasonable agreement with the experimental values of $\delta T_a(0)$.
From the foregoing it is clear that a better agreement between theoretical and experimental values might be expected if more detailed

information would be available about the various coefficients α_{tr}, g_r, g_{tr}, A_i and B_k.

4.4 Shape of the gas temperature distribution.

The shape of the thermocouple temperature distribution $T_t(r)$ depends on the gas temperature distribution $T_a(r)$ and the systematic difference $\delta T_a(r)$. As a matter of fact each experimental thermocouple temperature should be correct by an amount δT_a which is given by expression (4.9). In order to investigate the rough shape of the temperature distribution which is obtained after correction of the experimental thermocouple temperature distribution $T_t(r)$ with $\delta T_a(r)$, we shall follow a more general, although not absolutely accurate method. From Fig. 4.8 it follows that for the gas temperatures occuring in our experiments the following expression for $\delta T_a(r)$ is a reasonable approximation (Fig. 4.8).

$$\delta T_a(r) = A + k.T_t(r). \tag{4.10}$$

Substitution of this expression into the experimental thermocouple temperature distribution : $T_t(r)$, which is represented by expression (4.1), yields for $T_a(r)$ the following distribution function.

$$\frac{T_a(r)}{T_a(0)} = \theta' + \frac{1 - \theta'}{1 + \frac{r^2}{\beta^2}} \tag{4.11}$$

where:

$$\theta' = \frac{\theta.T_t(0) + \frac{A}{k+1}}{T_t(0) + \frac{A}{k+1}} \tag{4.12}$$

From expression (4.11) it follows that within the range of validity of this approximation the gas temperature distribution has essentially the same shape as the thermocouple temperature distribution. The values of θ presented in chapter 3 table III are corrected according to (4.12)

with A = - 500 Kelvin and k = 0,769.

Conclusion.

From the foregoing it follows that in the gas temperature range between 500 and 2000 Kelvin the thermocouple measurements contain a considerable systematic error. This deviation of the thermocouple temperature from the real gas temperature is caused in a first approximation by the thermal radiation of the thermocouple. With the aid of the simple energy transport model discussed in section 4, it is possible to calculate roughly the systematic error caused by this effect. The result of such calculations is in good agreement with the experimental facts. As a consequence, within this gas temperature range, the relative systematic error in the thermocouple measurements, which is of the order of magnitude of a few times ten percent may be reduced greatly by taking into account the thermal radiation of the thermocouple. It is expected that the remaining relative systematic error due to various other effects will not exceed 5 per cent.

Moreover it follows from the actual experiments that within these limits of error the gas temperature distribution in the constricted positive column in neon may be represented by a mathematical expression of the form (4.1.).

REFERENCES.

1) Kuch, R., Retschinsky, T., Ann.Phys. 22, 595 (1907).
2) Seeliger, R., Phys. Z. 27, 732 (1926).
3) Hayess, E., Venzke, D., Wojaczek, K., Beitr.Plasmaphys. 7, 461 (1967).
4) Hayess, E., Wojaczek, K., Beitr.Plasmaphys. 10, 407 (1970).

CHAPTER V MODEL FOR THE CONSTRICTED POSITIVE COLUMN

5.1.1 Introduction.

In recent decennia, both the low pressure positive column ($p < 50$ torr; $i < 100$ mA) and the high pressure arc ($p > 1$ atm; $i > 1$A) have been studied extensively. The arc mechanism can largely be understood by assuming for the arc plasma a local thermal equilibrium L.T.E. or a small deviation from it. Starting from this plasma model, the most important properties of these arcs with respect to line and continuum emission[1][2][3], heat transfer[4] and the mutual dependence of the various plasma parameters can be described reasonably well with the theories available up to now[5]. On the other hand, for the low pressure positive column a rather complex plasma model was developed. This model was obtained by extending the basic diffusion theory, proposed by Schottky, introducing a great number of processes that may play a more or less important part in the discharge mechanism. Among these processes the most important are; stepwise excitation and ionization[6][7], space charge effects, volume and wall recombination [8][9], deviations from the Maxwell electron energy distribution[10][11] [12], deviations from quasi-neutrality[13][14][15] and radial variation of the various plasma parameters[16][17]. With the diffusion theory extended in this way, various complex phenomena such as moving striations in and constriction of the low pressure positive column can be understood. The moderate pressure and the high pressure positive columns, however, are scarcely explored subjects of investigation.
Up till now several attempts[18][19][20][21] have been made to describe the high pressure column by solving the set of coupled differential equations governing the charged particle densities, the electron temperature and the gas temperature. The difficulty, however, is that to solve these equations, in which all quantities show radial dependence, so many simplifying assumptions have to be made that an accurate description of the discharge mechanism can hardly be expected.

In the present work a theory for the high pressure positive column is developed by working out the constriction mechanism proposed in a

previous paper[22]. This thermal constriction model is essentially based on a strong coupling of electron temperature and gas temperature. The relative gradient in the electron temperature approximately equals the relative gas temperature gradient and the latter is fully determined by thermal energy transfer. Therefore the radial variation of electron density and radiant flux, both strongly dependent on the electron temperature, are in principle determined by thermal effects.

5.1.2 Basic Model

Although the various assumptions to be made are discussed in detail in the next sections, we shall briefly outline here the plasma model to be considered. The investigation concerns a high pressure (a few hundred torr) moderate current (a few hundred mA) positive column, the length of which is large with respect to its diameter. The plasma is supposed to be inhomogeneous but radially symmetric whereas axial variations of the various plasma parameters are neglected. Because of the high gas pressure and discharge current it is assumed that the electron-electron and the electron-atom interactions are sufficiently strong to establish a local equilibrium situation.
As the reduced electric field E/p_0 and the electron temperature both are very low, the influence of inelastic collisions on the energy balance is neglected. Since metastable atoms are effectively destroyed in three body collisions, direct ionization is assumed to be the dominant ionization process, whereas the destruction of charged particles is governed by associative ionization and dissociative recombination. The balance equation for these processes leads to a Corona-like equilibrium that can be described with the aid of a modified Saha-equation expressing the relation between electron density, neutral particle density and electron temperature.

5.2 Calculation of the heat dissipation function.

In our model the constricted high pressure column is essentially determined by thermal effects. Therefore the gas temperature distribution

follows directly from the Heller-Elenbaas equation

$$\frac{1}{r}\frac{d}{dr}\left[r\lambda(T_a)\frac{dT_a(r)}{dr}\right] + \sigma E^2 = 0 \qquad (5.1)$$

where:

$T_a(r)$ = gas temperature at position (r),
λ = thermal conductivity,
σ = electrical conductivity,
E = electric field.

In this equation only the heat dissipation function σE^2 depends on the typical electrical discharge parameters. In this paragraph starting from the basic model outlined here, we shall derive an expression for this dissipation function and show that this function can be approximated very well by a Gauss function. The next paragraph presents an analytical solution of the Heller-Elenbaas equation for the case of a Gaussian heat dissipation function.

5.2.1 Electron energy distribution function.

With the aid of a 4 mm microwave interferometer the mean electron density in the positive columns investigated, was estimated to vary from 10^{11} to 10^{14} el/cm^3. In the upper range of this electron density region the electron-electron interaction is sufficiently strong to establisch a Maxwell energy distribution.
This is illustrated in Fig. 5.1, where according to a criterion given by Rother[23], the critical electron density n_e', above which the energy distribution is Maxwellian, is plotted versus the neutral gas density n_a with the average electron energy kT_e as parameter.
This critical electron density was calculated from the relation

$$n_e' = q_i U_i U_e^2 n_a \, 10^{-4} \ (\text{el/cm}^3)$$

where:

$q_i = 6.10^{-2}$ (for neon)[23]
U_i = ionisation potential
U_e = average electron energy.

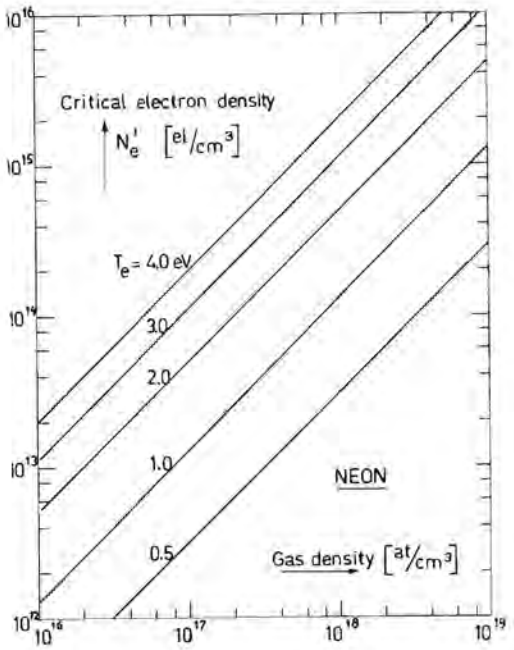

Fig. 5.1 Critical electron density as a function of the gas density with the electron temperature as parameter.

Both theoretical and experimental investigations[12][23] show that with increasing electron density, in the investigated region the electron energy distribution changes from a Druyvesteyn distribution into a Maxwell distribution.

- The low current high pressure positive column.
  In the low current ($i < 50$ mA) high pressure positive column the electron density is low ($n_e << 10^{14}$ el/cm^3). So the electron-electron interaction can be neglected.
  Moreover, the other important conditions for the establishment of a Druyvesteyn distribution in particular the dominant elastic losses, and a negligible gas temperature are fulfilled, so the Druyvesteyn distribution is at least a good approximation in this region.

- The high current high pressure positive column.
  Here the electron-electron interactions are dominant and consequently a Maxwell energy distribution is established. A high electron density cannot be realised without a large current in these discharges. Consequently there will be a large Joule dissipation and the gas temperature will no longer be negligible as was the case in the low current positive column.

Only the high current high pressure positive column will be considered in the following.

5.2.2 The energy balance.

Since in the constricted high pressure positive column both, the reduced electric field (E/p_0) and the average electron energy are very low, 10^{-2} V/cm torr and 1-2 eV resp., the greater part of the energy gain of the electrons in the electric field is transferred to the neutral gas atoms in elastic collisions. This is illustrated in Fig. 5.2 where for a Maxwell energy distribution in neon the reduced energy transfer $p = \frac{P}{P_{tot}}$ in exciting (p_{exc}), elastic (p_{elast}) and ionizing collisions (p_{ion}) is plotted versus the average electron energy kT_e. For the calculation of the numerical results presented in this figure use was made of the following empirical relations and data.

For the momentum transfer cross section use was made of the data given by Thomas[24], who constructed an empirical best fit to the data of Ramsauer and Kollath.
Unfortunately only for a few excited levels absolute values for the excitation cross sections are known. Therefore instead of separate values of $Q_j, \Sigma Q_j$ was used. To this end the value of the total excitation cross section was taken from recent data of Shaper and Scheibner[25] for $16{,}33 < U_e < 21{,}56$ eV. This curve was extrapolated to lower values of U_e with the help of data of Thomas[24].

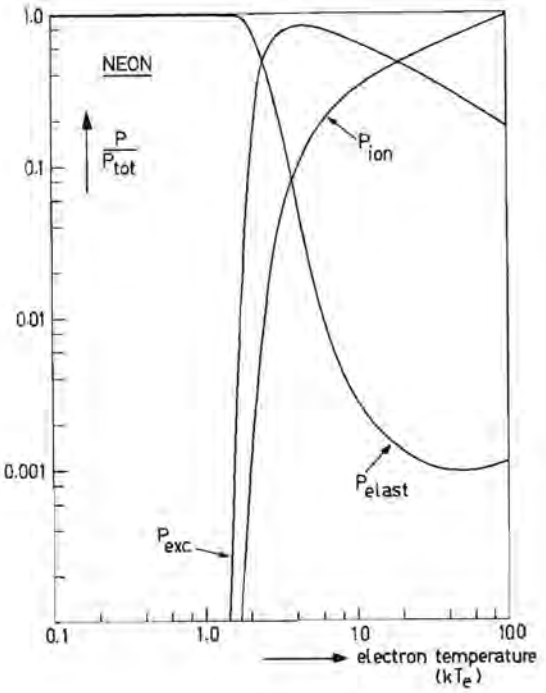

Fig. 5.2 Energy transfer in ionizing, exciting and elastic collisions.

For the ionization cross section use was made of absolute values given by Adamczyk et al[26]. The form of this cross section was derived from the data given by Rapp[27].

Empirical expressions were constructed for the momentum transfer cross section Q_m, the excitation cross section Q_{exc} and the ionization cross section Q_{ion} of which the results are listed below.

$$Q_m = Q_{m1} + Q_{m2}$$

$0 < u < 100$: $Q_{m1} = 149\ u^{0.3} \exp(-0.012u) \times 10^{-18}\ cm^2$

$100 < u$: $Q_{m2} = 178.5 \times 10^{-18}\ cm^2$

$$Q_{exc} = Q_{e1} + Q_{e2} + Q_{e3}$$

$$16.33 < u < \infty \quad : Q_{e1} = 1.38(u-16.33)\exp\left[-\frac{u-16.33}{43.67}\right] \times 10^{-18}\,cm^2$$

$$16.70 < u < 19.00 : Q_{e2} = 0.25 \times 10^{-18}\,cm^2$$

$$16.70 < u < 17.30 : Q_{e3} = \left[1.26 - 14(u-17)^2\right] \times 10^{-18}\,cm^2$$

$$Q_{ion}$$

$$21.56 < u < \infty \quad : Q_{ion} = \frac{0.53\,(u-21.56)^{1.1}}{1 + 4.43(u-21.56)^2 \times 10^5} \times 10^{-18}\,cm^2$$

(u in eV)

From Fig. 5.2 it follows that for the electron temperatures occuring in our experiments (1-2 eV) very nearly almost all energy gain of the electrons in the electric field is transferred to the neutral gas atoms in elastic collisions. Consequently the energy balance of the high pressure positive column can be written to a very close approximation as

$$P_{joule} = P_{elast.} \tag{5.2}$$

5.2.3 Relation between electron temperature and gas temperature

The energy dissipated in the plasma per second per unit volume P_{joule} is given by the general relation[28]

$$P_{joule} = -\frac{4\pi q^2 E^2}{3m_e} \int_0^\infty \frac{v^3}{\nu_c} \frac{\partial f_o(v)}{\partial v}\, dv \tag{5.3}$$

where:

$f_o(v)$ = isotropic part of the electron velocity distribution,
ν_c = the elastic electron-atom collision frequency,
v = the electron velocity,
q = charge of the electron,
m_e = mass of the electron,
E = the axial electric field.

When the electron energy distribution is assumed to be Maxwellian and the elastic cross section Q_{el} is taken constant (which is very nearly the case for neon[29]) expression (5.3) reduces to :

$$P_{joule} = \frac{8\pi q^2 E^2}{3m_e n_a Q_o v_o^2} \int_o^\infty v^3 f_o^m(v)dv \qquad (5.4)$$

where:

$$f_o^m(v) = \frac{n_e}{\pi^{3/2} v_o^3} \exp(-\frac{v^2}{v_o^2}),$$

$$v_o^2 = \frac{2kT_e}{m_e}$$

Q_o = (constant) elastic collision cross-section for neon.

Expression (5.4) may readily be evaluated, giving:

$$P_{joule} = \frac{2^{5/2} q^2 E^2}{3Q_o\sqrt{\pi k m_e}} \frac{n_e}{n_a} T_e^{-\frac{1}{2}} \qquad (5.5)$$

The expression for the elastic losses P_{elast} can, in the same general form, be written as

$$P_{elast} = -\frac{4\pi m_e^2}{m_a} \int_o^\infty \nu_c v^4 \{f_o(v) + \frac{kT_a}{m_e v} \frac{\partial f_o(v)}{\partial v}\}dv . \qquad (5.6)$$

Again, assuming a Maxwell distribution for the electrons and a constant elastic collision cross section, (5.6) reduces to:

$$P_{elast} = -4\pi \frac{m_e^2}{m_a} (1 - \frac{T_a}{T_e}) \int_o^\infty \nu_c v^4 f_o(v)dv \qquad (5.7)$$

where:

m_a = atomic mass.

After some elementary calculus this expression can be written as

$$P_{elast} = 24\sqrt{\frac{2}{\pi}}\ \frac{m_e^{1/2}k^{3/2}Q_o}{m_a}\ n_a n_e T_e^{1/2}(T_e - T_a) \qquad (5.8)$$

Substitution of expressions (5.5) and (5.8) into the balance equation (5.2) finally yields the following relation between the electron temperature and the gas temperature

$$\frac{T_e^2}{T_a}\left(1 - \frac{T_a}{T_e}\right) = \frac{m_a q^2}{18\, m_e Q_o^2}\left(\frac{E}{p}\right)^2 \qquad (5.9)$$

From this relation it follows that for a specific discharge gas the ratio $\frac{T_e}{T_a}$ depends only on the reduced electric field (E/p). This is illustrated in Fig. 5.3 where for neon the value of $\frac{T_e}{T_a}$ is plotted versus (E/p) .

5.2.4 The dissipation function.

In expression (5.5) the heat dissipation function P_{joule} is expressed in terms of n_e, n_a, E and T_e. When we introduce the usual approximation stating that the electric field is approximately constant over the cross-section of the discharge, the expression for the Joule dissipation in the case of a Maxwell electron energy distribution reduces to

$$P_{joule} = S_j\ \frac{n_e}{n_a}\ T_e^{-1/2} \qquad (5.10)$$

where

$$S_j = \frac{4}{3}\sqrt{\frac{2}{\pi}}\ \frac{q^2E^2}{Q_o\sqrt{km_e}} \qquad (5.11)$$

From this relation it follows that once the electron temperature dependence of the electron density is known, the energy dissipation function can be expressed as a function of T_e and therefore with the

aid of eq.(5.9) as a function of T_a. Then the Heller-Elenbaas equation can be solved in principle. In order to find the relationship between n_e and T_e, however, a detailed discussion of the various particle balances is necessary.

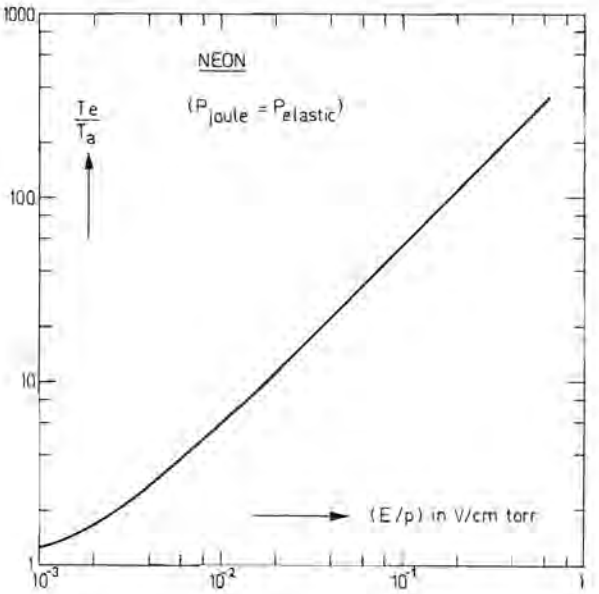

Fig. 5.3 Relationship between electron temperature and gas temperature as a function of (E/p).

5.3 Relevant atomic processes

Under the conditions of the experiment it is expected that two processes are in principle responsible for the formation of electrons and atomic ions i.e. direct ionization and stepwise ionization. Although it is known that in the low pressure and the moderate pressure discharges stepwise ionization via the metastable state is the dominant ionization process, it is questionable if in the high pressure discharge the same

situation occurs, since here the metastable atoms are destroyed efficiently in two and three body collisions[30]. In order to conclude which ionization mechanism is dominant in the constricted positive column we shall consider first the coupled particle balances of resonant and metastable atoms.

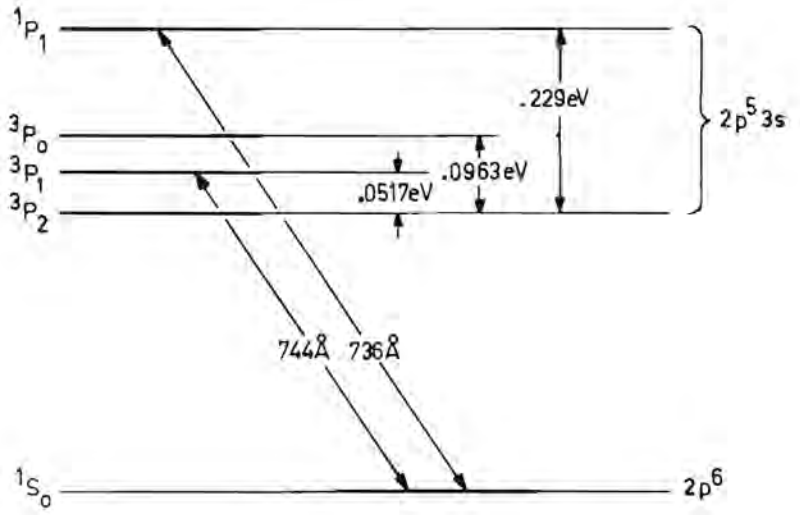

Fig. 5.4 Simplified energy level diagram for neon showing the ground state and the four levels of the $1S^2\ 2S^2\ 2P^5\ 3S$ configuration

In their most general form these particle balances are extraordinary complicated. Fortunately in the high pressure positive column there are only a few processes dominating the formation and destruction of metastable and resonant atoms. For that reason various formation and destruction mechanisms are neglected of which it is expected that they play only a minor part in these particle balances. In this category fall: decay from higher energy states to the resonant state, diffusion of metastable and resonant atoms, stepwise ionization and excitation from the resonant state. Under these conditions, the particle balance for metastable atoms can be written as

$$n_e n_a \nu_{em} + A n_R n_a = n_e n_m \nu_{im} + a A n_a n_m + \gamma_m n_m n_a^2 \qquad (5.12)$$

where:

n_R = concentration of atoms in the resonant ($^3P_1$) state.
n_m = concentration of atoms in the metastable ($^3P_2$) state.
A = two body collision coefficient
γ_m = three body collision coefficient
ν_{em}; ν_{im} are the collision frequencies per unit electron density for direct excitation to and for stepwise ionization from the metastable state.

This collision frequency per unit density is defined in a general form by

$$\nu_c = \frac{1}{n_e} \int_0^\infty 4\pi v^3 f_o(v)\, Q_c(v) dv \qquad (5.13)$$

where:

v = relative speed of the colliding particles
$Q_c(v)$ = cross section for the collision process involved.

For the atoms in the resonant state, the balance equation reads

$$n_e n_a \nu_{eR} + a A n_m n_a = \nu_n n_R - \nu_n \iiint_{vol} n_R(\vec{r}') G(\vec{r}-\vec{r}') d\vec{r}' + A n_R n_a \qquad (5.14)$$

where:

ν_{eR} = collision frequency per unit electron density for direct excitation to the resonant state.
ν_n = frequency for spontaneous decay
$G(\vec{r}-\vec{r}')$ = the probability that radiation emitted at r will be absorbed ar r'.
a = ratio of the frequency per unit metastable atom density of excitation to the frequency per unit resonant atom density of deexcitation from the metastable to the resonant state.

This ratio: a may be obtained from the principle of detailed balancing

$$a = \frac{(2J_m+1)}{(2J_R+1)} \exp(-\frac{\Delta E_{RM}}{kT_a}) \qquad (5.15)$$

where:

J_R and J_M are the J values of the resonant and metastable state resp.

ΔE_{RM} = the energy separation between these states.

An approximate calculation carried out by Phelps.[30] shows that the terms in eq. (5.14), representing the "diffusion" of resonance radiation, are of the order $10^5(sec^{-1})$ under the conditions of our experiments, so that their influence on the balance equation may be neglected since all other terms are several orders of magnitude larger. In this case n_R can be solved from eq. (5.14) giving

$$n_R = \frac{n_e n_a \nu_{eR} + aAn_m n_a}{A\, n_a} \qquad (5.16)$$

Substitution of this expression into the balance equation for n_m yields the following expression for the ratio of the concentration of metastables to the concentration of neutral atoms

$$\frac{n_m}{n_a} = \frac{n_e \nu_{em} + n_e \nu_{eR}}{n_e \nu_{im} + \gamma_m n_a^2} \qquad (5.17)$$

To compare the decay rates of metastable atoms in stepwise ionisation and in three body collisions, one needs reliable values of the rate coefficient for the latter effect, especially for the high gas temperatures occuring in the constricted column. Unfortunately, rate coefficients in neon for this process are only available in the gas temperature range from 70 to 500 Kelvin. In this region the three body collision coefficient may be represented by the following empirical relation

$$\gamma_m = \gamma_{mo} \exp\left(\frac{T_a}{T_3}\right) \tag{5.18}$$

where:

γ_{mo} and T_3 are numerical constants

An extrapolation of the temperature dependence of γ_m according (5.18) to higher gas temperatures is only allowed if the reaction products created in the three body collisions have a very short lifetime. Following the suggestions of Edwin and Turner[31], Prince and Robertson[32] and Colli[33], we assume that in the three body collisions an excited neon molecule is formed which has a high transition probability to the ground state. Consequently both the density of excited molecules and the intensity of molecular U.V. radiation must increase rapidly with increasing gas temperatures. This is in agreement with experimental investigations of Tanaka[34] who observed a large U.V. continuum of molecular origin and only two weak atomic resonance lines in a similar discharge as the one considered here. Moreover it may be concluded from the investigations of Wilkinson[35] that the energy of the excited molecules responsible for the strong U.V. continuum must be close to the energy of the resonant state. This experimental fact also suggests a temperature dependence of γ_m as given by (5.18) at high temperatures. As no more information about these excited molecules concerning lifetime, dissociation energy etc., is available, it is assumed as a hypothesis that their formation and decay is governed by the processes proposed in the foregoing. Starting from a temperature dependence for γ_m given by (5.18) it may easily be shown that under the actual experimental conditions

$$\gamma_m n_a^2 \gg n_e \nu_{im} \tag{5.19}$$

This is illustrated in Fig. (5.5), where the decay frequency for stepwise ionization from the metastable state is compared as a function of the electron temperature with the decay frequency for metastables in three body collisions at various gas temperatures. For the calculation of ν_{im} use was made of an empirical approximation for the energy dependence

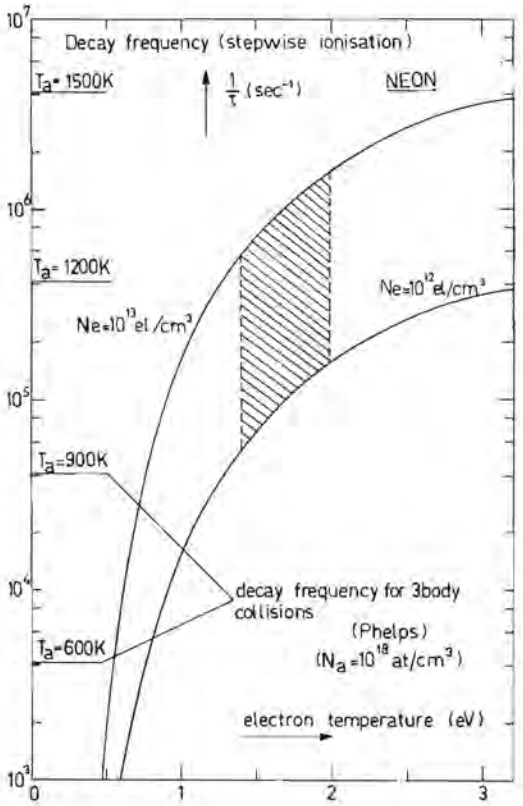

Fig. 5.5 Decay rates for stepwise ionization and 3 body collisions as a function of the gas temperature.

of the cross section for stepwise ionization,(Fabrikant)

$$u < u_o \quad Q(u) = 0$$

$$u \geq u_o \quad Q(u) = eQ(U_m)\left[\frac{U-U_o}{U_m-U_o}\right] \exp\left[-\frac{U-U_o}{U_m-U_o}\right] \qquad (5.20)$$

where:

U_m = energy for which Q reaches its maximum value. $Q(U_m)$.

e = 2.73 .....

U_o = energy difference between ionization energy and energy of atoms in the metastable state.

The various numerical values were taken from Rutscher[36]. The values of T_3 and γ_m were calculated from experimental values of γ_m given by Phelps[30].

From Fig. (5.5) it follows that for the conditions of the experiment (5.17) reduces to

$$\frac{n_m}{n_a} = \frac{n_e \nu_{em} + n_e \nu_{eR}}{\gamma_m n_a^2} \tag{5.21}$$

5.3.2 The ionization mechanism.

The metastable atom density largely influences the ionization mechanism in the positive column. This can be seen by considering relation (5.22) where the ratio of the number of ions formed per second per unit volume in stepwise ionisation z_{im} to the number of ions formed per second per unit volume in direct ionization z_{di} is given.

$$\frac{z_{im}}{z_{di}} = \frac{n_m}{n_a} \frac{\nu_{im}}{\nu_{di}} \tag{5.22}$$

where:

ν_{di} = collision frequency for direct ionization.

With the aid of expression (5.21) this formula can be written as

$$\frac{z_{im}}{z_{di}} = \frac{\nu_{im}}{\nu_{di}} \frac{n_e \nu_{em} + n_e \nu_{eR}}{\gamma_m n_a^2} \tag{5.23}$$

For the numerical calculation of this ratio, use has been made of an approximation for the cross-sections for direct and stepwise ionization given by Fabrikant. Moreover the simplifying assumption $\nu_{eR} = \nu_{em}$ was made. The various values of the relevant parameters were again taken from Rutscher. By making these approximations a relative error of about 100 per cent may be introduced, so that this calculation has to be considered as an order of magnitude estimation rather than as an exact description of the ionization mechanism. In spite of these

uncertainties, the numerical results presented in Fig. (5.6) provide a lot of information about the ratio of direct to stepwise ionization in the high pressure discharge.

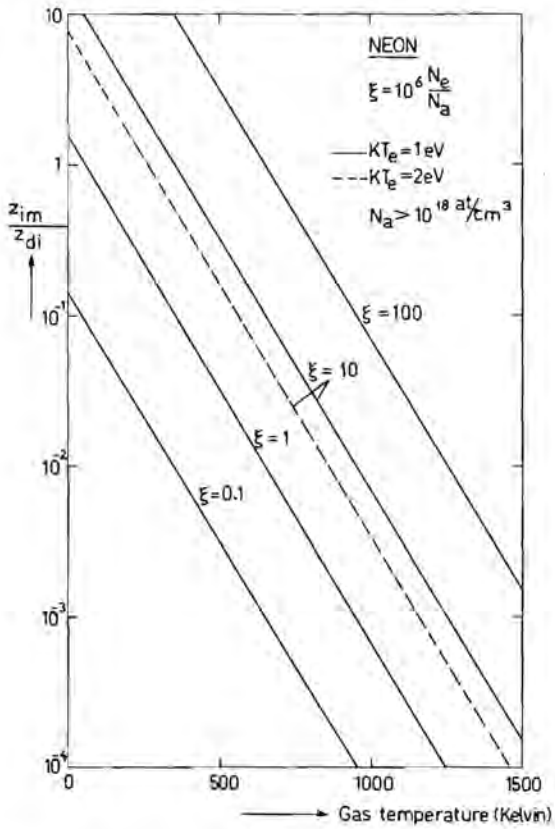

Fig. 5.6 Ratio of stepwise to direct ionization as a function of the gas temperature.

In this figure we can see that at low gas temperatures and high electron densities the ionization mechanism is largely stepwise whereas at high gas temperatures the ionization mechanism is direct, even at high electron densities.

5.3.3 Charged particle balance.

In the preceding section it was shown that the atomic ions are formed in direct ionizing collisions with the neutral atoms. The destruction of the charged particles, in particular of the electrons, is a somewhat more complicated process. While in the low pressure column the electrons and ions are transported to the wall by ambipolar diffusion, where they recombine, at high pressures this wall recombination can be neglected with respect to volume recombination. This can be seen from the following expressions for the transport c.q. destruction of electrons by ambipolar diffusion and volume recombination resp.

$$\frac{\partial n_e}{\partial t} = \frac{kT_e}{q_i \lambda_a^2} \mu_i n_e \simeq 20\ n_e\ \text{el/cm}^3\ \text{sec} \quad \text{(ambipolar diffusion)}$$

Where:

μ_i = mobility of ions in their own gas.

λ_a = a parameter characterising the first diffusion mode

$$\lambda_a = \frac{2{,}4}{R}$$

R = radius of the discharge tube.

$$\frac{\partial n_e}{\partial t} \simeq \alpha_r n_e^2 \simeq 10^{-7}\ n_e^2\ \text{el/cm}^3\text{sec.} \quad \text{(volume recombination)}$$

where:

α_r = recombination coefficient.

A comparison of the numerical values of both expressions for electron densities in the range (10^{12} - 10^{14} el/cm^3), immediately shows that for our experimental conditions the influence of ambipolar diffusion on the charged particle balances can be neglected.

The most important destruction process for the atomic ions is the so-called conversion process in which an atomic ion is converted into a molecular ion in a collision with two neutral gas atoms.

$$Ne^+ + 2Ne \rightarrow Ne_2^+ + Ne \tag{5.24}$$

Since the rate coefficient of this process is proportional to n_a^2, this process becomes very probable at high gas densities.[37]

The molecular ions formed in this way capture electrons with a great efficiency to form instable neon molecules, each decaying to an excited and a neutral atom. This process, called: dissociative recombination is schematically described in eq. (5.25)

$$Ne_2^+ + e^- \rightarrow (Ne_2) \rightarrow_{\text{instable}} Ne' + Ne + E_{kin}. \tag{5.25}$$

For neon, this process and in particular the temperature dependence of the recombination coefficient was studied extensively by O'Conner, Biondi, Frommhold and Mehr[38][39][40].

If the influence of other possible formation and destruction processes is neglected the charged particle balances can be written as

$$\begin{aligned} \frac{\partial n_e}{\partial t} &= n_e\, n_a\, \nu_{di} - \alpha_r\, n_2^+\, n_e = 0 \\ \frac{\partial n^+}{\partial t} &= n_e\, n_a\, \nu_{di} - \beta\, n_a^2\, n^+ = 0 \\ \frac{\partial n_2^+}{\partial t} &= \beta\, n_a^2\, n^+ - \alpha_r\, n_2^+\, n_e = 0 \end{aligned} \tag{5.26}$$

Since in the plasma atomic ions (n^+) as well as molecular ions (n_2^+) are present the quasi-neutrality conditions reads

$$n_e = n^+ + n_2^+ \tag{5.27}$$

The purpose of the calculations presented in this paragraph is to find an expression for n_e. This expression can be found by solving the set of coupled equations presented in (5.26) and (5.27), giving for n_e:

$$\frac{n_e}{n_a} = \frac{\nu_{di}}{\alpha_r} + \frac{n_e \nu_{di}}{\beta n_a^2} \qquad (5.28)$$

For the actual experimental conditions

$$\nu_{di} << \beta n_a,$$

so that eq. (5.28) reduces to:

$$\frac{n_e}{n_a} = \frac{\nu_{di}}{\alpha_r} \qquad (5.29)$$

If ν_{di} is calculated according to (5.13), the expression (5.29) can be written as

$$\frac{n_e}{n_a} = \frac{4}{\alpha_r} \sqrt{\frac{2}{\pi m_e}} e \frac{Q_i(U_m) U_o' U^{\frac{1}{2}}}{(U_m - U_o')} (1 + 2 \frac{U}{U_o'}) \exp(- \frac{U_o'}{U}) \qquad (5.30)$$

where:

$Q_i(U_m)$ = maximal value for the cross section for direct ionization.
U_m = electron energy for which Q_i is maximal.
U_o' = threshold energy of Q_i.
U = electron energy (kT_e).

This equation, that was obtained by a detailed consideration of the various particle balances in the plasma, may be considered as a modified Saha-equation, describing the equilibrium in the formation and destruction of charged particles in the constricted high pressure positive column.

5.3.4. The heat dissipation function.

After this extensive discussion of the relevant atomic processes, we focus our attention on the calculation of the heat dissipation function.

Elimination of $\frac{n_e}{n_a}$ from the general relation for P_{joule} (eq. 5.5) and the modified Saha-equation, obtained in the preceding sections, (eq. 5.30) yields for P_{joule}:

$$P(U)_{joule} = \frac{32e}{3\pi} \frac{q^2E^2\, Q(U_m)U_o'}{m_e\alpha_r\, Q_o(U_m-U_o')} (1 + 2\frac{U}{U_o'}) \exp(-\frac{U_o'}{U}) \qquad (5.31)$$

Since we are especially interested in the shape of P_{joule} as a function of r, the ratio $P(r) = \frac{P_j(r)}{P_j(o)}$ was calculated.

$$P(r) = \left[1 + 2U'(S(r) -1)\right] \exp\left[-\frac{1}{U'}\left(\frac{1}{S(r)} - 1\right)\right] \qquad (5.32)$$

where:

$$S(r) = \frac{U(r)}{U(o)}$$

$$U' = \frac{U(o)}{U_o'}$$

For the actual values of $T_a(r)$ and $T_e(r)$ equation (5.9) can be approximated with a relative inaccuracy of less than 1 per cent by the following simple relation

$$\frac{T_e(r)}{T_e(0)} = \frac{T_a(r)}{T_a(o)} \quad \text{or} \quad S(r) = \frac{T_a(r)}{T_a(o)} \qquad (5.33)$$

Although P(r) can now be expressed in terms of $T_a(r)$ with the aid of eq. 5.33, a direct solution of the Heller-Elenbaas equation written in this form gives rise to a lot of mathematical difficulties. For that reason we have chosen another procedure.

If the gas temperature distribution is known, the shape of P(r) can be calculated from eqs. 5.33 and 5.32. In chapter IV it was shown, that the experimental gas temperature distribution can in a large range of plasma parameters be represented by an empirical relation of the form

$$S(r) = \theta + \frac{1-\theta}{1 + \frac{r^2}{\beta^2}}$$

With the aid of this empirical gas temperature distribution and after some elementary calculus P(r) can be expressed as

$$P(r) = (1 + \theta \frac{r^4}{r_o^2 \beta^2}) \quad \exp(- \frac{r^2}{r_o^2}) \tag{5.34}$$

where:

$$r_o^2 = \frac{\beta^2 U'}{(1-\theta)} \tag{5.34b}$$

Since under the conditions prevailing in the high pressure high current discharge $r_o << R$, this expression shows that P(r) may in the first order approximation be written as a Gauss function multiplied by a correction term deviating only slightly from unity. The influence of the correction function did not exceed 5% in our experiments. In Fig. (5.7), for a discharge with a filling pressure of 415 torr and a discharge current of 300 mA, P(r) calculated according to eq. (5.34) is presented. The experimental gas temperature distribution used in this calculation is also plotted in the figure.
From the foregoing it is clear that in the constricted high pressure positive column the heat dissipation function may be represented by the general relation

$$P(r) = \sum_{\mu=0}^{\infty} a_\mu (\frac{r}{\rho})^{2\mu} \exp(- \frac{r^2}{\rho^2}), \tag{5.35}$$

where ρ is introduced as an unknown parameter, characterising the width of the dissipation function and $a_0 = 1$. It follows from what has been

said before, that the power series for $\mu > 0$ in expression (5.35) must be considered as a small correction term to the Gauss function : $\exp(-\frac{r^2}{\rho^2})$.

With the help of eq. (5.35) the dissipation term in the Heller-Elenbaas equation can be written as a function of the independent variable r only, which enables a direct solution of this equation.

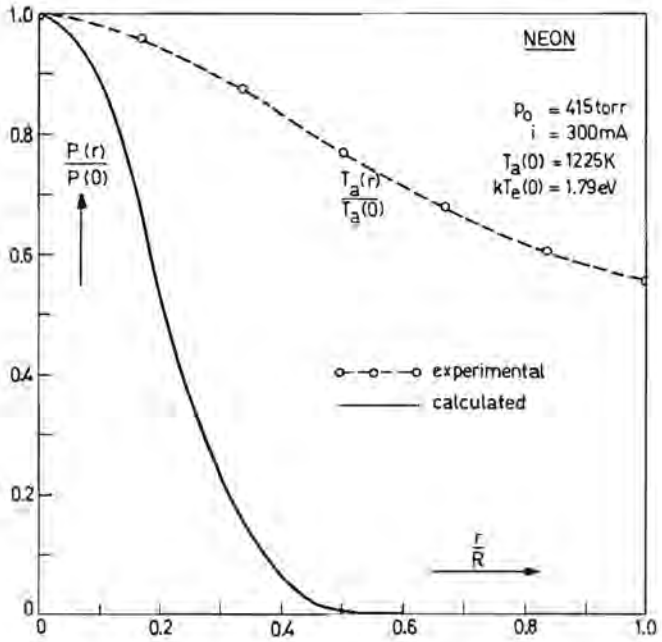

Fig. 5.7 The shape of the dissipation function P(r) calculated from the experimental gas temperature distribution presented in the figure.

5.4 The solution of the Heller-Elenbaas equation.

For a heat dissipation function as given by (5.35) the Heller-Elenbaas equation can be written as

$$\frac{1}{r}\,\frac{d}{dr}\Big[\, r\,\lambda(T_a(r))\,\frac{dT_a(r)}{dr}\,\Big] = -\,P(o)\sum_{\mu=0}^{k} a_\mu\,\Big(\frac{r}{\rho}\Big)^{2\mu}\exp\Big(-\frac{r^2}{\rho^2}\Big), \qquad (5.36)$$

with the boundary conditions

$$T_a(r) = T_a(0) \text{ and } \frac{dT_a(r)}{dr} = 0 \text{ for } r = 0 \qquad (5.37)$$

This equation can be solved by direct integration giving

$$r\,\lambda(T_a(r))\,\frac{dT_a(r)}{dr} = -\,\frac{P(0)}{2}\sum_{\mu=0}^{k}\Big[a_\mu\,\rho^{2(\mu+1)}\{\mu!-\exp\Big(-\frac{r^2}{\rho^2}\Big)\sum_{j=0}^{\mu}\frac{\mu!}{j!}\Big(\frac{r}{\rho}\Big)^{2j}\}\Big] \qquad (5.38)$$

When for λ the usual temperature dependence is assumed

$$\lambda(T_a(r)) = \lambda_o\,T_a^m(r), \qquad (5.39)$$

a second integration of (5.38) leads to the final general solution of the Heller-Elenbaas equation

$$T_a^{(m+1)}(\xi) - T_a^{(m+1)}(0) = -\,\frac{P(o)}{4\lambda_o}(m+1)\sum_{\mu=0}^{k} a_\mu\rho^{2(\mu+1)}\mu!\Big[\sum_{n=1}^{\infty}\frac{(-1)^n}{nn!}\xi^n + \sum_{p=1}^{\mu}\frac{1}{p}(1-e^{-\xi})\times$$

$$\times\sum_{j=o}^{(p-1)}\frac{\xi^j}{j!}\Big)\Big] \qquad (5.40)$$

Where:

$$\xi = \frac{r^2}{\rho^2}$$

In case the polynomial in eq. (5.36) has such a small influence that it may be neglected, the complex expression (5.40) is considerably simplified and after some rearrangements reduced to

$$\frac{T_a(r)}{T_a(o)} = \left[1 + K \sum_{n=1}^{\infty} \frac{(-1)^n}{n.n!} \left(\frac{r}{\rho} \right)^{2n} \right]^{\frac{1}{(m+1)}} \qquad (5.41)$$

where:

$$K = \frac{(m+1)\ P(0)\rho^2}{4\lambda_o\ T_a^{(m+1)}(o)}\ , \qquad (5.41b)$$

The most important property of this solution is that, apart from the scale factor ρ, its shape is uniquely determined by the total input per unit column length ($\simeq \pi P(o)\rho^2$). The gas temperature distribution according to (5.41) is plotted in Fig. (5.8) for some values of K as a function of the dimensionless parameter $\left(\frac{r}{\rho} \right)$.
From this figure it follows that with increasing K, the gas temperature distribution varies from nearly a constant ($K < 0{,}1$), via a Lorentzlike distribution function ($0{,}1 < K < 0{,}3$) to a nearly parabolic one.

As it is assumed for the solution of the Heller-Elenbaas equation that the heat conductivity of the wall largely exceeds that of the plasma, the temperature distribution inside this wall is not affected by the presence of such a wall. This assumption enables us to represent a wall with radius R in Fig. (5.8) by a vertical line at a distance $\frac{R}{\rho}$ from the origin. So when the presence of the wall is taken into account, the gas temperature distribution to be expected in a certain discharge, apart from K, depends also on the value of the dimensionless parameter $\frac{R}{\rho}$.

An other important conclusion that can be drawn from an investigation of solution (5.41) is, that for each value of K there exists a maximum discharge tube radius: R_m, above which the gas temperature gradient is too low to transport the amount of input energy, characterised by K, by conduction. This maximal value $(\frac{R_m}{\rho})$ is found from the boundary conditon

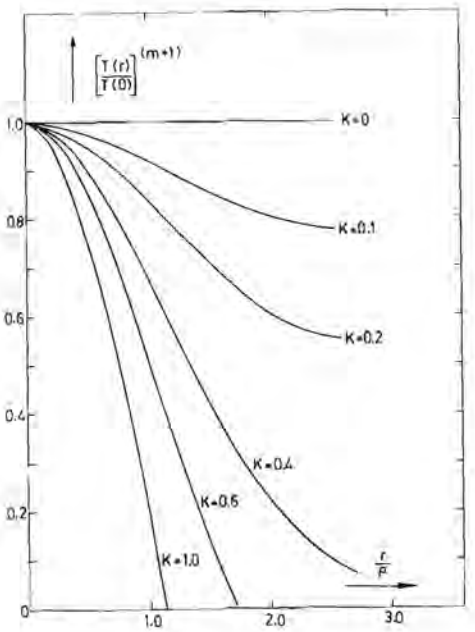

Fig. 5.8 Some theoretical gas temperature distributions plotted for various values of K.

$$T_a\left(\frac{R_m}{\rho}\right) = 0 \tag{5.42}$$

Its value can be calculated from the implicite equation

$$\sum_{n=1}^{\infty} \frac{(-1)^n}{n\, n!} \left(\frac{R_m}{\rho}\right)^{2n} = -\frac{1}{K} \tag{5.43}$$

Although the model developed in the present work is, strictly speaking, only valid for the constricted high pressure positive column, the general solution of the Heller-Elenbaas equation written in the form of (5.36) appears to be valid in a much wider range of plasma parameters. This is illustrated in Fig. (5.9) and Fig. (5.10), where for a moderate

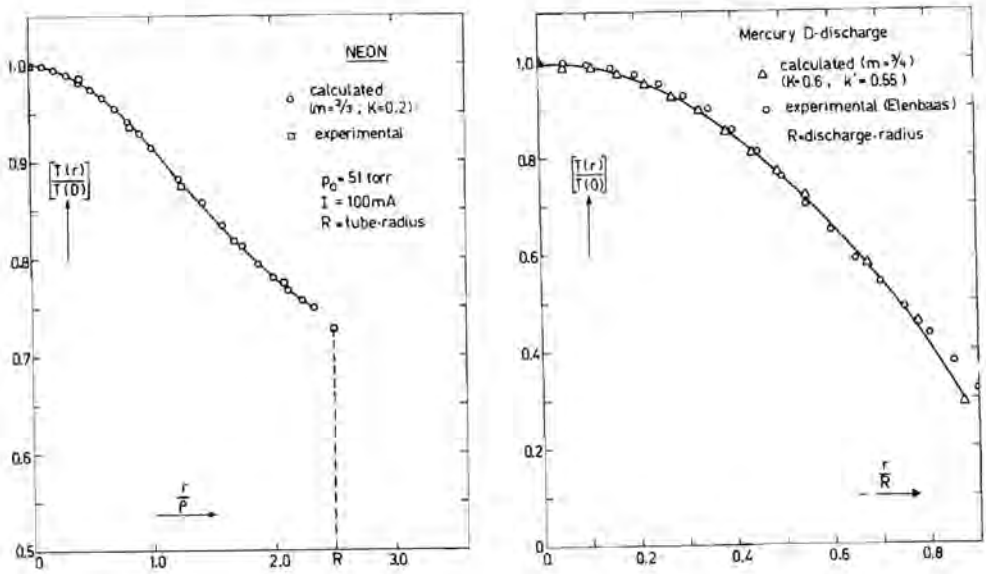

Fig. 5.9; 5.10 Some experimental gas temperature distributions for non-constricted discharges. The best fits to the theoretical gas temperature distribution (5.41) are also shown.

pressure discharge ($p_0 \approx 50$ torr) and a high pressure arc in mercury ($p_0 \approx 1$ atm) the theoretical distributions given in (5.41) are fitted to the experimental gas temperature distributions. The best fits are presented in the figure.

5.5 Approximate solutions.

5.5.1 The gas temperature distribution.

Although expression (5.41) is a very good representation of the gas temperature, for practical purposes and for many theoretical calculations a simpler approximation of this solution will do. Mostly one is only interested then in the exact form of the behaviour of the gas temperature

distribution function near the axis of the discharge tube whereas only a rough approximation of the temperature distribution near the discharge wall is needed . A typical example of such a simple temperature distribution is the frequently used parabolic one. This special distribution can be obtained from expression (5.41) by assuming that both K and $\frac{r}{\rho}$ are much smaller than unity. Under these conditions eq. (5.41) reduces to

$$T_a(r) = T_a(0)\left[1 - \frac{K}{m+1}\frac{r^2}{\rho^2}\right] \tag{5.44}$$

Following the conventional procedure to fit this function to the experimental values $T_a(0)$ and $T_a(R)$ we obtain

$$T_a(r) = T_a(0)\left[1 - (1 - \frac{T_a(R)}{T_a(0)})\frac{r^2}{\rho^2}\right] \tag{5.45}$$

Although relation (5.44) provides a good approximation of the real temperature distribution for small r-values, an extrapolation to large r-values may lead to a considerable systematic error. This is illustrated also in Fig. (4.1) , where this parabolic function is compared with expression 5.41 and with the experimental distribution.

A better approximation of the gas temperature distribution is the empirical distribution presented in chapter 4.

$$\frac{T_a(r)}{T_a(0)} = \theta + \frac{(1-\theta)}{1 + \frac{r^2}{\beta^2}} \tag{5.46}$$

This distribution function, which appeared to be a good approximation for all our experimental gas temperature distribution functions is theoretically valid for K values between 0,1 and 0,3. In terms of plasma parameters this conditions corresponds with low, moderate and high pressures, and moderate discharge currents.
Since the behaviour of this function must be identical to that of expression 5.41 for low r-values, a comparison of the first terms in the series representations of both functions yields the following relations:

$$(1-\theta)\frac{\rho^2}{\beta^2} = \frac{K}{(m+1)} \quad \text{and} \quad \rho^2 = \frac{\beta^2}{2m(1-\theta)+4} \tag{5.47}$$

If the expression for K, (5.41b) is rewritten in the form,

$$T_a(0)^{(m+1)} = \frac{(m+1)}{4\pi\lambda_o K} P_t \tag{5.48}$$

where:

P_t = the total power input per unit column length.

This equation predicts a linear relationship between $T_a(0)^{(m+1)}$ and P_t. For the special case of a constricted positive column in neon where m = 2/3 this theoretical result is in good agreement with the experiments as can be seen from Fig. (5.11)

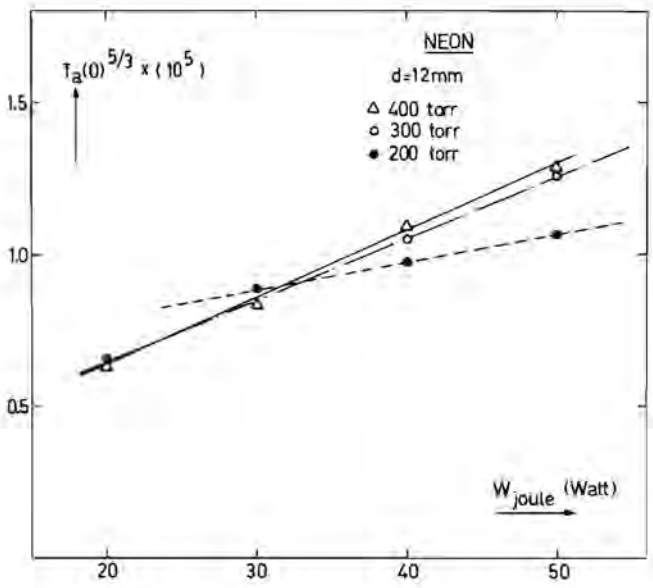

Fig. 5.11 Gas temperature at the axis as a function of the total power input W(= IxV).

5.5.2 The electron temperature distribution.

From eq.(5.33) it follows that the electron temperature distribution has the same shape as the gas temperature distribution. However, this relationship is only valid for the active part of the plasma. Consequently the similarity of the shapes of the gas temperature and the electron temperature distributions holds only for r-values given by the following inequality.

$$r < 2\rho \tag{5.49}$$

Within the scope of the approximations presented in the foregoing, P(r) may be represented by a pure Gauss function as can be seen in eq.(5.34); so the variable ρ in eqs. (5.36) through (5.48) may be replaced by the quantity r_o defined in eq. (5.34b). From the identity of r_o and ρ using eq. (5.47), an expression for the electron temperature in the axis, $T_e(0)$, can be derived which reads

$$kT_e(0) = \frac{qV_i(1-\theta)}{2m(1-\theta) + 4} \tag{5.50}$$

This relation offers the possibility to find a good approximation of the electron temperature at the axis if the parameter θ is known. The electron temperatures $T_e(0)$ calculated with the aid of the experimental θ-values according to eq. (5.50) are plotted in Fig. 5.12 versus the total input P_t(= IxV).
It can be seen from this figure, that the electron temperature is independent of gas pressure and discharge current; it is uniquely defined by the total power input P_t. Since in a first apprximation the ratio of $T_a(0)$ and $T_e(0)$ is constant, this experimental fact is in good agreement with the theoretical and experimental results expressed in eq. (5.48) and Fig. (5.11) resp.

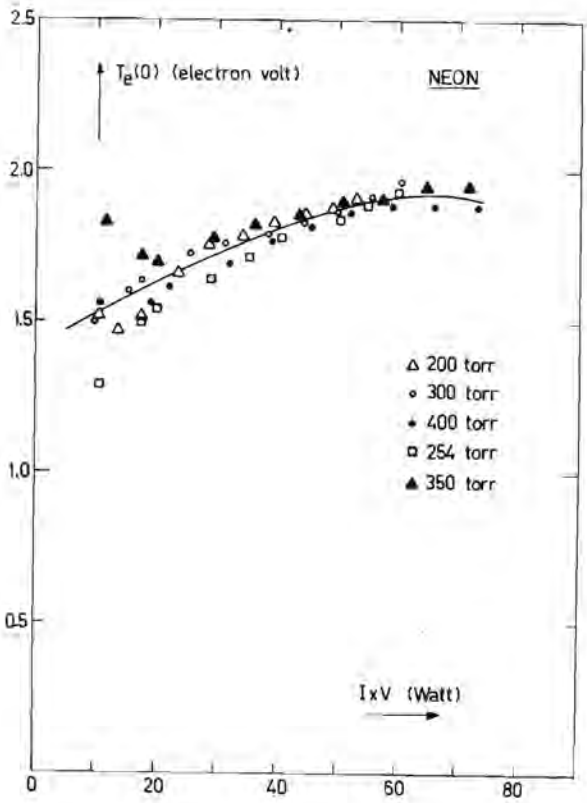

Fig. 5.12 Electron energy kT_e as a function of the total power input $W(= IxV)$.

5.5.3 The spatial distribution of spectrum line radiation.

The high pressure positive column is characterised by a very strong constriction. This can visually be observed by looking at the light emission of such a column. It appears that this emission takes place in a very narrow channel around the longitudinal axis, whereas the space between this luminous cylinder and the wall remains completely dark. This strong constriction of the light intensity distribution can only be understood by assuming a strong electron temperature

dependence of the excitation mechanism. From a consideration, analogous to that developed for the treatment of the ionization mechanism, it follows that the excitation mechanism is in a first approximation direct as well. If filling up from higher energy states is neglected, one may write for the power emitted per unit volume in a spectral line with central frequency ω_{nm}:

$$L_{nm}(r) \sim n_e n_a \nu_{en} \tag{5.51}$$

where:

ν_{en} = the collision frequency for direct excitation of the n^{th} energy state.

With the usual approximation of a cross-section given by (5.20) and a Maxwellian electron energy distribution, it is possible to write $L_{nm}(r)$ in the form

$$L_{nm}(r) = \text{const. } n_e n_a T_e^{\frac{1}{2}} \exp\left(-\frac{qV_n}{kT_e}\right) \tag{5.52}$$

where:

V_n = excitation potential of the n^{th} energy state.

Using the modified Saha-equation discussed in section 5.3.3, n_e can be eliminated to give

$$L_{nm}(r) = \text{const. } \exp\left(-\frac{r^2}{\chi^2}\right) \tag{5.53}$$

where:

$$\chi^2 = \frac{V_i}{(V_i + V_n)} \frac{\beta^2}{2m(1-\theta) + 4} \tag{5.54}$$

In the calculation of eq. (5.53) , terms containing lower powers of T_e or T_a were omitted. From this relation it follows that to a first order approximation $L_{nm}(r)$ may be represented by a Gauss-function. This in in good agreement with the experimental results which showed that for high discharge currents ($i > 100$ mA), the function $L_{nm}(r)$ could be

approximated by such a function, with a relative deviation of less than 3 per cent. The experimental values of the parameter χ, which characterises the width of the function $L_{nm}(r)$, were in good agreement with the theoretical values.

5.5.4 The constriction mechanism.

Starting from the theoretical results obtained in the foregoing sections, the constriction mechanism can easily be understood now from a macroscopic point of view. This can be seen as follows.

If in a moderate pressure discharge both the gas pressure and the discharge current are increased, the power input per unit column length P_t increases also. From eq. (5.48) it follows that by increasing P_t, the gas temperature in the axis of the discharge tube increases too. Since the temperature raise of the wall (ΔT_w) is limited ($\Delta T_w \leq 100K$), by increasing P_t to high values ($T_a(0) \approx 1200$-$2000K$), a large gradient in the gas temperature is created. However, in the active part of the discharge plasma ($r < 2\rho$) the relative gradients in the electron temperature and the gas temperature are equal (eq.5.33) so that there also exists a large gradient in the electron temperature. Consequently all characteristic plasma parameters show a strong dependence on the radius. As the gradient in the electron temperature is negative, going from the discharge axis to the discharge wall, the power emitted in a spectrum line per unit volume rapidly decreases. This means that this phenomenon, generally referred to as constriction, has a thermal origin.

5.5.5 Conclusion.

The model for the high pressure positive column presented in this chapter is essentially based on the assumption that the greater part of the energy gain of the electrons in the electric field is transferred to the neutral gas atoms in elastic collisions. This condition in fact causes the strong coupling of electron temperature and gas temperature which in its turn is responsible for the most characteristic properties of the high pressure constricted positive column. Moreover a number of assumptions had to be made for working out the model in more detail. These assumptions, however, are of only minor importance for the plasma model as such. The most important assumptions of this kind are, the Maxwell electron energy distribution, the Fabrikant approximation for the various cross sections and the extrapolation of the three body collision coefficient of metastables to high gas temperatures. If these assumptions are not fulfilled, the model presented can easily be adapted to other more adequate suppositions, which, in particular cases may be in better agreement with reality. The influence of such modifications should not be overestimated, however, since the systematic error in the numerical results introduced by the use of various experimental cross sections can hardly be compensated by a refinement of the model as such. Therefore the model presented here will provide a qualitative description of the complex relationship of the various parameters involved. Only in special cases, where the relative behaviour of the cross section is important in the calculations rather than its absolute magnitude, a good description of the behaviour of various quantities can be expected .

Although the validity of the plasma model is limited, the general solution of the Heller-Elenbaas equation (5.41), appears to have a much wider range of applicability than the one discussed here. This has its origin in the fact that experiments as well as calculations have shown that in many practical cases $P(r)$ may in a first approximation be written as a pure Gauss-function. As a consequence, the gas temperature distribution calculated with a pure Gauss-function for $P(r)$ is only determined by two parameters K and ρ resp. This two-parameter representation of the gas temperature distribution has the

great advantage of simplicity, whereas in many practical cases it provides a better approximation than the frequently used parabolic one.

References

1) Kruithof, A.A., Riemens, J., Proc.VIIIth.Conf.Ion.Phen.Gas, 223 (1967).
2) Mouwen, C.A.M., Physica, 44, 381 (1969).
3) Elenbaas, W., The high pressure mercury vapour discharge, North-Holl.Publ.Comp.(Amsterdam) (1951).
4) Maecker, H., Z.Phys, 157, 1 (1959).
5) Hoyaux, M.F., Arc Physics, Springer Verlag (Berlin)(1968).
6) Wojaczek, K., Beitr.Plasmaphys, 6, 211 (1966).
7) Venzke, D., Wojaczek, K., Monatsberichte, 10, 431 (1968).
8) Wojaczek, K., Beitr.Plasmaphys, 9 243 (1969).
9) Forrest, J.R., Franklin, R.N., Brit.J.Appl.Phys, 1, 1357 (1968).
10) Rutsher, A., Beitr.Plasmaphys, 7, 43 (1967).
11) Pfau, S., Beitr.Plasmaphys, 7, 57(1967).
12) Golubowsky, Ju.B., Kagan, Ju. M., Ljagustschenko, R.J., Michel, P., Beitr.Plasmaphys, 8, 423 (1968).
13) Rutsher, A., Pfau, S., Beitr.Plasmaphys, 7, 187 (1967).
14) Rutsher, A., Pfau, S., Beitr.Plasmaphys, 8, 85 (1968).
15) Rutsher, A., Pfau, S., Beitr.Plasmaphys, 8, 73 (1968).
16) Wojaczek, K., Beitr.Plasmaphys, 7, 149 (1967).
17) Belousova, L.E., Sovj.Phys. Techn.Phys, 15, 396 (1970).
18) Ecker, G., Zoller, O., Phys. Fluids, 7, 1996 (1964).
19) Baranov, V.Ju., Uljanov, K.N., Sovj.Phys. Techn.Phys, 14, 183 (1969).
20) Golubowsky, Ju.B., Kagan, Ju.M., Ljagustschenko, R.J., Beitr.Plasmaphys, 10, 427, (1970).
21) Eletskii, A.V., Smirnov, B.M., Sovj.Phys.Techn.Phys, 15, 1308 (1971).
22) Mouwen, C.A.M., Claassens,J.M.M., Phys.Lett, 31A, 123 (1970).
23) Rother, H., Z.Phys, 173, 441 (1963).
24) Thomas, W.R.L., J.Phys.B, 2, 551 (1969).

25) Shaper, M., Scheibner, H., Beitr.Plasmaphys, 9, 45 (1969).
26) Adamczyk, B., et.al, J.Chem.Phys, 44, 4640 (1966).
27) Rapp, D., Englander-Golden, P., J.Chem.Phys, 43, 1464 (1965).
28) Delcroix, J.L., Plasma Physics, John Wiley & Sons. LTD (1968).
29) Hoffmann, C.R., Skarsgard, H.M., Phys.Rev, 178, 168 (1968).
30) Phelps, A.V., Phys. Rev, 114, 1011 (1958).
31) Edwin, R.P., Turner, R., J.Chem.Phys, 50, 4388 (1969).
32) Prince, J.F., Robertson, W.W., J.Chem.Phys, 46, 3309 (1967).
33) Colli, L., Phys. Rev., 95, 892 (1954).
34) Tanaka, Y., Jursa, A.S., LeBlanc, F.J., J.Opt.Soc.Am, 48, 304 (1958).
35) Wilkinson, P.G., Can.J.Phys, 45, 1715 (1967).
36) Rutsher, A., Beitr.Plasmaphys, 6, 195 (1966).
37) Beaty, E.C., Patterson, P.L., Phys.Rev, 170, 116 (1968).
38) Connor, T.R., Biondi, M.A., Phys. Rev, 140, 778 (1965).
39) Frommhold, L., Biondi, M.A., Phys. Rev, 185, 244 (1969).
40) Frommhold, L., Biondi, M.A., Mehr, F.J., Phys.Rev, 165, 44 (1968).

Summary.

In this thesis the contricted positive column in neon is studied. Since it is believed that the most prominent general characteristics of this discharge type have a thermal origin, most attention has been paid to the behaviour of the gas temperature distribution as a function of the various plasma parameters. These gas temperature distributions have been determined in two essentially different ways. On the one hand these distributions have been obtained directly from thermocouple measurements, while on the other hand they could be calculated from combined gas pressure measurements and spectrum line broadening experiments. In order to obtain some more detailed information about specific phenomena, incidentally various well-known plasma diagnostic methods have been applied. They are briefly reviewed in chapter II.

In chapter III, the results of the spectrum line broadening measurements, performed on a resonance broadened neon line are reported. The spectrum line profile emitted from a homogeneous plasma can be represented by a pure Lorentz function. Since the plasma of the contricted positive column is strongly inhomogeneous, a theory has been developed describing the spectrum line broadening in inhomogeneous plasmas. It appeared that the inhomogeneity of the plasma, as far as it is relevant for the line broadening, can be characterised by only one representative parameter called "the spectral inhomogeneity". Further it was shown that for low values of this parameter the observed line profile could be approximated very well with a Lorentz function. Starting from this concept a new method has been developed and verified experimentally to determine the gas temperature in the axis of a strongly inhomogeneous plasma. The results calculated from this theory are in good agreement with the experimental results of both the line broadening experiments and the thermocouple measurements.

In chapter IV the results of the thermocouple measurements are discussed . Since only little is known about the systematic error of such measurements, performed in plasmas, this diagnostic method was scarcely used in plasma physics. From the present work, however, it follows that the systematic error in the thermocouple measurements is

mainly caused by thermal radiation of the thermocouple. By taking into account this loss of heat, the systematic error in the interpretation of the thermocouple measurements has been reduced to about 5 per cent of the absolute value of the temperature found. Moreover a simple empirical formula for the gas temperature distribution has been obtained which gives a better representation of this distribution in a much wider range of plasma parameters than the frequently used parabolic one.

Based on the numerous experimental results obtained from the experiments mentioned, in chapter V a new model for the constricted positive column has been developed. Since in this column both the reduced electric field and the electron temperature are very low, the greater part of the energy gain of the electrons in the electric field is transferred to the neutral gas atoms in elastic collisions. Consequently the electron temperature and the gas temperature are strongly coupled. Starting from this basic concept some distribution functions for relevant plasma quantities have been calculated. These theoretical distribution functions and especially the gas temperature distributions are in good agreement with those obtained from the experiments mentioned.

Samenvatting.

In dit proefschrift wordt een onderzoek beschreven naar de eigenschappen van de positieve zuil van een gecontraheerde ontlading in neon. Daar wij menen dat de meest kenmerkende eigenschappen van dit ontladingstype een thermische oorzaak hebben, is bijzonder veel aandacht besteed aan het gedrag van de radiale verdeling van de gastemperatuur als functie van een aantal relevante ontladingsparameters. Deze gas temperatuursverdelingen zijn bepaald met behulp van twee essentieel verschillende meetmethoden. Enerzijds werden deze verdelingen rechtstreeks verkregen uit thermokoppelmetingen, anderzijds konden ze berekend worden uit de resultaten van gecombineerde metingen van gasdruk en spectrale lijnverbreding. Om een beter inzicht te verkrijgen in bepaalde details van het gedrag van de gecontraheerde zuil werden bovendien een aantal bekende plasma diagnostische methoden gebruikt die kort zijn beschreven in hoofdstuk II.

In hoofdstuk III worden de resultaten vermeld van de lijnverbredingsexperimenten. Deze hebben voornamelijk betrekking op de metingen van de halfwaardebreedte van een door resonantieverbreding bepaalde spectraallijn uitgezonden door de gecontraheerde neon zuil. Het profiel van een door resonantieverbreding bepaalde spectraallijn, geemitteerd door een homogeen plasma kan mathematisch worden beschreven door een zuivere Lorentzfunctie.

Aangezien het plasma van deze zuil echter sterk inhomogeen is, moest een theorie ontwikkeld worden voor de interpretatie van de lijnverbreding in een inhomogeen plasma. Uit deze theorie bleek dat de inhomogeniteit van het plasma, voor zover deze van belang is voor de lijnverbreding, kan worden gekarakteriseerd door één parameter die we hebben genoemd de "spectrale inhomogeniteit". Verder is aangetoond dat voor kleine waarden van deze parameter het gemeten lijnprofiel zeer goed benaderd kan worden door een Lorentzfunctie. De numerieke resultaten berekend met deze theorie waren in goede overeenstemming met de experimentele resultaten van zowel de lijnverbredingsexperimenten als van de thermokoppelmetingen.

In hoofdstuk IV worden de resultaten besproken van de gastemperatuursmetingen met behulp van thermokoppels. Aangezien over de nauwkeurigheid hiervan in wijde kring veel onzekerheid bestaat is speciale aandacht besteed aan de systematische fouten in dergelijke metingen. Hieruit is gebleken dat deze systematische fout voornamelijk wordt veroorzaakt door de thermische straling van het thermokoppel. Door de metingen te corrigeren voor dit storend verschijnsel, kon de relatieve systematische fout in deze metingen worden teruggebracht tot ongeveer 5 procent van de gevonden absolute temperatuur. Bovendien volgde uit dit onderzoek een empirische formule voor de verdeling van de gastemperatuur in een zuilontlading. Deze verdelingsfunctie geeft een betere beandering en is algemener geldig dan de veel gebruikte parabolische verdelingsfunctie.

Uitgaande van de talrijke experimentele resultaten van de genoemde metingen is in hoofdstuk V een nieuw model van de gecontraheerde positieve zuil ontwikkeld. Aangezien in deze zuil zowel de gereduceerde veldsterkte als de electronentemperatuur laag zijn, wordt het overgrote deel van de energie, die de electronen winnen in het electrische veld, in elastische botsingen overgedragen op de neutrale gasatomen. Hierdoor ontstaat een zeer sterke koppeling tussen de electronentemperatuur en de gastemperatuur. Uitgaande van dit fundamenteel gegeven, worden een aantal verdelingsfuncties berekend van relevante plasmaparameters. Deze theoretische verdelingsfuncties en met name de berekende verdelingen van de gastemperatuur kwamen goed overeen met de experimenteel gevonden verdelingsfuncties.

CURRICULUM VITAE.

19 januari	1944	Geboortedam
5 juli	1961	Eindexamen HBS-B
30 september	1966	Doctoraal examen technische natuurkunde met specialisatie: gasontladingsphysica (T.H.Eindhoven)
1 october	1966	Datum indiensttreding als wetenschappelijk medewerker aan de T.H. Eindhoven bij de groep Atoomfysica
1 september	1970	Benoeming tot hoofddocent-natuurkunde aan het Moller-instituut voor de opleiding van leraren te Tilburg.

Elk lid van de sectie Atoomphysica heeft op eigen wijze bijgedragen tot de realisering van dit werk.
Ik ben allen hiervoor zeer erkentelijk.
Mijn speciale dank gaat hierbij uit naar Mej. M.A. van Basten , die op zeer nauwgezette wijze dit proefschrift heeft getypt en naar Mej. R. Gruyters die de tekeningen heeft verzorgd.

STELLINGEN

1

De gangbare benaming "Drukverbreding" voor een bepaalde verzameling spectrale lijnverbredingsprocessen is principieel onjuist.

G.Traving, Uber die Theorie der Druckverbreiterung von Spektrallinien, 1960.

2

Bij de opstelling van een model voor de gecontraheerde positieve zuil gaan Baranov en Uljanov uit van twee onverenigbare voorwaarden.

V.Ju.Baranov, K.N.Uljanov, Sovj.Phys.Tech.Phys. 14, 183 (1969).

3

De vaak gehanteerde benadering dat de gastemperatuursverdeling in een positieve zuil kan worden voorgesteld door een parabolische functie van de straal is slechts onder zeer beperkte condities geldig.

Dit proefschrift, hoofdstuk V.

4

De door Betz gebruikte methode ter bepaling van de reflectiecoëfficiënt van een germanium-sulfide oppervlak is gebaseerd op een onjuiste extrapolatie procedure.

C.R.Betz, Thesis, North Western University, Evanston,Illinois, U.S.A.

5

Zowel Lang als Edwin en Turner gaan er bij de interpretatie van hun spectrale lijnprofielmetingen ten onrechte van uit dat het door hen beschouwde emitterende plasma homogeen is.

K.Lang, Acta Phys. Austriaca 5, 376 (1951).
R.P.Edwin, R.Turner, J.Opt.Soc.Am. 60, 448 (1970).

6

Bij de experimentele lerarenopleidingen wordt voor de derde-graads studie de combinatie van de vakken natuurkunde en scheikunde ten onrechte als één studierichting beschouwd.

7

De aanduiding "klassiek" voor een aantal lijnverbredingstheorieën is misleidend daar hierdoor ten onrechte wordt gesuggereerd dat geen gebruik wordt gemaakt van quantum-mechanisch berekende resultaten.

8

De door Wojaczek en Hayess gegeven interpretatie van door hen uitgevoerde thermokoppelmetingen in een positieve zuil in argon is aanvechtbaar.

E.Hayess, K.Wojaczek, Beitr.Plasmaphys. 10, 407 (1970).

Wanneer men er van uit gaat dat een eerste-graads opleiding tot leraar een doctoraal niveau moet hebben, lijkt de instelling van een leraren doctoraal een zinvolle consequentie.

10

Het ontladingsmodel, gehanteerd door Schaper en Scheibner bij de interpretatie van metingen van de totale werkzame doorsnede voor aanslag van edelgasatomen, leidt tot betrouwbare uitkomsten dankzij het feit dat de invloeden van twee verschillende vereenvoudigingen in dit model elkaar nagenoeg opheffen.

M.Schaper, H.Scheibner, Beitr.Plasmaphys. 9, 45 (1969).

11

Het verdient aanbeveling om de aan de instituten voor de opleiding van leraren geldende verplichting tot studie in twee verschillende vakken te veranderen in de mogelijkheid tot het verwerven van meerdere akten van bekwaamheid op grond van een met succes afgesloten multidisciplinaire studie.

12

Gezien het succes van de Stichting Ether Reclame in het tot stand brengen van een conversatie tussen twee gehaktballen moet overwogen worden de vitrines van slagerijen van geluidsisolerend materiaal te voorzien.

8 juni 1971, Tilburg. C.A.M. Mouwen.